CO_2 fluxes between land and atmosphere in catchments with contrasting land cover

By

Bertrand Teodosio

Under the supervision of

Dr. Edoardo Daly

and

Assoc. Prof. Valentijn Pauwels

Department of Civil Engineering
Monash University

A dissertation submitted to Monash University in accordance with the requirements of the degree of Master of Engineering Science (Research) in the Faculty of Engineering.

March 2017

Abstract

The project is part of a collaborative effort of Monash University, La Trobe University, Department of Economic Development, Jobs, Transport and Resources, and Australian Research Council to study the effect on carbon and water fluxes as a result of conversion of agricultural landscapes to plantations.

Productive ephemeral catchments are more prone to environmental degradation and play an important role in the economy of Australia. However, few managed ecosystems are currently being monitored in Australia to understand the impact of managed landscapes on CO_2 fluxes. The main aim of this research is to investigate soil carbon efflux (R_S) through field experimentation and numerical analysis in productive ephemeral catchments with contrasting land use. The study sites are two adjacent catchments in Southwestern Victoria; one catchment is mainly a livestock-grazed pasture and the other is a blue gum plantation. Based on the soil respiration chamber (SRC) and eddy-covariance (EC) measurements, the catchments were water-limited resulting into R_S mainly controlled by soil water content. The spatial variability of R_S measured by SRCs in the Mediterranean study sites resulted in an inverse relationship with soil temperature (T_S). This R_S-T_S relationship opposed the common relationship observed in temperate regions where R_S as T_S increases. Furthermore, the wavelet and Granger causality analyses of the EC field data from the pasture suggested that considering soil moisture (θ) and air temperature (T_a) in estimating R_S may be useful rather than relying on a single parameter, T_S. Since the spatial variability and key drivers investigation suggests that θ plays an important role in regulating R_S in productive ephemeral catchments, simulations employing root water compensation and hydraulic redistribution in the root water uptake formulation (RWU) were performed. A one-dimensional model was presented to couple the soil water flow with heat and CO_2 equations. One of the aims of the numerical simulations is to compare how different formulations of RWU, accounting for root water compensation and hydraulic redistribution, affect transpiration and soil CO_2 efflux. The other aim is to investigate the diurnal phase of R_S. The comparison resulted into a difference of around 15% to 20% for transpiration (T_{ac}) and R_S, respectively. The out of phase relationship of the daily pattern of R_S and T_S can be explained by reducing soil heat flux due to shading and applying hydraulic redistribution capturing empirical daily pattern from field studies. In summary, the magnitude and pattern of R_S are mainly affected by θ.

Dedication and acknowledgements

I would like to dedicate my humble effort to my family, Luisito, Eufemia, Bill, and Noemi, who has been a constant source of encouragement. To my lifetime partner, Chris, for inspiring me through your love and care. And to God, for always guiding my path.

I would like to express my sincere gratitude to my supervisor, Dr. Edoardo Daly, for his knowledge and guidance. To the Australian Research Council (Project LP140100871) and the Monash University - Civil Engineering Department for funding my candidature. To Assoc. Prof. Valentijn Pauwels, Dr. Steven Loheide, and Dr. Chris Rudiger for their technical advice. To Dr. Malcolm McCaskill for providing weather station data. To Peter, James, Eva, Elise, Anne, Caitlin of OzFlux. To Frank, Ian, Paul, and Kiri for assisting me during my site visits. And to my Monash University mates, especially Jamie and Giselle, for the awesome moments!

"It always seems impossible until it's done."

- Nelson Mandela (1918-2013)

Author's declaration

I declare that the work in this dissertation was carried out in accordance with the requirements of the University's Regulations and Code of Practice for Research Degree Programmes and that it has not been submitted for any other academic award. Except where indicated by specific reference in the text, the work is the candidate's own work. Work done in collaboration with, or with the assistance of, others, is indicated as such. Any views expressed in the dissertation are those of the author.

SIGNED:  ... DATE: ..05/06/2017..

Table of Contents

List of Tables

List of Figures

Figure **Page**

Chapter 1

Introduction

Land use of agricultural catchments plays an important role in our economy and environment. With the aim to increase productivity (e.g. crop yield), management may cause land degradation and affect precious water resources. For instance, tree plantations are grown to sustain the demand for timber and paper production, but also offer natural carbon sequestration to mitigate global warming (*Campioli et al.*, 2015). However, tree plantations commonly use more water than grasslands and pastures (*Benyon et al.*, 2009). In southern Australia, plantations are often found in ephemeral catchments and they might access groundwater to satisfy the demand for higher amounts of water (*Benyon et al.*, 2006). The impact of plantations on groundwater recharge and stream flow in ephemeral catchments is a progressive drawdown in groundwater levels and drying up of tributary flows (*Adelana et al.*, 2015; *Dean et al.*, 2016). Furthermore, excessive use of water resources led to soil salinization, acidity increase, and aridation of catchments, all of which directly affect ecosystems (*Jackson et al.*, 2005; *Robson*, 2008; *Robson et al.*, 2013). This may be prevented through sustainable management of productive landscapes.

Managed lands in the state of Victoria in Australia, specifically pastures and plantations, play an important role in its economy. Livestock-grazed pastures are often mainly devoted to beef and dairy products, and sheep and wool (*Henzell*, 2007). The agriculture industry in Victoria is vast, making it the largest milk producing state, with around 60-70% of the total national milk production. Furthermore, the sheep and wool industry in Victoria is very important; for instance, in 2007 it was worth 11% of the total gross value of the agricultural production of Australia for domestic use and an additional 2% as export earnings (*Wolfe*, 2009). On the other hand, blue gum plantations supply hardwood chips for the Port of Portland in

Victoria which is now the biggest exporter of blue gum hardwood chips in the world. The port has shipped out 2.65 million tonnes during the 2014/15 financial year. The exportation has been forecasted to increase and stay high until the mid-2020s (*Grindlay*, Updated: August 2015).

While productive ephemeral landscapes are very important in the economy of Australia and more prone to environmental degradation, few managed sites are currently being monitored to understand the impact of land use on water and carbon fluxes. According to the Australian and New Zealand Flux Research and Monitoring (OzFlux), the national ecosystem research network that provides consistent observations of carbon and water exchange between land and atmosphere, most sites in the database being monitored at the moment are natural forests and grasslands.

Due to the dearth of studies of carbon efflux on productive ephemeral catchments, the main aim of this research is to investigate CO_2 efflux in two catchments with contrasting land use. One catchment is mainly a livestock-grazed pasture, which will be referred to hereafter as pasture, and the other catchment is a blue gum plantation, which will be referred to as plantation.

This thesis presents the field experiments and modelling components of the research. Firstly, the aims of the research are outlined and put in the context of current research efforts. Afterward, the experimentation and modelling methodologies and results are discussed. Finally, conclusions are presented. The acronyms and nomenclature are presented in Appendix A. Appendices B to E present supplementary data necessary to fully understand this thesis.

CHAPTER 2

Literature review

This literature review critically evaluates experimental studies concerning the effect of land use on carbon efflux. Many of these studies used the eddy-covariance (EC) method to measure the net ecosystem exchange (NEE), which was then partitioned to estimate the ecosystem respiration (R_E). Other studies used soil respiration chambers (SRCs) to obtain soil C efflux or soil respiration (R_S). This literature review also evaluates models focusing on soil C efflux and its relationship to root water uptake.

2.1 CO_2 efflux measurements

Land use has a significant effect on the atmospheric CO_2 concentration and has been of great interest due to yield production and climate change. Different terrestrial ecosystems have been assessed based on field experimentations and numerical modelling to quantify their capacity to sequester carbon and to produce biomass (*Baldocchi*, 2014). For instance, *Schulze* (2006) determined that sustainable land use can sequester around 25% of the annual human-induced CO_2 net flux.

The carbon budget provides potential carbon sequestration capabilities of terrestrial ecosystems depending on various biotic and abiotic factors. In analysing the carbon budget of a landscape, NEE, R_E, gross primary productivity (GPP), and net primary productivity (NPP) are necessary to be explained (Figure 2.1). NEE is the net accumulation of carbon of an ecosystem, which can be measured using the EC method. The sign convention for the CO_2 fluxes is positive if carbon is transferred to the atmosphere and negative if carbon is transferred into the ecosystem. Thus, positive NEE values indicate carbon emission while negative NEE values

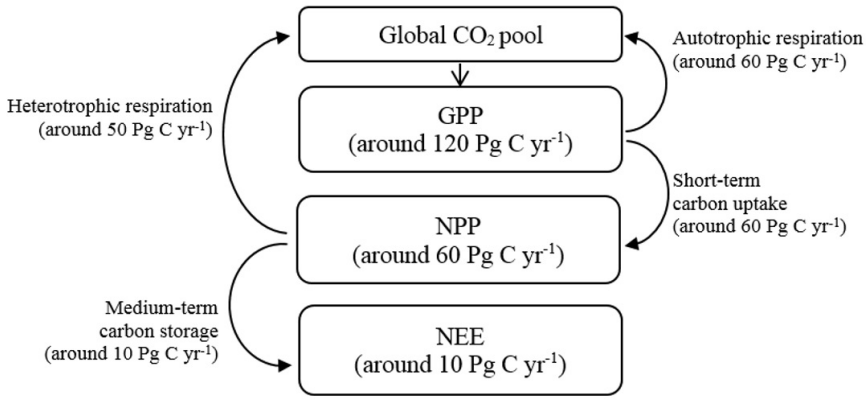

FIGURE 2.1. Terrestrial ecosystem uptake.

indicate carbon sink. The relationship between NEE, R_E, and GPP is given by:

$$NEE = GPP + R_E, \tag{2.1}$$

where GPP represents the overall carbon fixed through photosynthesis by vegetation in an ecosystem. R_E is the sum of autotrophic (R_a) and heterotrophic respiration (R_h): R_a is the derivative of metabolism of organic matter by vegetation, while R_h is that of microbes. NPP denotes the net production of organic matter, which is equivalent to GPP reduced by losses due to R_a.

The differences in carbon budget estimates of each site are driven mainly by land use (*Abdalla et al.*, 2013). Tables 2.1 and 2.2 show the carbon fluxes of diverse land uses investigated in a number of studies. In these studies, carbon fluxes (i.e. NEE) were collected using EC systems. Some other sites used additional methods to measure carbon emission (i.e. R_E) that verified the common method of partitioning of NEE into GPP and R_E.

The NEE of natural forests, plantations, grasslands, pastures, croplands, savanna, and peat bogs differed in range. Grasslands were observed to have values of NEE ranging widely from 0.05 to -0.40 gC m^{-2} d^{-1}. It can be observed that the range of values of NEE of grasslands can be positive values (indicating carbon sources), values close to zero (indicating a carbon neutral ecosystem), or negative values (indicating carbon sink). This range indicates that grasslands were sensitive to location and environmental factors as they shift from carbon sinks to sources (*Serrano-Ortiz et al.*, 2014). The average NEE of managed pastures ranged from -0.60 to -1.40 gC m^{-2} d^{-1}. The range of NEE of croplands was wide, having a range of -0.60 to -4.30 g gC m^{-2} d^{-1} based on the reviewed studies. The NEE of croplands was strongly dependent on the type of plants cultivated in the particular landscape. The average NEE of natural forests based on the study sites reviewed ranged from -0.80 to -1.40 gC m^{-2} d^{-1}. A higher average NEE of

Table 2.1: NEE, GPP, and R_E of natural forests and plantations

Location	Vegetation	Period	NEE ($gCm^{-2}d^{-1}$)	GPP ($gCm^{-2}d^{-1}$)	R_E ($gCm^{-2}d^{-1}$)	Reference
Natural forests						
Victoria, AUS	*Eucalyptus regnans*	2005-2007	-0.26 to -2.07	-4.84 to -8.55	4.49 to 7.60	(*Kilinc et al.*, 2013)
South Zealand, DNK	*Fagus sylvatica*	2006-2010	-0.70±0.09	-5.18±0.35	4.49±0.52	(*Wu et al.*, 2013)
Southeast, GBR	*Quercus robur*	2007-2010	-0.78 to -1.38	-3.72 to -5.62	3.02 to 4.15	(*Heinemeyer et al.*, 2012)
Jura, CHE	Mixed deicuous	2005-2009	-1.12±0.17	-5.01±1.21	3.80±0.95	(*Etzold et al.*, 2011)
Davos, CHE	*Picea abies*	2005-2009	-0.43±0.17	-2.85±0.69	2.51±0.60	(*Etzold et al.*, 2011)
Hesse, FRA	*Fagus sylvatica*	1996-1997	-0.60 to -0.69	-2.76 to -3.37	2.16 to 2.68	(*Granier et al.*, 2000)
Prince Albert, CAN	*Picea mariana*	1995-1998	-0.60 to -0.69	-2.76 to -3.37	2.16 to 2.68	(*Malhi et al.*, 1999)
Oak Ridge, USA	Oak-hickory mix	1995-1998	-0.17	-2.68	2.51	(*Malhi et al.*, 1999)
Manaus, BRA	Evergreen	1995-1998	-1.64	-8.29	6.74	(*Malhi et al.*, 1999)
Plantations						
South Tyrol, ITA	*Malus domestica*	2009-2010	-1.04±0.09	-3.46±0.01	2.42±0.43	(*Zanotelli et al.*, 2013)
North Carolina, USA	*Pinus taeda*	1998-2003	-0.95 to -2.16	-3.46 to -6.83	3.28 to 5.53	(*Stoy et al.*, 2006)
Christchurch, NZL	*Pinus radiata*	1994-1996	-1.64	-11.23	7.60	(*Arneth et al.*, 1998)
Laois, GBR	*P. stichensis*	2003-2007	-2.48	-5.51	4.04	(*Arneth et al.*, 1998)

Table 2.2: NEE, GPP, and R_E of natural grasslands, pastures, and other ecosystems.

Location	Vegetation	Period	NEE ($gCm^{-2}d^{-1}$)	GPP ($gCm^{-2}d^{-1}$)	R_E ($gCm^{-2}d^{-1}$)	Reference
Grasslands						
Granada, ESP	*Festuca indigesta*	2006-2008	-0.35 to -0.43	-1.04 to -1.21	0.78	(*Serrano-Ortiz et al.*, 2014)
Almeria, ESP	*Festuca scariosa*	2006-2008	-0.09	-0.26 to -0.60	0.43	(*Serrano-Ortiz et al.*, 2014)
Almeria, ESP	*Stipa tenacissima*	2006-2008	0.35	-0.60 to -0.69	0.78 to 0.95	(*Serrano-Ortiz et al.*, 2014)
North Carolina, USA	C_3 grass	2001-2002	0.26	-3.28	3.54	(*Novick et al.*, 2004)
Oklahoma, USA	Bluestem, etc.	1997	-3.45	-14.30	10.85	(*Gilmanov et al.*, 2003)
Pastures						
Carlow, GBR	*Lolium perenne*	2003-2005	-0.58	-4.53	3.95	(*Abdalla et al.*, 2013)
Oklahoma, USA	Mixed prairie	1997	-1.42	-8.31	6.25	(*Gilmanov et al.*, 2003)
Oklahoma, USA	Bluestem	1997	-0.90	-11.11	10.36	(*Gilmanov et al.*, 2003)
Cropland						
Carlow, GBR	*Hordeum vulgare*	2003-2007	-0.52	-2.48	1.96	(*Abdalla et al.*, 2013)
Oklahoma, USA	Wheat crop	1997	-4.31	-12.30	7.98	(*Gilmanov et al.*, 2003)
Savanna						
Kruger, ZAF	*C. apiculatum*	2000-2005	-0.38	-	-	(*Archibald et al.*, 2009)
Peat bog						
Te Ika-a-Maui, NZL	*S. ferrugineus*	1999-2000	-0.64	-3.11	2.47	(*Archibald et al.*, 2009)

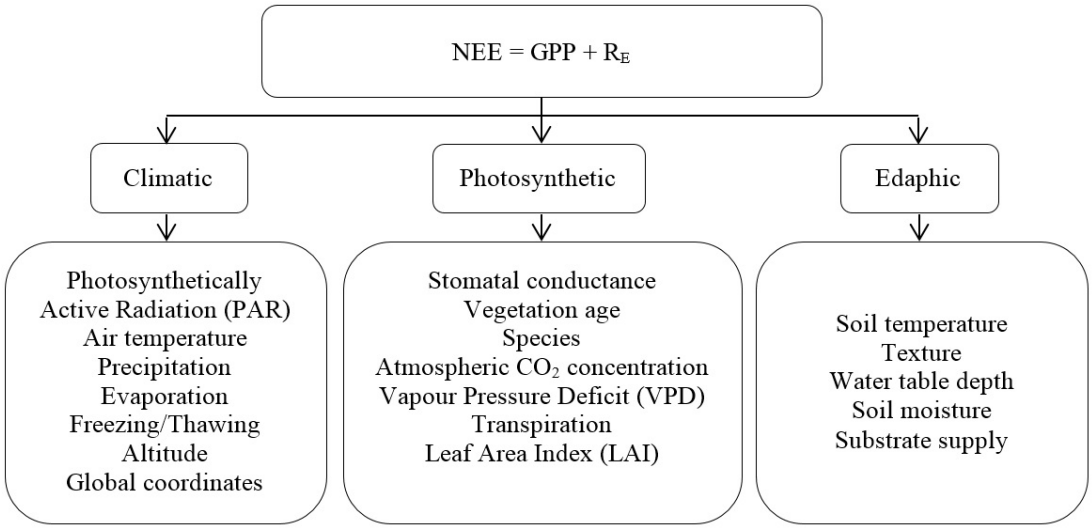

FIGURE 2.2. CO_2 fluxes key drivers.

plantations was observed, from -1.20 to -2.20 gC m^{-2} d^{-1}. Plantations and pastures sequestered more carbon compared to natural forests and grasslands due to land management (*Luyssaert et al.*, 2014). Based on the reviewed studies, NEE was driven by the variables presented in Figure 2.2. Since NEE is calculated by equation (2.1), these abiotic and biotic factors may also affect GPP and R_E.

GPP was affected by land management that led to a more active photosynthesis of plants (Tables 2.1 and 2.2). The average value of GPP in grasslands was -1.20 gC m^{-2} d^{-1}. The average GPP of natural forests was approximately -5.10 gC m^{-2} d^{-1}, while that of plantations was around -6.10 gC m^{-2} d^{-1}. Croplands had an average GPP of -7.40 but the minimum and maximum values were -2.48 and -12.30 gC m^{-2} d^{-1} for a spring barley and winter wheat crop, respectively. This large difference was due to the type of crops present in the study sites. Pastures had an average GPP of -8.0 gC m^{-2} d^{-1}.

The R_E of the studied croplands ranged from 2.00 to 8.00 gC m^{-2} d^{-1}. The average R_E of grasslands (1.40 gC m^{-2} d^{-1}) and natural forests (3.60 gC m^{-2} d^{-1}) were lower than that of plantations (4.40 gC m^{-2} d^{-1}) and pastures (6.90 gC m^{-2} d^{-1}). This suggested more active root and microbial respiration in managed landscapes (*Campioli et al.*, 2015).

R_E is commonly assumed to equal soil respiration (R_S), the below-ground respiration due to carbon emission of roots (autotrophic respiration) and microbes (heterotrophic respiration). For low stature plants this assumption proved to be acceptable since SRCs include the foliar

respiration during measurements. However, for high stature plants, R_S was between 60% to 80% of R_E (*Davidson et al.*, 1998). R_S is a strong indicator of biological activity that reflects whether the soil conditions are conducive to biological processes (e.g. photosynthesis). The biological activity in the soil is related to physical and chemical environment, which can either be inherent (e.g. soil texture) or extrinsic (e.g. soil organic carbon (SOC) and soil aeration). R_S is a useful measure as a short-term and a long-term response to land use management. Furthermore, R_S plays a significant part in the carbon cycle (*Bond-Lamberty and Thomson*, 2010; *Reichstein et al.*, 2013) and has a profound impact on atmospheric carbon concentrations, thus contributing to global warming (*Yiqi and Zhou*, 2010).

Measured R_S by past studies used SRCs, which investigated the magnitude of C emission in both natural and managed ecosystems as shown in Tables 2.3 and 2.4. The average magnitude of R_S in natural forests was lower (1.01 t 4.23 gC m^{-2} d^{-1}) than those in grasslands (1.21 t 5.43 gC m^{-2} d^{-1}) and shrublands (0.46 t 6.09 gC m^{-2} d^{-1}) according to the reviewed literature. For managed ecosystems, plantations (1.35 t 4.09 gC m^{-2} d^{-1}) had lower R_S than croplands (2.23 t 6.50 gC m^{-2} d^{-1}) and pastures (0.96 t 8.79 gC m^{-2} d^{-1}). It can further be observed that the average R_S of croplands and pastures were relatively higher than those of grasslands and shrublands. On the other hand, plantations have slightly lower R_S compared to those of natural forests. R_S of grasslands, shrublands, and croplands had a wider range compared to the ranges of natural forests and plantations. In addition, the reviewed literature for both pastures and plantations was limited; this requires for more site investigations. Specifically, in Australia, where managed ephemeral catchments play an important role in the economy of the nation (*Grindlay*, Updated: August 2015) and these managed ecosystems are prone to environmental degradation due to abrupt changes in the ecosystem (*Jackson et al.*, 2005; *Robson*, 2008; *Robson et al.*, 2013), further investigations of R_S are necessary.

At the present time, R_S is still not well understood due to its high spatial variability (*Buysse et al.*, 2016). Studies designed to investigate its spatial variation depending on land use at a catchment scale are required. Few studies focused on spatial variability of R_S using SRCs. Early studies include *Rochette et al.* (1991) who measured R_S on bare soil, in maize, and in wheat crops. The investigation resulted to an indefinite spatial auto-correlation on bare soil measurements along transects. In the maize crop transect, when the soil is dry, R_S along rows was significantly higher than that of between rows. Under wet conditions, R_S between rows and along rows had no significant difference. However, compacted soil between rows due to tractor wheels has lower R_S than that of the uncompacted soil in between rows. *Hanson et al.* (1993) conducted chamber measurements on a forest floor, together with soil temperature and soil moisture measurements. R_S measurements of different topographic features of the forest did not have observable patterns. *Almagro et al.* (2009) conducted a comparison of R_S between

Table 2.3: Soil respiration (R_S) measurements in natural ecosystems using SRCs.

Location	Climate	Soil	Vegetation	Period	R_S ($gCm^{-2}d^{-1}$)	Reference
			Natural forest			
Prades Mt., ESP	Mediterranean	Xerochrepts	Pine & Oak	2010 growing season	2.54-3.15	(*Barba et al.*, 2013)
California, USA	Mediterranean	Haploxerpts	Bishop pine	06/2008-10/2009	1.03-4.99	(*Carbone et al.*, 2011)
Kiskunsag, HUN	Pannonian	Arenosol	Steppe	04/2010-11/2012	0.11-2.57	(*Lellei-Kovács et al.*, 2016)
Cahegin, ESP	Mesomediterranean	Petric calcisol	Oak	12/2006-04/2007	2.10±0.18	(*Almagro et al.*, 2013)
Tennessee, USA	Temperate	Loam	Oaks	03/1991-01/1992	0.83-5.91	(*Hanson et al.*, 1993)
Harvard, USA	Temperate	Canton	Red oak & Maple	1995	0.60-6.00	(*Davidson et al.*, 1998)
Western AUS	Mediterranean	Chromosol	*E. marginata*	10/2005-05/2006	0.72-2.16	(*Livesley et al.*, 2009)
Monte Novo, PRT	Mediterranean	-	*Pinus pinea*	2005-2006	0.93-3.63	(*Correia et al.*, 2012)
Coruche, PRT	Mediterranean	-	*Quercus suber*	2008-2096	1.66-3.94	(*Correia et al.*, 2012)
Alfarrobeira, PRT	Mediterranean	-	*Quercus ilex*	1999	0.73-5.70	(*Correia et al.*, 2012)
			Grasslands			
Oregon, USA	Mediterranean	clay-rich	annuals	2010 (spring to fall)	0.70-6.20	(*Reynolds et al.*, 2015)
Oregon, USA	Mediterranean	clay-rich	perrenials	2010 (spring to fall)	0.25-7.00	(*Reynolds et al.*, 2015)
Washington, USA	Mediterranean	clay-rich	perrenials	2010 (spring to fall)	0.50-6.10	(*Reynolds et al.*, 2015)
Vila Vicosa, PRT	Mediterranean	-	C_3	2006-2007	0.80-4.50	(*Correia et al.*, 2012)
Montemor, PRT	Mediterranean	-	C_3	2006-2007	1.60-4.00	(*Correia et al.*, 2012)
Elvas, PRT	Mediterranean	-	C_3	2003-2005	0.60-4.20	(*Correia et al.*, 2012)
Inner-Mongolia, CHN	Temperate	Calcic Luvisol	*S. krylovii*	2005-2007	2.26	(*Liu et al.*, 2009)
Utah, USA	Semi-arid	Loam	*Q. gambelii*	07/2008-11/2008	4.00-6.00	(*Moyes and Bowling*, 2013)
			Shrublands			
Mols, DNK	Atlantic	Haplic podzol	Heath	05/2011-09/2012	0.65-17.66	(*Lellei-Kovács et al.*, 2016)
Brandbjerg, DNK	Atlantic	Haplic podzol	Heath	03/2011-12/2012	0.02-8.48	(*Lellei-Kovács et al.*, 2016)
Oldebroek, NLD	Atlantic	Haplic podzol	Heath	07/2010-06/2012	0.26-3.05	(*Lellei-Kovács et al.*, 2016)
Clocaenog, GBR	Atlantic	Ferric podzol	Heath	01/2010-10/2012	0.13-4.00	(*Lellei-Kovács et al.*, 2016)
Garraf, ESP	Mediterranean	Petric Calcisol	Garrigue	04/2002-12/2003	0.27-2.60	(*Lellei-Kovács et al.*, 2016)
Caccia, ITA	Mediterranean	Petric Calcisol	Garrigue	02/2010-11/2011	0.98-5.38	(*Lellei-Kovács et al.*, 2016)
Ningxia, CHN	Arid	Sandy soil	*Artemisia*	06/2012-10/2012	0.90-1.49	(*Wang et al.*, 2015)

Table 2.4: Soil respiration (R_S) measurements in managed ecosystems using SRCs.

Location	Climate	Soil	Vegetation	Period	R_S ($gCm^{-2}d^{-1}$)	Reference
Croplands						
Selhausen,DEU	Temperate	Haplic Luvisol	Bare	05/2009-06/2009	1.33-4.17	(*Herbst et al.*, 2009)
BEL	Temperate	Dystric Luvisol	Wheat & Maize	05/2012-12/2012	0.20-9.70	(*Wiaux et al.*, 2015)
Cahegin, ESP	Mesomediterranean	Calcaric Regosol	Cereal	12/2006-04/2007	1.77±0.18	(*Almagro et al.*, 2013)
Cahegin, ESP	Mesomediterranean	Petric Carcisol	Olive	12/2006-04/2007	1.17±0.08	(*Almagro et al.*, 2013)
Western FRA	Temperate	Haplic Albeluvisols	Maize, Cereal	05/2014-04/2015	2.10-5.63	(*Buysse et al.*, 2016)
Plantations						
Buckley, CAN	Temperate	Gravelly loam	Douglas fir	08/2005-12/2006	2.07-7.78	(*Jassal et al.*, 2008)
Pegoes, PRT	Mediterranean	-	*E. globulus*	2002 & 2006	1.04-3.73	(*Correia et al.*, 2012)
Mitra, PRT	Mediterranean	-	*Quercus suber*	2008-2009	0.83-5.60	(*Correia et al.*, 2012)
Western AUS	Mediterranean	Chromosol	*E. globulus*	10/2005-06/2006	0.24-1.44	(*Livesley et al.*, 2009)
Western AUS	Mediterranean	Chromosol	*P. radiata*	10/2005-06/2006	0.48-1.92	(*Livesley et al.*, 2009)
Pastures						
Bugac, HUN	Semi-arid	Sandy soil	Festuca, Carex	07/2011-11/2012	0.24-16.00	(*Balogh et al.*, 2015)
Western AUS	Mediterranean	Chromosol	Clover	10/2005-06/2006	0.84-1.32	(*Livesley et al.*, 2009)

canopy and inter-canopy measurements of a forest, an abandoned field, and an Olive grove. This study observed higher R_S measurements on canopies than those R_S measurements on the inter-canopy. The highest R_S was measured in the canopy of the forest while the R_S in the inter-canopy of the Olive grove was half of the abandoned field and forest. According to *Herbst et al.* (2009), the spatial variability of R_S was also high in their bare soil test plot field experiment. *Barba et al.* (2013) also showed that the spatial variability of R_S during growing season was high and showed no spatial auto-correlation. R_S was highest in soils near to dead pines and trees. *Wang et al.* (2015) concluded that spatial variability of R_S was dependent on plant distribution based on their experiment in a desert sand dune.

The large uncertainty due to lack of R_S measurements that have been taken in the past requires thorough investigations on its key drivers, since the roles of abiotic and biotic factors are still unknown. Past studies showed that soil temperature (T_S), soil moisture (θ), climate, vegetation phenology, soil C and N pools, and evapotranspiration controlled the R_S dynamics. R_S was primarily driven by T_S, which mostly accounted for seasonal and daily variation (*Davidson et al.*, 1998; *Valentini et al.*, 2000; *Wiaux et al.*, 2015). *Subke and Bahn* (2010) showed that there is an exponential increase in R_S due to soil temperature or Q_{10} (i.e. measure of rate of change of R_S due to a soil temperature increase by 10°C) for sites with temperate condition. However, T_S had been found to have confounding relationship with θ when it comes to controlling the magnitude of R_S (*Davidson et al.*, 1998; *Lellei-Kovács et al.*, 2016). *Jassal et al.* (2008) and *Carbone et al.* (2011) argued that R_S was dependent on T_S; however, it was modulated by a θ threshold, which affected its seasonal pattern. In drier regions, θ predominantly controlled R_S (*Liu et al.*, 2009; *Correia et al.*, 2012; *Suseela et al.*, 2012; *Almagro et al.*, 2009). Furthermore, *Reynolds et al.* (2015) determined that latitudinal climate gradient in Mediterranean regions affected the monthly R_S response due to θ limitation and episodic droughts. *Moyes and Bowling* (2013) and *Wang et al.* (2015) assessed the relative importance of plant phenology on R_S during seasonal transitions. Moreover, *Almagro et al.* (2013) presented the importance of vegetation pattern and soil C and N content on R_S. Evapotranspiration also controls R_S in some dry ecosystems (*Balogh et al.*, 2015).

In Australian sites with Mediterranean climate, R_S appears to be strongly related to soil moisture. R_S clearly shows response to rainfall events. Furthermore, there were no observed consistent relationship between R_S and soil temperature in water-limited sites (*Livesley et al.*, 2009). R_S varied significantly with soil moisture, which was affected by soil drainage patterns (*Davidson et al.*, 1998). Soil drainage patterns had significant effect on the spatial heterogeneity of R_S.

Understanding the spatial variability and key drivers of R_S thus lead to deeper understanding of

the variables affecting the process of root and microbial respiration. This may aid in partitioning NEE into GPP and R_E by incorporating essential parameters in a model (*Reichstein et al.*, 2005; *Livesley et al.*, 2009; *Lasslop et al.*, 2010).

2.2 Soil CO_2 models

Soil water extracted by plant roots for transpiration not only constitutes a significant portion of the hydrological cycle, but has an important role on the CO_2 and energy exchange between the land and the atmosphere (*Bonan*, 2015). Thus, key mechanisms regulating root water uptake, such as root water compensation and hydraulic redistribution, are essential to be included in models for ecohydrological applications.

Root water compensation refers to the ability of vegetation to adjust root water uptake as a function of soil water content, while hydraulic redistribution refers to the movement of soil water from wetter to drier layers through the root system (*Aroca et al.*, 2012). These mechanisms have been observed to be significant in modulating actual transpiration (T_{ac}) (*Caldwell et al.*, 1998; *Da Rocha et al.*, 2004; *Domec et al.*, 2010; *Howard et al.*, 2009; *Neumann and Cardon*, 2012; *Prieto et al.*, 2010), nursing seedlings (*Neumann and Cardon*, 2012; *Prieto et al.*, 2011, 2012), enhancing nutrient uptake (*Caldwell et al.*, 1998; *Neumann and Cardon*, 2012; *Prieto et al.*, 2012), prolonging root life span (*Caldwell et al.*, 1998; *Domec et al.*, 2006; *Neumann and Cardon*, 2012; *Prieto and Ryel*, 2014), and preventing evaporation through hydraulic descent in extremely dry conditions (*Neumann and Cardon*, 2012). Accordingly, root water compensation and hydraulic redistribution have been incorporated in mathematical models to provide a more realistic description of root water uptake.

Many mathematical models for ecohydrological applications use the Richards equation with a sink term to describe soil water dynamics. When using a macroscopic approach, the soil water extraction rate from different soil layers is assumed to depend on the soil water content, root density and potential transpiration (*Molz*, 1981; *Skaggs et al.*, 2006). Root water compensation is often included by adjusting the distribution of root water uptake from different soil layers (*Jarvis*, 1989; *Simunek and Hopmans*, 2009; *Jarvis*, 2011). Other models describe root water uptake as a function of water potential gradients between soil and root xylem (*Molz*, 1981; *Mendel et al.*, 2002; *Siqueira et al.*, 2006; *Amenu and Kumar*, 2007; *Verma et al.*, 2014), thereby accounting for compensatory mechanisms. Some of these latter models have been extended to include a detailed description of the root architecture (*Couvreur et al.*, 2012; *Javaux et al.*, 2013). Although providing a three dimensional detailed description of soil water dynamics, these models of root architecture are computationally expensive and involve a large number

of parameters often difficult to quantify. The sink term introduced by *de Jong van Lier et al.* (2013) models root water uptake as a function of the difference between the matric flux potential in the soil and a constant value of matric flux potential characterizing the root surface. This model has been observed to be somehow equivalent to the model introduced by *Jarvis* (1989), as discussed in *Jarvis* (2010). Comparisons between models of soil water fluxes using these different expressions for root water uptake have been presented by *de Willigen et al.* (2012) and *Camargo and Kemanian* (2016) for some virtual experiments. On the other hand, *Santos et al.* (2017) evaluated the capability of some empirical models to reproduce the water extraction distribution under varying environmental conditions from numerical simulations of a detailed physical model.

Since soil water content is one of the key variables regulating soil CO_2 production and efflux (*Hanson et al.*, 1993; *Davidson et al.*, 1998; *Almagro et al.*, 2009; *Liu et al.*, 2009; *Carbone et al.*, 2011; *Suseela et al.*, 2012; *Balogh et al.*, 2015; *Reynolds et al.*, 2015; *Lellei-Kovács et al.*, 2016), root water uptake mechanisms might play an important role in defining CO_2 fluxes. Mechanistic models have been developed for CO_2 production and transport to adequately describe vertical gaseous diffusion and dispersion as a function of soil water content and temperature (*Patwardhan et al.*, 1988; *Simunek and Suarez*, 1993; *Fang and Moncrieff*, 1999). These models have been calibrated and validated against experimental data (*Suarez and Simunek*, 1993; *Moncrieff and Fang*, 1999; *Goffin et al.*, 2015), have been coupled to soil water and temperature models at catchment scale (*Welsch and Hornberger*, 2004; *Riveros-Iregui et al.*, 2011), and have been combined with experimental data of soil moisture, soil temperature, and air-phase soil CO_2 concentrations to estimate soil CO_2 production and surface efflux (*Hirano et al.*, 2003; *Chen et al.*, 2005; *Jassal et al.*, 2008; *Daly et al.*, 2009; *Liang et al.*, 2010; *Latimer and Risk*, 2016).

The evolution of root water uptake calculation is improving significantly, however, models are still not thoroughly compared. The difference in model formulation should be investigated since this may affect the end results crucial for ecohydrological forecasting. Root water compensation calculation using (1) adjustment of distribution of root water uptake from different soil layers (*Jarvis*, 1989; *Simunek and Hopmans*, 2009; *Jarvis*, 2011) and (2) water potential gradients between soil and root xylem (*Molz*, 1981; *Mendel et al.*, 2002; *Siqueira et al.*, 2006; *Amenu and Kumar*, 2007; *Verma et al.*, 2014) should be compared to know the quantitative difference of each formulation. Moreover, quantitative analysis of the effect of hydraulic redistribution on actual transpiration may be significant to be considered in models. Hydraulic redistribution might also have substantial impact on soil CO_2 efflux, which is important in carbon budget calculations.

2.3 Research gaps

The reviewed literature showed the importance to further monitor and analyze CO_2 flux data from managed productive ephemeral catchments. Specifically, in Australia, where managed ephemeral catchments play an important role in the economy and these managed ecosystems are more prone to environmental degradation, further investigations of R_S are necessary.

R_S, commonly assumed to be equal to R_E, is still not well understood due to its high spatial variability. Studies designed to investigate the spatial variability of R_S depending on land use at a plot-scale in catchments are required. Plot-scale investigations are advisable to collect datasets depending on location with similar spatial features, through this, the influence of the variables (i.e. soil temperature, soil moisture, soil C and N content) on soil respiration can be analysed. Furthermore, the large uncertainty in R_E measurements and estimations due to lack of data collection, which requires thorough investigations on its key drivers. Understanding the spatial variability and key drivers of R_E using SRCs and EC time series analyses may lead to deeper understanding of the variables affecting the process of soil CO_2 efflux. This may also help the partitioning of NEE into GPP and R_E by accounting for essential variables in partitioning models.

Moreover, in drier regions, root water compensation and hydraulic redistribution are usually prevalent and are essential to be included in models for ecohydrological applications. The difference in model formulation of root water compensation calculation using (1) adjustment of distribution of root water uptake from different soil layers (*Jarvis*, 1989; *Simunek and Hopmans*, 2009; *Jarvis*, 2011) and (2) water potential gradients between soil and root xylem (*Molz*, 1981; *Mendel et al.*, 2002; *Siqueira et al.*, 2006; *Amenu and Kumar*, 2007; *Verma et al.*, 2014) should be effectively compared to know the quantitative effect to actual transpiration and soil respiration. Moreover, analysis of the effect of hydraulic redistribution on root water uptake and soil respiration will be significant to be considered in models. These root water uptake mechanisms affect soil water content, which regulates soil CO_2 production and efflux. Hydraulic redistribution might also have substantial impact on soil CO_2 efflux, which is important in carbon budget calculations. Thus, the effect of different formulations of root water uptake, considering root water compensation and hydraulic redistribution, on CO_2 efflux should be investigated.

Chapter 3

Research aims

The main aim of this research is to investigate the possible links between land use and soil carbon efflux. Two adjacent productive ephemeral landscapes, a *Eucalyptus globulus* (blue gum) plantation and a livestock-grazed pasture, are the study sites of this research project.

The specific research aims are:

1) To investigate soil carbon efflux in two managed and productive ephemeral catchments with different land use

A limited number of sites in Australia have investigated soil carbon efflux (R_S) in water-limited productive landscapes. Although past studies discovered that pasture usually have higher soil carbon efflux than the plantation, this aim focus on the comparison of the role of the spatial distribution of soil temperature, soil moisture, carbon and nitrogen content on the heterogeneity of R_S of a pasture and a plantation, which are both managed and parts of ephemeral catchments.

Even though the importance of R_S has been highlighted by past studies, the response of R_S to environmental factors is not yet generally understood. This aim investigates the role of environmental parameters that may lead to a better understanding of the variability and drivers of R_S. Knowing the drivers of R_S is necessary in improving methods for partitioning Net Ecosystem Exchange (NEE) into Gross Primary Productivity (GPP) and Ecosystem Respiration (R_E).

2) To develop a model of soil carbon efflux using different formulations of root water uptake

Since soil water content is one of the key variables regulating soil carbon efflux, root water uptake mechanisms might play an important role in defining CO_2 fluxes. Mechanistic models have been developed for CO_2 production and transport to adequately describe vertical gaseous diffusion and dispersion as a function of soil water content and temperature. Given the links between soil water and R_S, the inclusion of root water compensation and hydraulic redistribution in models of soil water dynamics will also affect the modelling of soil CO_2 dynamics. The focus of this aim is to investigate the effect that different formulations of root water uptake have on the modelling of soil moisture and R_S.

CHAPTER 4

CO_2 efflux in ephemeral productive landscapes

4.1 Site description

The adjacent study sites in Gatum, a blue gum plantation and a livestock-grazed pasture, lie around 300 km west of Melbourne in Southwestern Victoria (Figure 4.1). The climate of the sites is Mediterranean characterized by warm wet winters and hot dry summers. The average annual rainfall is 611 mm (1954-2012) based on the data from the Bureau of Meteorology station at Gatum (Station number 089043) and the average annual pan evaporation is around 1400 mm (*Adelana et al.*, 2015).

The pasture covers an area of 166 ha with an elevation ranging from 235 to 261 m according to the Australian Height Datum (AHD). The main plant species in the pasture are phalaris and subterranean clover. The site is used mainly for cattle and sheep grazing with some cropping of canola and wheat. There are lines of Eucalyptus trees (*E. camaldulensis* and *cladocalyx*) planted for windbreaks.

The plantation covers an area equivalent to 339 ha with an elevation ranging from 236 to 265 m (AHD) with McGill Creek as the primary drainage. Blue gum trees were planted in 2005 at a stand density of approximately 800 trees per ha (*Adelana et al.*, 2015). The recent count of blue gum trees is 727 trees per ha as of Dec. 2, 2015. Around 62% of the land is covered by blue gum, while the remaining area is covered with grass and access trails.

In the plantation and pasture, soil characterization was conducted and groundwater levels were monitored. Three holes were dug for each site for soil sampling to estimate the mean soil bulk density and mean soil porosity, with values equal to 1.5 g cm^{-3} and 0.10 to 0.15, respectively;

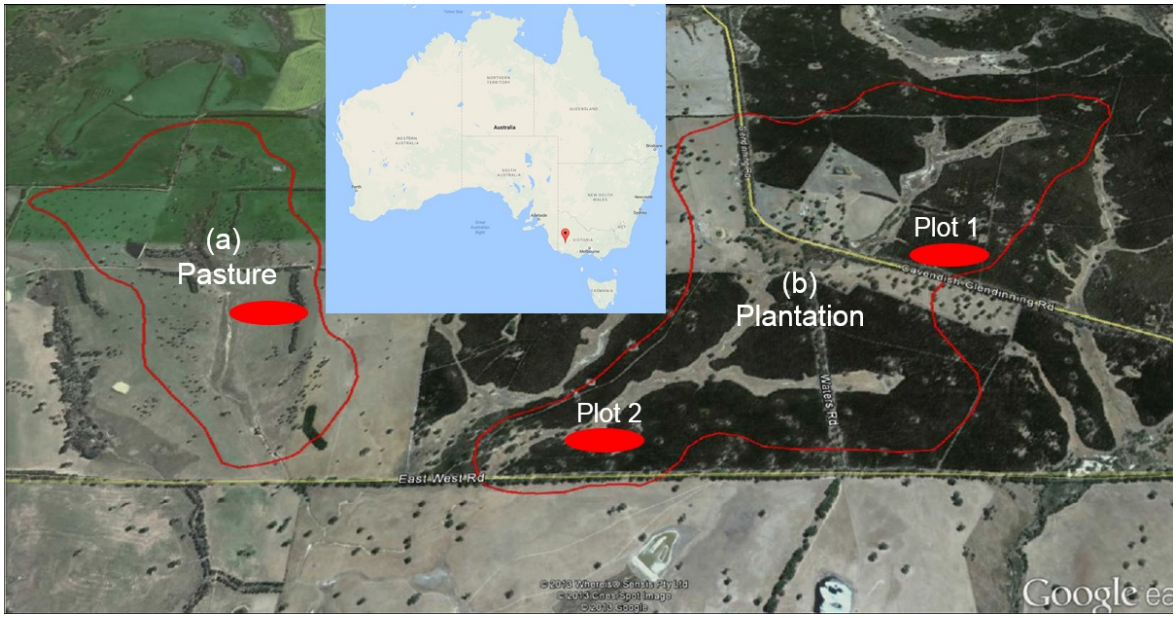

FIGURE 4.1. Study sites at Gatum, Victoria, Australia: (a) livestock-grazed pasture and (b) blue gum plantation from Google Earth *Adelana et al.* (2015).

these values were assumed to be representative for the overall soil. Groundwater levels are monitored (Schlumberger diver dataloggers which were installed in 2009) in 10 new bores in the plantation and 14 bores in the pasture (*Adelana et al.*, 2015). Infiltration rate ranges from $1.16{\cdot}10^{-3}$ to $3.47{\cdot}10^{-3}$ cm s^{-1}. The hydrogeology of the sites was discussed by *Adelana et al.* (2015).

4.2 Soil respiration chamber measurements

A limited number of sites in Australia have investigated soil carbon efflux (R_S) in water-limited productive landscapes. The focus of this chapter is to compare the role of the spatial distribution of soil temperature (T_S), soil moisture (θ), carbon (C), and nitrogen (N) content on the heterogeneity of R_S of the pasture and plantation. To determine the impact of land use on soil carbon flux in productive ephemeral catchments, soil respiration chamber measurements together with T_S and θ were conducted monthly across 2 years. Soil C and N content were measured quarterly, together with some monthly soil respiration chamber measurements.

4.2.1 Methodology

To investigate the key drivers of the spatial variability of soil respiration, measurements were conducted in both plantation and pasture using SRCs and statistical analyses were then per-

formed.

4.2.1.1 Data collection

The equipment used was an assembly of an environmental gas monitor for CO_2 (PP Systems, EGM-4), a closed-dynamic chamber (PP Systems, SRC-1), and a soil temperature probe (PP Systems, STP-1) to measure soil respiration and T_S (5 cm below the ground surface). The volumetric soil water content averaged over 5 cm was measured using the Hydraprobe Data Acquisition System (HDAS) (*Panciera and Walker*, 2006). The measurements of respiration, temperature, and moisture were taken at the same time near the same location. The equipment used for this study is shown in Figure 4.2.

FIGURE 4.2. Soil respiration, soil temperature, and soil moisture equipment used in both plantation and pasture.

The pasture has one plot near an established eddy-covariance (EC) system (Figure B.1) with SRC measurements and soil sampling points (for C and N) at interval of 5 m in space. The total number of measurement and soil sampling points for the pasture plot is 32 points, 8 points for each transect. On the other hand, 2 plots in the plantation were established for the soil respiration measurements. One is in a 1-ha plot (Figure B.2) with 38 points, 8 points for each

transect with a spacing of 2.5 m, and has biometric measurements (i.e. 30 dendrometers and 10 litterfall traps), and another one is located in the lower elevation near the McGill Creek (Figure B.3) with 28 points. The soil respiration measurements in the plantation had 3 different cases of measurements: SRC measured on mounds (below the canopy), trails (between tree canopies or inter-canopy), and open spaces (away from the canopies).

4.2.1.2 Statistical analysis

Statistical analyses were performed to investigate the difference in R_S magnitude for each case (pasture, mound, trail, and open space). The statistical tests conducted were Kolmogorov-Smirnov and Wilcoxon tests to evaluate the probability distribution and median of datasets in each case. Boxplot and scatter graphs were also plotted to compare the datasets and to identify possible relationships of T_S, θ, Soil Organic Carbon (SOC) and Total Nitrogen (TN) with R_S for each case depending on the land use (i.e. pasture or plantation). A non-linear regression analyses were also performed for each case to investigate the relationship of soil respiration with the collected independent variables.

4.2.2 Data presentation and analysis

Presented in this section are the monthly R_S, T_S, and θ measurements collected from June 2015 to December 2016 (Figure 4.3). The measured carbon (SOC) and nitrogen (TN) content of the soil, conducted quarterly (data collected in December 2015, March 2016, June 2016, and October 2016), are also described.

The pasture and the open space were observed to have the largest measured soil CO_2 efflux across all plots during late-autumn, winter, and early-spring (Figure 4.3). The missing data in October 2015, May and September 2016 were due to too much rainfall experienced in these months, making it impossible to collect soil respiration data. The probability distributions (Kolmogorov Smirnov test, $p>0.01$) and medians (Wilcoxon rank sum test, $p>0.01$) of R_S in the pasture and the open space were statistically similar during the mentioned seasons. T_S in the pasture and open space were similar during winter and spring and highest during late-spring, summer, and early-autumn. Soil moisture in the pasture and the open space were highest in the late-autumn, winter, and early-spring while relatively similar throughout the remaining periods.

On the other hand, mounds had the highest magnitude of R_S during late-spring, summer, and early-autumn due to canopy shading; this resulted in a relatively higher soil moisture and a relatively lower T_S in the mound during late-spring, summer, and early-autumn compared to other cases (pasture, trail, and open space). The trail R_S measurements had lower R_S than that of the mound, except for the August 2015 dataset. Moreover, the soil C and N content of

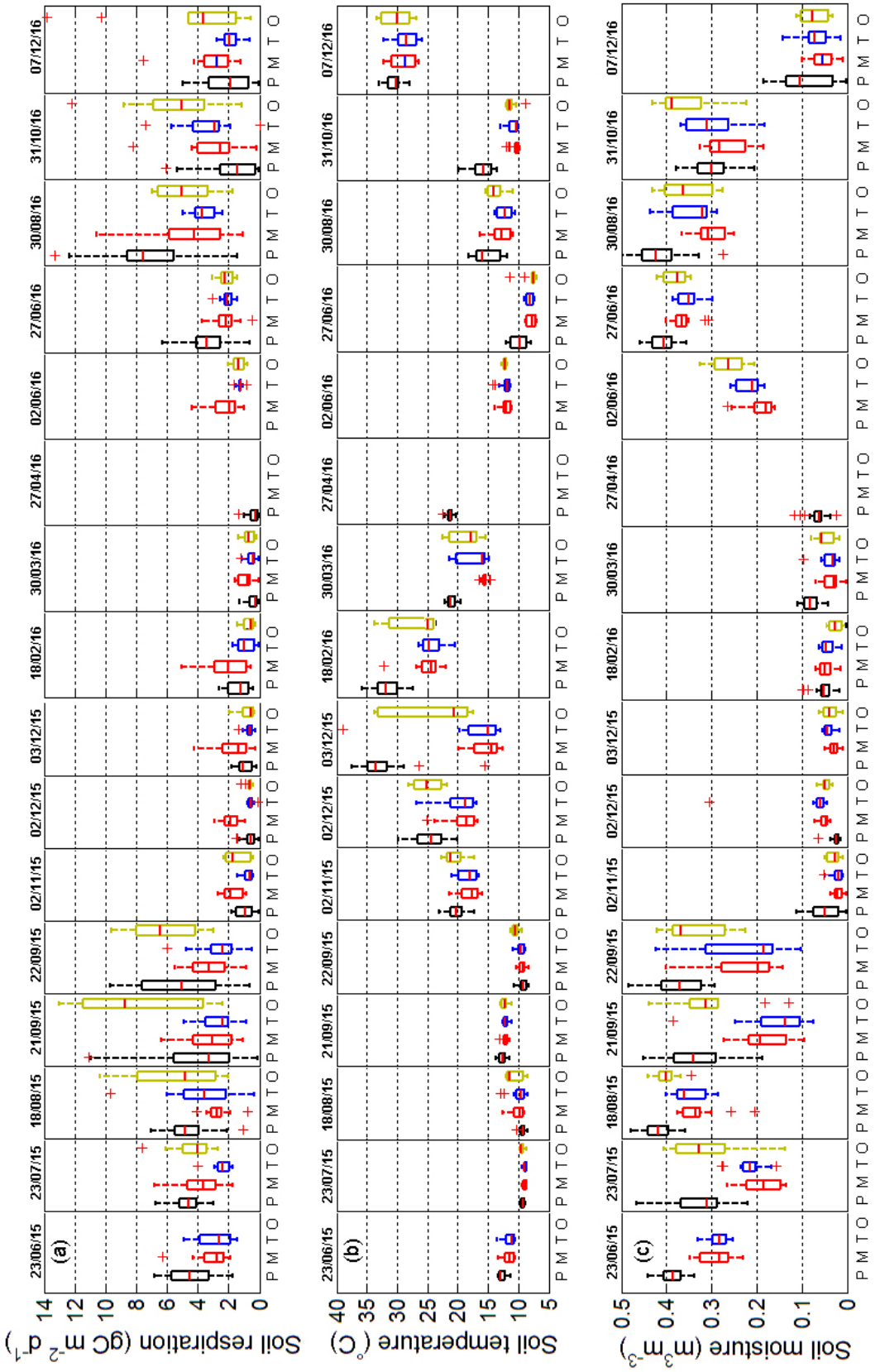

FIGURE 4.3. Boxplots of (a) soil respiration, (b) soil temperature, and (c) soil moisture in different cases (P=pasture; M=mound; T=trail; O=open space).

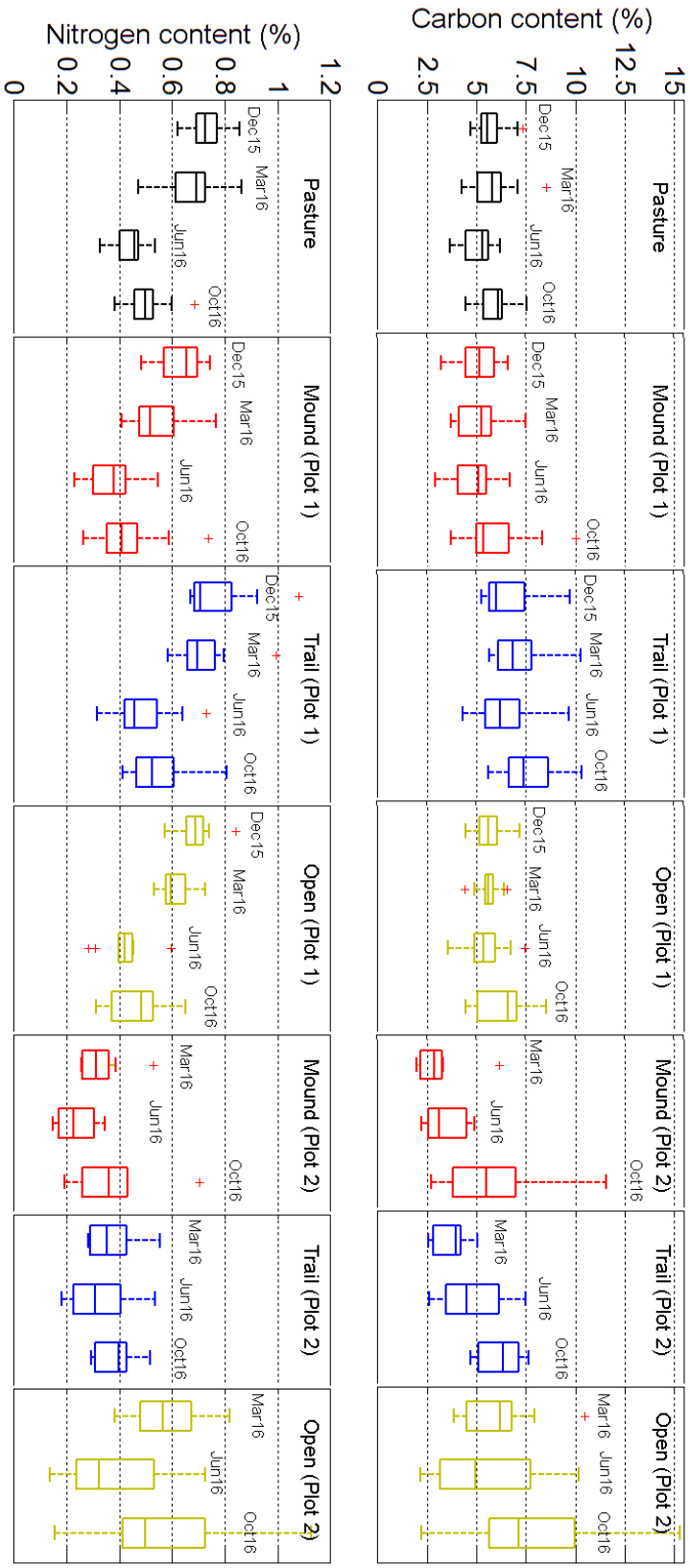

FIGURE 4.4. Boxplots of (a) soil carbon and (b) soil nitrogen content.

the trail was relatively higher compared to the other cases (Figure 4.4).

The relationship between R_S, T_S, and θ is shown using scatter plots. There was an inverse relationship between R_S and T_S (Figure 4.5). R_S was highest at T_S around 12°C. R_S plummeted for T_S larger than 12°C and increased again around 30°C. Furthermore, the relationship between R_S and T_S were different from the relationship presented in temperate measurements (*Subke and Bahn*, 2010) where T_S is directly proportional to R_S. R_S and T_S relationship in the mound is more scattered; this may be due to microtopography effect, root water compensation of plants, or shading. On the other hand, there was a directly proportional relationship between R_S and θ (Figure 4.6).

In Mediterranean climates, where high soil moisture and temperatures are not in phase, R_S is mostly driven by soil moisture. In the pasture, mound, and open space, we can observe that there are instances when R_S and T_S were high having a direct proportionality, due to an acceptable value of θ content. However, in the pasture, there were instances when θ and T_S were high but the R_S was low; this might be due to patchy vegetation in the pasture.

The quarterly soil C and N content, the C content in the pasture and the plantation plot 1 was similar in all the seasons (Figure 4.4). The C content collected in October 2016 in the plantation plot 2 increased. The N content of all the cases (pasture, mound, trail, and open space measurements) decreased during the June and October 2016 measurements, with an exception of the measurements conducted on the trail in the plot 2 of the plantation. Furthermore, the C and N content of the trail in the plantation plot 1 had a relatively higher value compared to other treatments. The relationship between R_S and C-to-N ratio is presented in Figure 4.7. There was an inverse relationship between R_S and C-to-N ratio, which is comparable to the relationship between R_S and T_S.

A regression model was developed to explain the relative influences of T_S and θ on R_S given by

$$R_S = c_1 \left(\frac{\exp(c_2\theta)}{\exp(c_3 T_S)} \right), \tag{4.1}$$

where c_1, c_2, and c_3 are the constants depending on the location where R_S was taken. The models are presented in Table 4.1. An exponential relationship of R_S, T_S, and θ gave acceptable R^2 and RMSE values. With the negligence of outliers, acceptable R^2 were obtained ranging from 0.50 to 0.77. However, the models tended to be inaccurate for θ greater than 0.35. Furthermore, the relationships of soil respiration with C and N soil content were scattered that resulted to a low R^2 for all cases (0.10 to 0.25), thus, were not presented.

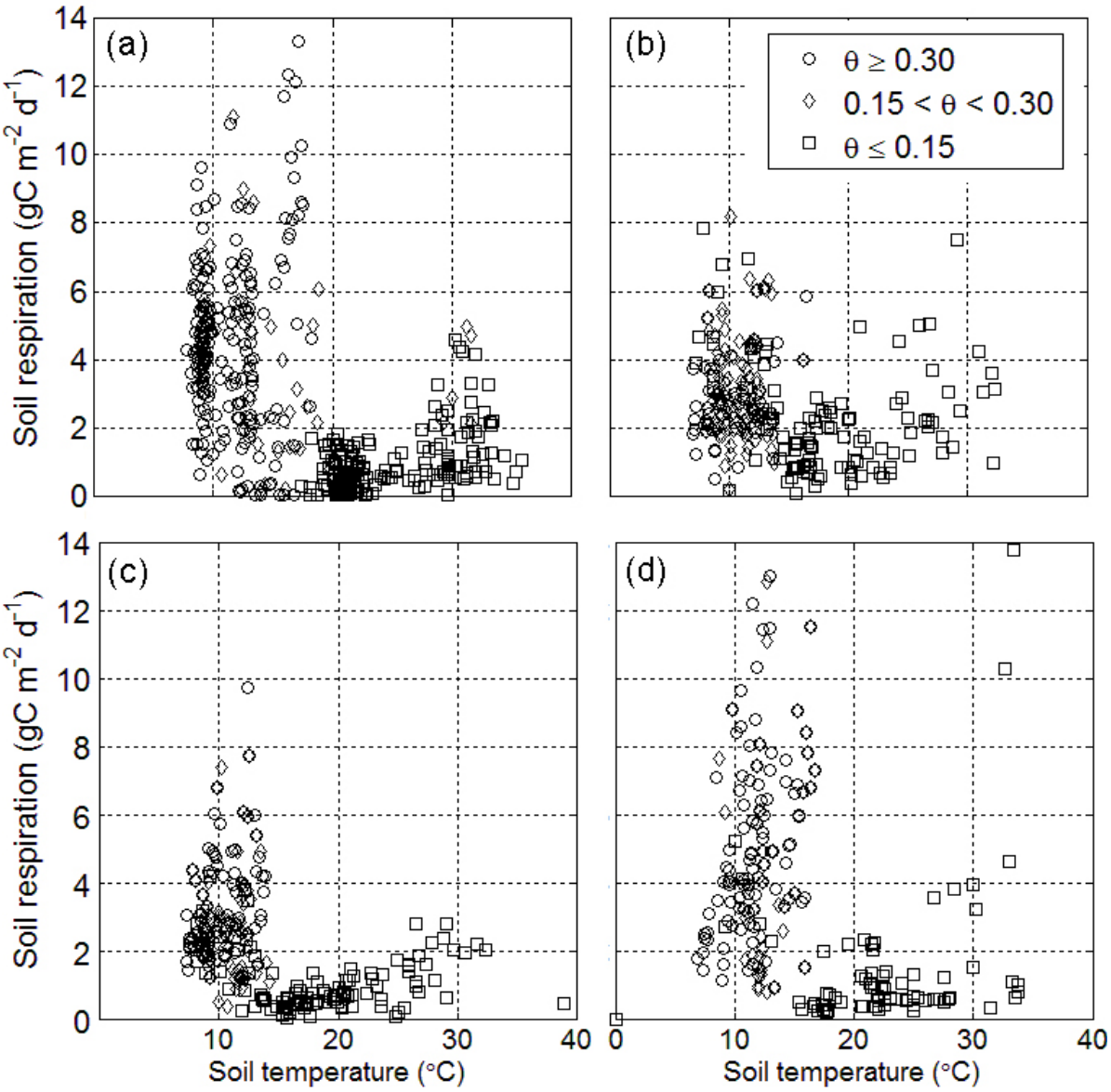

FIGURE 4.5. Scatter plots between soil respiration and soil temperature in (a) pasture, (b) mound, (c) trail, and (d) open space.

Based on the R^2 of the regressed model, the mound had a more scattered dataset compared to the other cases (R^2=0.50). This is in accordance with the findings of *Almagro et al.* (2009), where the R_S under the canopy had more scattered datasets. The values R^2 of were lower ranging from 0.39 to 0.55 and the values of RMSE were higher ranging from 2.99 to 18.32 compared to other cases (i.e. trail and open space). From the model presented, R_S had an acceptable fit when T_S and θ are confoundedly considered using exponential relationships (*Almagro et al.*, 2009; *Jassal et al.*, 2008).

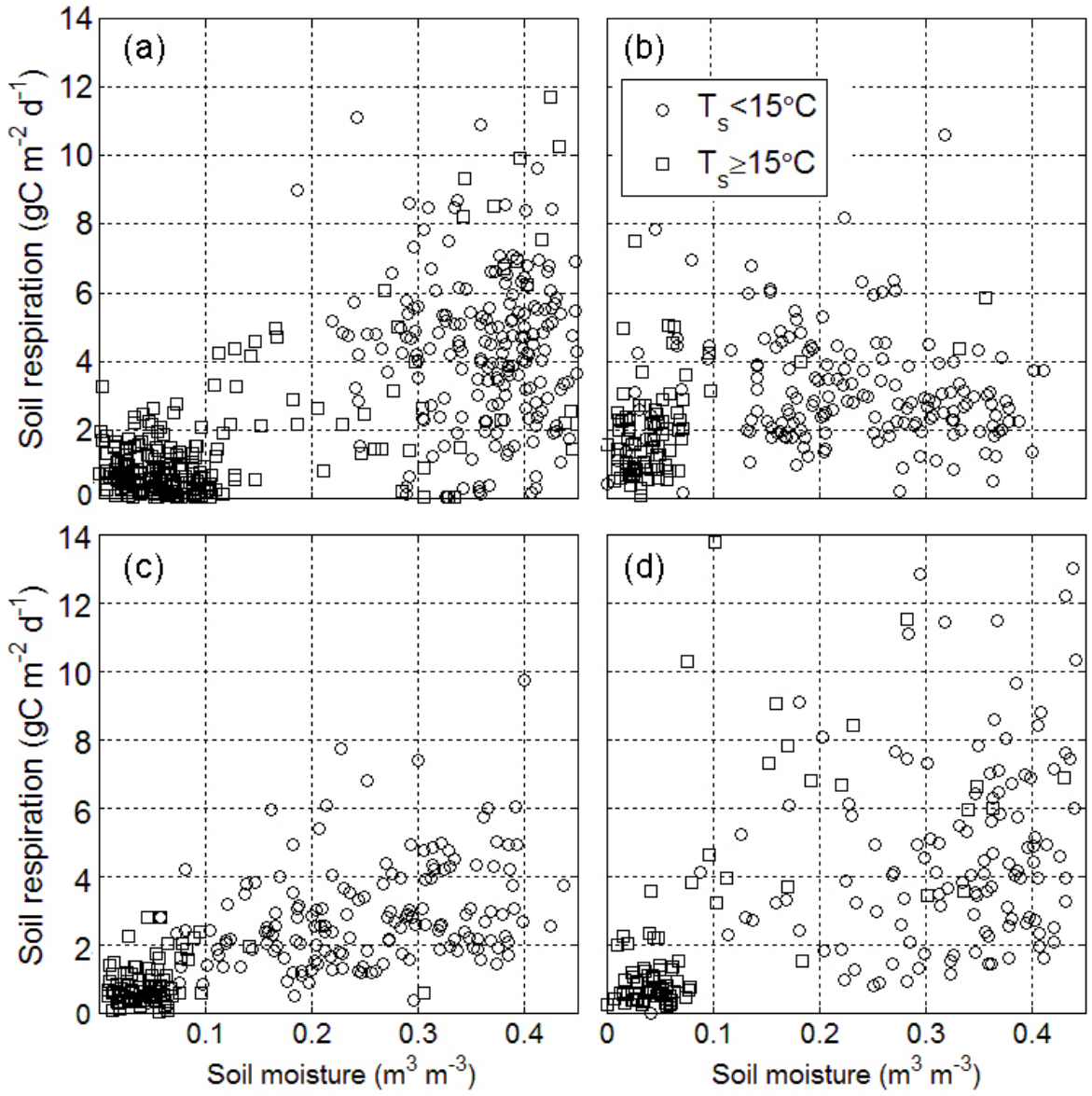

FIGURE 4.6. Scatter plots between soil respiration and soil moisture in (a) pasture, (b) mound, (c) trail, and (d) open space.

4.2.3 Conclusions

The variability of R_S was investigated considering land use (i.e. livestock-grazed pasture and blue gum plantation) using SRC measurements. The measurements were taken in four different conditions: pasture, mounds near trees, trail between trees, and open areas in the plantation.

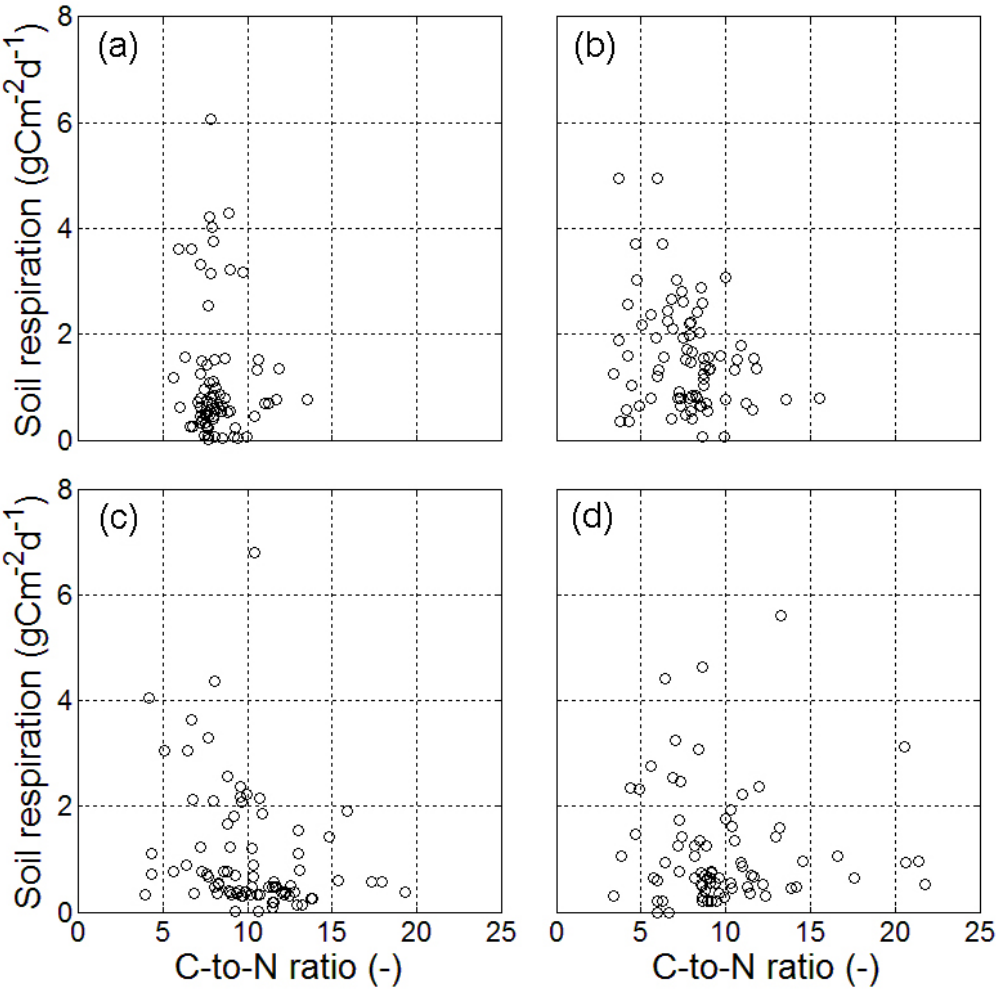

FIGURE 4.7. Scatter plots between soil respiration and C-N ratio in (a) pasture, (b) mound, (c) trail, and (d) open space.

Table 4.1: Model fitting for soil respiration using soil temperature and soil moisture

Location	c_1	c_2	c_3	R^2	RMSE	n
Pasture	0.5682 ± 0.1741	4.993 ± 0.532	-0.01616 ± 0.01132	0.65	0.539	457
Mound	1.401 ± 0.4215	3.346 ± 0.685	-0.007802 ± 0.01375	0.50	0.932	183
Trail	0.5682 ± 0.2119	4.83 ± 0.703	-0.01524 ± 0.01765	0.64	0.826	233
Open	0.3086 ± 0.1812	6.644 ± 0.987	-0.01524 ± 0.02258	0.77	1.321	132

The pasture emitted more C to the atmosphere specifically during late-autumn, winter, and early-spring when the soil moisture was higher. On the other hand, the plantation had relatively higher R_S during drier periods (late-spring, summer, and early-autumn); however, the magnitude of R_S during wetter periods in the pasture is a magnitude higher than that of

drier periods in the plantation. Thus, the pasture had higher R_S or soil C efflux compared to the R_S of the plantation. The spatial variability was mainly driven by the soil moisture distribution. For instance, the pasture and open space had higher R_S during the growing seasons since they had higher soil moisture content. This is also true during the summer when the mound and the trail had relatively higher R_S. Furthermore, the relationship between R_S and T_S were different from the relationship presented in temperate measurements (*Subke and Bahn*, 2010) where T_S is directly proportional to R_S. In the field observations presented, the opposite relationship were obtained because the sites were in a water-limited ecosystems. The regressed model developed was found to have an acceptable fit when T_S and θ are confoundedly considered using exponential relationships. The model estimates R_S in the pasture, trail, and open space more accurately than the mound. The mound has lower accuracy de to a more scattered dataset used for the model regression compared to the other cases. However, this was also observed in the paper of *Almagro et al.* (2009).

4.3 CO_2 fluxes in the pasture

An EC system in the pasture was installed together with an ancillary weather station. This will investigate the role of environmental parameters (i.e. net radiation (F_n), soil heat flux (F_g), soil temperature (T_S), soil moisture (θ), specific humidity (q), vapor pressure deficit (VPD), and air temperature (T_a)) to fluxes (i,e, net ecosystem exchange (NEE), evapotranspiration (ET), sensible heat flux (F_H), and ecosystem respiration (R_E)) based on EC measurements and link the observations with R_S for a better estimation and NEE partitioning.

4.3.1 Methodology

The methods performed to collect and analyze the EC data collected from the pasture are presented in this section. Data collection, quality control measures, C flux partitioning, and Granger causality test will be discussed herein.

4.3.1.1 Data collection

Carbon, latent, and sensible heat fluxes were measured using an EC system installed near the soil respiration measurement plot of the pasture (Figure 4.8). EC data were collected from February 9, 2015 to November 2, 2015 with a sampling frequency of 10 Hz by a closed-path eddy covariance system (IRGA EC155, CPEC200 by Campbell Scientific). Air was sampled through a polyethylene tube (2.7 mm inner diameter with a length of 58.4 cm) with a flux rate of 7 L min^{-1} provided by an external pump. The separation between the sonic anemometer and the IRGA was 15.60 cm. Wind velocity was measured by a 3-D sonic anemometer (CSAT-3,

Campbell Scientific) at a height of 2.90 m. From February 19, 2016 to December 7, 2016, EC data were collected by an open-path eddy covariance system (IRGASON, Campbel Scientific).

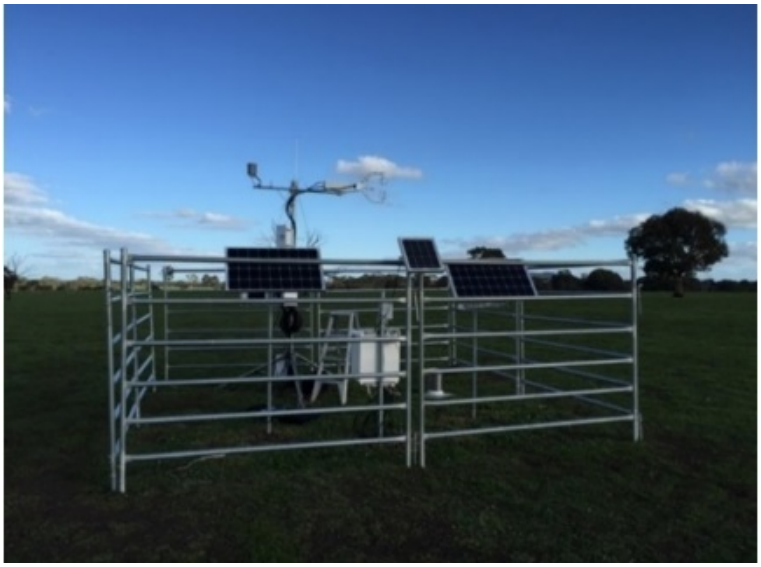

FIGURE 4.8. Eddy covariance system in the Gatum pasture site, Southwestern Victoria, Australia.

4.3.1.2 Data quality control and C flux partitioning

The collected EC data from February 2015 to December 2016 in the pasture were processed using EddyPro (*Biosciences*, 2012) and OzFluxQC (*Cleverly and Isaac*, 2015) software to apply some filters and corrections. Using the 10 Hz data, EddyPro applied axis rotation for tilt correction and time lag compensation. Compensation for density fluctuation was applied only for data collected from February 2016 to December 2016 using IRGASON since this period used an open-path eddy-covariance system dependent on pressure and temperature changes. Statistical tests for raw data screening were performed; these are the application of spike or count removal, amplitude resolution, drop-outs, absolute limits skewness and kurtosis. Spectral analysis and corrections were also conducted; these are spectral filter and analytic correction of high-pass and low-pass filters. Then, the Reichstein method (*Reichstein et al.*, 2005) was used to partition the NEE collected from February 2015 to December 2016.

OzFluxQC has 6 levels of quality control including gapfilling and partitioning. Level 1 is for importing the data, Level 2 is for variable filtering, Level 3 is for applying corrections and merging data, Level 4 is for gap-filling using climate data, Level 5 is for gap-filling using Artificial Neural Network (ANN), and Level 6 is for C flux partitioning. All these steps were

performed for the EC data collected from February 2015 to December 2016.

The gap-filling of Reichstein method (*Reichstein et al.*, 2005) includes an algorithm that considers three different conditions. First, only the data of direct interest are missing and all meteorological data are available. Second, the data of direct interest are missing, together with T_a or VPD, but F_n is available. Third, the data of direct interest are missing, together with T_a or VPD, and radiation is also missing. In the first condition, the missing data is replaced by the average value under similar meteorological conditions withinm a time-window of 7 days and increased to 14 days, if no similar meteorological conditions are observable. For the second condition, same approach is taken, however, similar meteorological conditions can be defined using radiation and window size remains 7days. In the third condition, the missing data is replaced by the average value at the same time of the day using mean diurnal course. The window size starts from 0.5 day comparable to a linear interpolation from available data at adjacent hours. The window size is then increased if after the preceding step is unsuccesful. The method, window size, missing data value, and standard deviation are recorded to estimate uncertainties.

OzFlux uses a two stages to perform gap-filling. First, OzFLux fill gaps in the meteorological data using alternative data from Bureau of Meteorology Automatic Weather Station (AWS), Bureau of Meteorology Numerical Weather Prediction (NWP), and the Australian Community CLimate and Earth-System Simulator (ACCESS) weather model. Second, a neural network is used to perform gap-filling in the flux measurements. The neural network is first trained on the "gappy" drivers (meteorological data) and target (flux), then, the missing flux data are predicted. The drivers used were θ, F_n, F_g, q, T_a and T_S.

The flux partitioning of Reichstein method (*Reichstein et al.*, 2005) only uses the original data. All original data flagged with a quality indicator greater than 1 (with non-turbulent conditions) are neglected. Data collected during nigh-time was selected assumed to be below the global radiation threshold of 20 W m^2, cross-checked against sunset and sunrise data, and defined as R_E. Afterward, the data set is split into consecutive periods with constant day length. For each period, data points are checked if there are more than six, and whether T_S is more than 5°C to have reasonable regressions of R_E and T_S. For the period where criteria are met, the Lloyd-Taylor equation (*Lloyd and Taylor*, 1994) is used given by

$$R_E(T) = R_{E,ref} e^{E_o\left(\frac{1}{T_{ref}-T_o}-\frac{1}{T_S-T_o}\right)}. \tag{4.2}$$

where T_o is a constant equal to -46.02°C, E_o is the varying activation energy, T_{ref} is the reference temperature set to 10°C, and $R_{E,ref}$ is the soil respiration at reference temperature.

Equation 4.2 is fitted the scatter of R_E versus T_S.

Ozflux estimates R_E from nocturnal NEE after unreliable low-turbulent data are removed, using the Change Point Detection (CPD) Method (*Cleverly and Isaac*, 2015). Then, R_E is predicted using a neural network, wit T_S and θ as drivers.

4.3.1.3 Wavelet analysis

Wavelet principal component analysis (PCA), wavelet coherence, and wavelet multiple linear regression were performed as part of the OzFLuxQC protocol. Wavelet PCA were conducted for the EC data from February 2015 to December 2016. The data were divided into two groups, the fluxes and the drivers. The fluxes were NEE, ET, and F_H, while the possible drivers were F_n, F_g, T_S, θ, q, VPD, and T_a. Wavelet PCA was performed to reveal the internal structure of the data in a procedure that best explains its variance. The wavelet coherence analysis was then conducted to investigate the period of influence of possible drivers to the fluxes. Finally, the wavelet multiple linear regression was performed to have an idea of the relationship affecting the fluxes.

4.3.1.4 Granger causality test

Since NEE is related to GPP and R_E (Equation 2.1), the key drivers controlling the fluxes in the wavelet analysis can be tested for time series causality using Granger test. The Granger causality test addresses the questions of whether the time series of x causes that of y, how much of the current y can be explained by the past values of y, and if the addition of lagged values of x can improve the connection. This has been used in many applications in economics implying that correlation does not necessarily imply causation. Thus, y is said to be Granger-caused by x if x helps in explaining and predicting y. It is important to take note that the meaning of the statement "x Granger causes y" does not imply that y is the effect of x; the Granger causality test measures precedence and information content, but does not itself indicate causality. The model for the Granger causality test is given by

$$y_t = \alpha_0 + \alpha_1 y_{t-1} + ... + \alpha_l y_{t-l} + \beta_1 x_{t-1} + ... + \beta_l x_{-l} + \epsilon_t, \tag{4.3}$$

and

$$x_t = \alpha_0 + \alpha_1 x_{t-1} + ... + \alpha_l x_{t-l} + \beta_1 y_{t-1} + ... + \beta_l y_{-l} + \upsilon_t, \tag{4.4}$$

where, l is the lag length that corresponds to the time over which the variable could predict the other, α and β are coefficients, ϵ and υ are the residuals. The null hypothesis is that x does not Granger cause y in the first regression model (Equation 4.3). The second regression model (Equation 4.4) has a null hypothesis of y does not Granger cause x.

4.3.2 Data presentation and analysis

In the EC data collected in 2015, the carbon assimilation and sequestration of plants started around early July (DOY 190); that was due to an increase in precipitation (Figure 4.9). The carbon sequestered during September and October was larger compared to the other period. In the EC data collected in 2016, the carbon assimilation and sequestration of plants started around late-April (DOY 121), when precipitation increased (Figure 4.10). Year 2016 had a prolonged carbon sequestration from May to December. This might be due to more rainfall in the Year 2016.

The monthly NEE in April showed an early carbon sink in 2016 for the pasture (Figure C.1). Furthermore, carbon sequestration was relatively higher in 2016 from April to July. In 2015, carbon sequestraion was higher than 2016 from August until October; there was a sharp decrease in carbon sequestration in November (Figure C.1). Photosynthesis (GPP) were relatively higher in 2016 from April to June (Figure C.2). Photosynthesis in July was similar for both years. However, in 2015, GPP was higher than 2016 from August until October; there was a similar sharp decrease in carbon sequestration in November.

Evapotranspiration in February, March, and May was similar in both years (Figure C.3). The magnitude of evapotranspiration was sustained in 2016 from April to December. On a different note, sensible heat flux in 2015 from February to October was relatively higher than 2016, except in September (Figure C.4).

4.3.3 CO_2 efflux partitioning

The OzFluxQC and REddyProc methods seemed to have similar magnitude in both years (Figure 4.11). Also, the collected R_S in 2015 was in accordance with the partitioned R_E. In 2016, the deviation of R_E using the methods was due to gap-filling during November where the EC system stopped collecting data due to a technical issue. In August 2016, the collected R_S was in accordance with the REddyProc partitioning method. However, in November 2016, OzFluxQC estimated the R_E better than REddyProc; REddyProc overestimated the R_E. OzFluxQC and REddyProc had around 300 g C m^{-2} difference in cumulative R_E throughout the data collection period due the difference in gap-filling methods performed for the data gaps in May and August 2017 due to technical issues. In the OzFluxQC partitioning method, the monthly R_E in 2015 was mostly consistent higher than that of 2016, with the exception of March (Figure C.5).

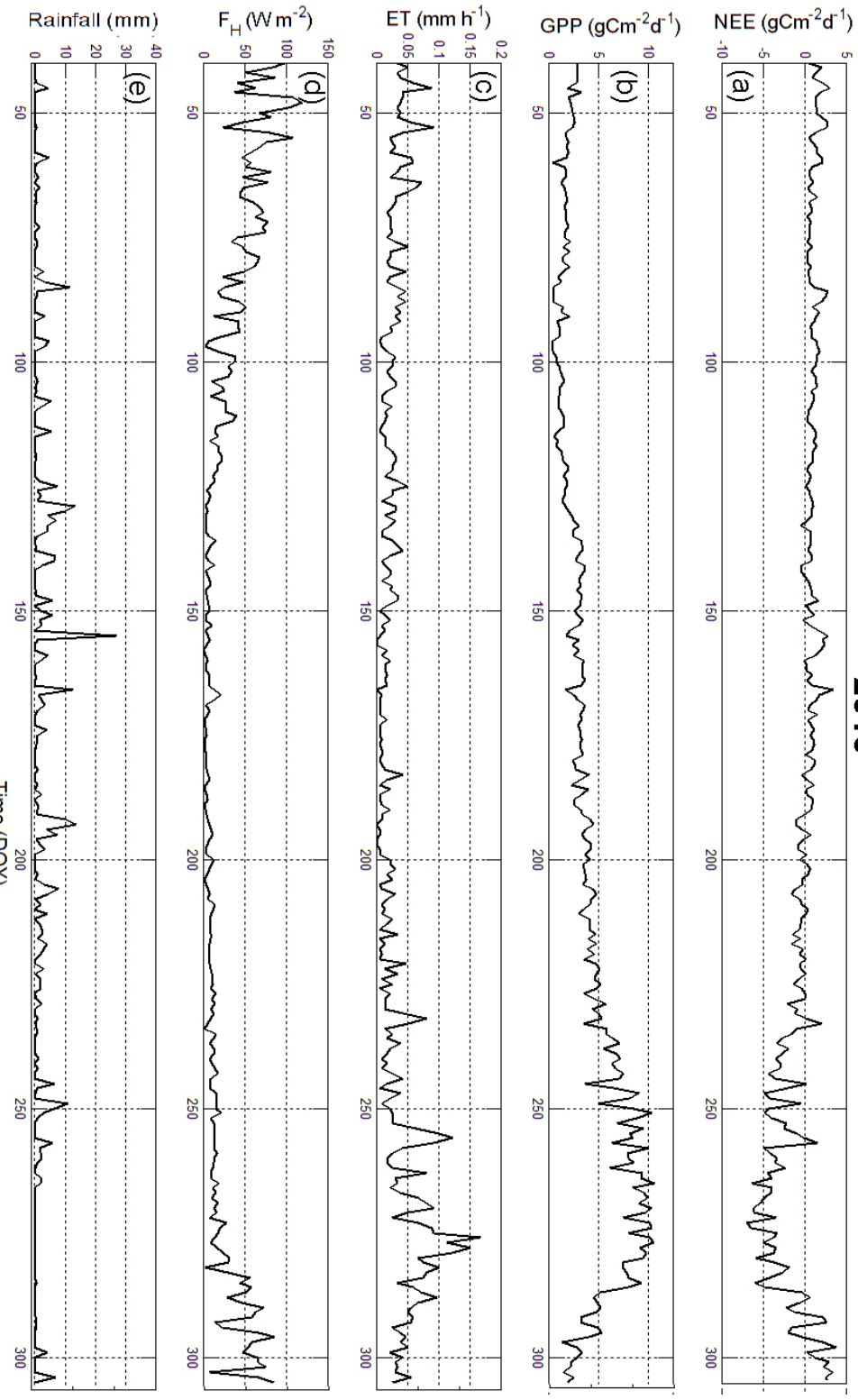

FIGURE 4.9. (a) Net Ecosystem Exchange, (b) Gross Primary Productivity, (c) Evapotranspiration, and (c) Sensible heat fluxes collected using eddy-covariance system for the year 2015.

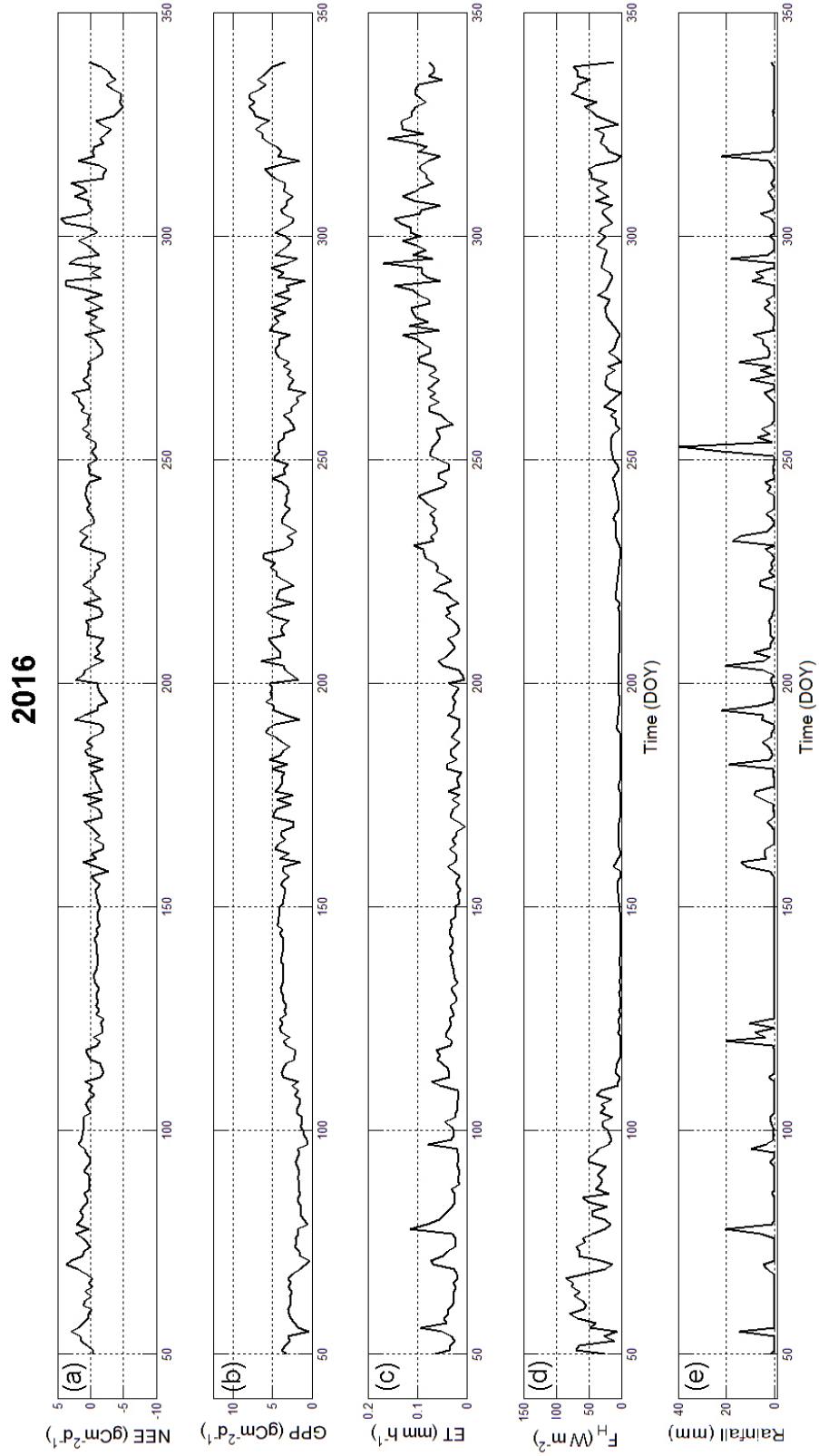

FIGURE 4.10. (a) Net Ecosystem Exchange, (b) Gross Primary Productivity, (c) Evapotranspiration, and (c) Sensible heat fluxes collected using eddy-covariance system for the year 2016.

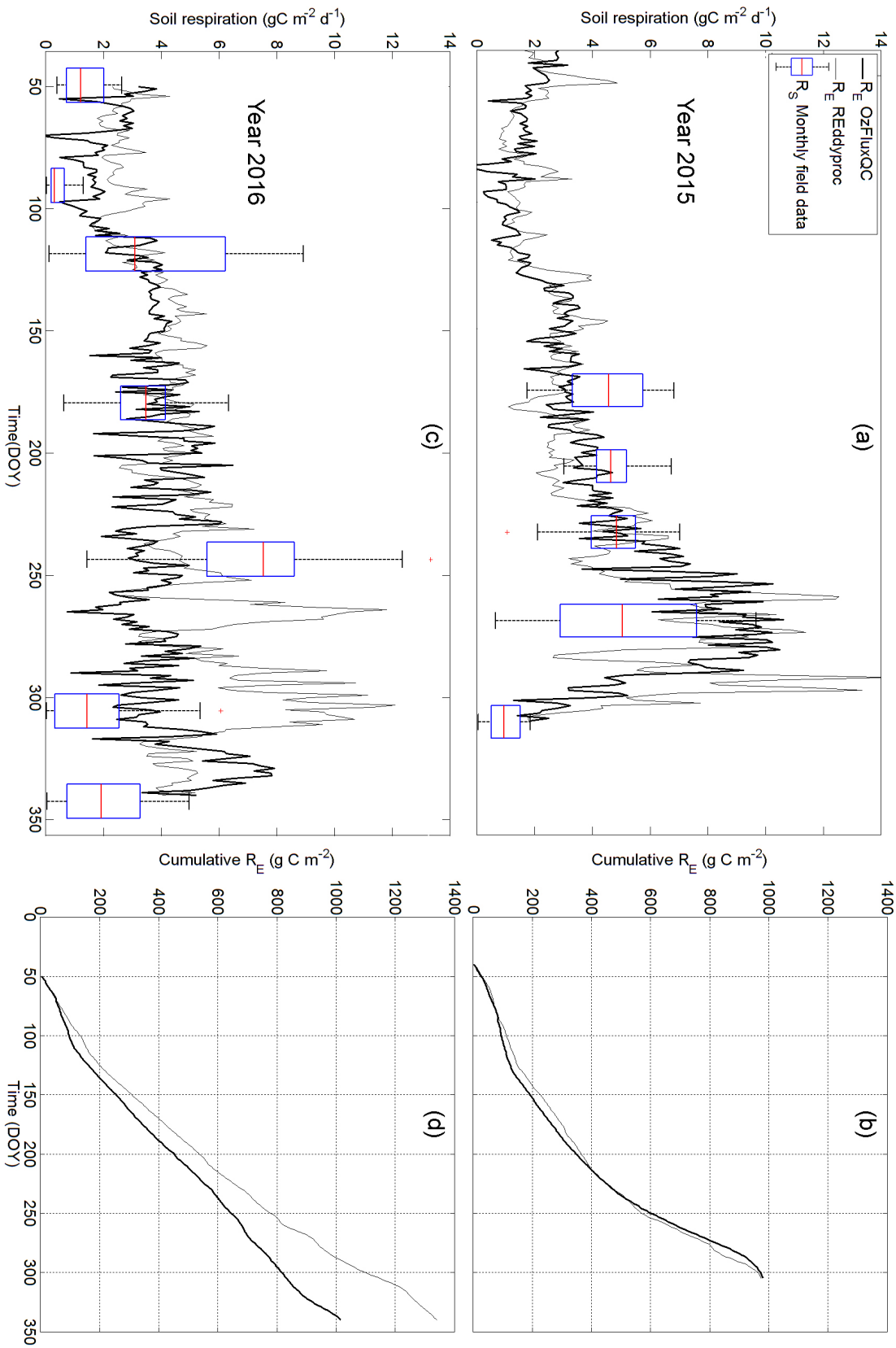

FIGURE 4.11. Partitioned ecosystem respiration (R_E) using OzFluxQC and REddyProc for the year (a) 2015 and (c) 2016. Cumulative ecosystem respiration for the year (b) 2015 and (d) 2016.

4.3.4 Wavelet analysis

Wavelet analysis was conducted for the fluxes NEE, ET, and F_H, together with the drivers F_n, F_g, T_S, θ, q, VPD, and T_a. The PCA for the fluxes and drivers for the year 2015 and 2016 is given by Table 4.2.

The results of the wavelet PCA analysis for the 2015 data (Table 4.2) suggested that the variability of the PCA fluxes in the pasture was due to F_H (0.9498) and ET (0.2972). Any parameters that affected F_H and ET had equally affected NEE because NEE (-0.0973) did not introduce any variability into the dataset that is not already explained by F_H and ET. Furthermore, the fluxes were driven by θ (-0.6617) and T_S (0.5476) for the first PCA coefficient of drivers (1), and were driven by F_n (-6.331) and F_g (-0.5697) for the second PCA coefficient of drivers (2).

On the other hand, the results of the wavelet PCA analysis for the 2016 data suggested that the variability of the PCA fluxes in the pasture was due to F_H (0.7284), ET (0.2971), and NEE (-0.4514). Furthermore, the fluxes were driven by F_n (-0.9929) for the first PCA coefficient of drivers (1), and were driven by F_g (0.9216), T_a (0.2308), and T_S (0.2258) for the second PCA coefficient of drivers (2).

Table 4.2: Wavelet principal component analysis (PCA) for the year 2015 and 2016 with fluxes, and first PCA coefficient of drivers (1) and second PCA coefficient of drivers (2).

Fluxes	**2015**	**2016**	**Drivers**	**2015 (1)**	**2015 (2)**	**2016 (1)**	**2016 (2)**
NEE	-0.0973	-0.4514	F_n	0.3716	-0.6331	-0.9929	-0.0795
ET	0.2972	0.5155	T_a	0.2308	0.0129	-0.0895	0.2308
F_H	0.9498	0.7284	θ	-0.6617	-0.2904	-0.0003	0.0011
			VPD	0.1583	-0.0963	-0.058	0.1933
			q	-0.0715	0.2503	-0.0120	-0.0521
			T_S	0.5476	0.3438	-0.0073	0.2258
			F_g	0.2019	-0.5697	-0.050	0.9216

After performing the wavelet PCA analysis, the wavelet coherence analysis was performed to investigate the temporal effect of the drivers to the fluxes. There were 4 combinations for the wavelet coherence analysis, these are the analysis between (i) fluxes and primary drivers of 2015, (ii) fluxes and secondary drivers of 2015, (iii) fluxes and primary drivers of 2016, and (iv) fluxes and secondary drivers of 2016. The wavelet coherence suggested that the drivers affected the fluxes from 16 to 64 hours (Figure 4.12). The other wavelet coherence results for the year 2015 and 2016 are shown in Figures C.6 to C.8, having the same temporal effect of drivers to the fluxes equivalent to 16 to 64 hours.

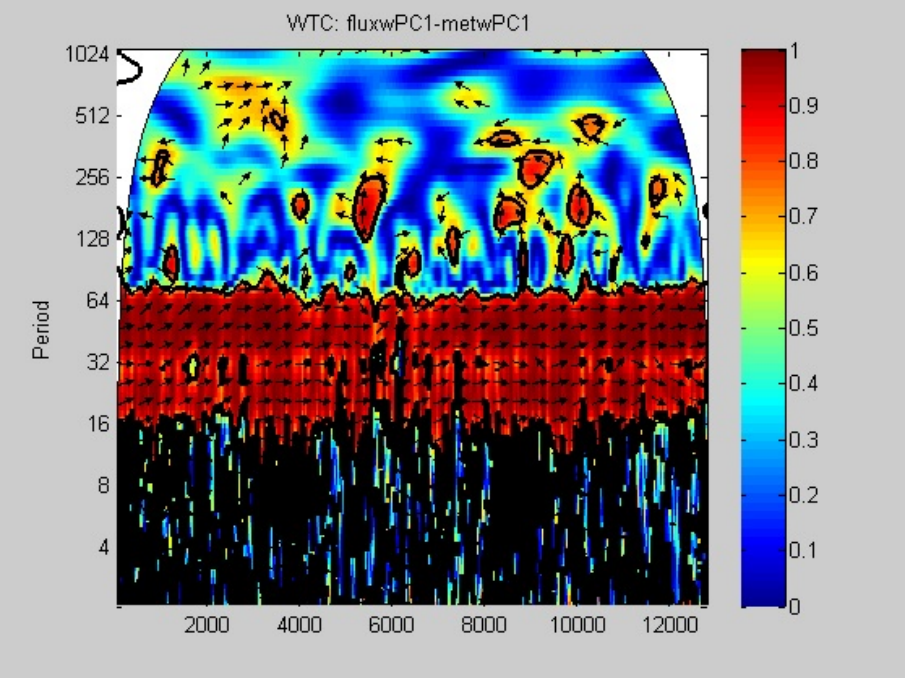

FIGURE 4.12. Wavelet coherence between fluxes and the first PCA term of the drivers (1) of the 2015 data.

The results of the scaled wavelet multiple linear regression analysis for the 2015 data (Table 4.3) suggested that the variability of the fluxes (NEE, ET, and F_H) in the pasture was mainly due to F_n and F_g. The larger absolute value of the coefficient of secondary drivers in comparison with the primary drivers suggested that variation in the fluxes were driven by energy fluxes (F_n and F_g) with indirect effects of θ and T_S.

Table 4.3: Wavelet multiple linear regression from February 2015 to November 2015.

	Coefficient	Standard Error	t-Stat	p-Value
fluxes	0.01172	0.00163	7.205	$6.14{\cdot}10^{-13}$
drivers (primary)	0.08637	0.00399	21.653	$5.37{\cdot}10^{-102}$
drivers (secondary)	-0.46016	0.00705	-65.284	≈ 0

On the other hand, the results of the wavelet multiple linear regression analysis for the 2016 data (Table 4.4) suggested that the variability of the fluxes (NEE, ET, and F_H) in the pasture was due to F_n with indirect effects of F_g, T_a, and T_S. It is observable that in 2015, the influence of the primary drivers are weaker and has an inverse relationship with the fluxes. On the other hand, in 2016, the primary driver is stronger and has a direct relationship with the fluxes.

The change in influence of the primary drivers was due to the lower precipitation in 2015, amounting to 370.2 mm d^{-1}, than that of 2016, around 632.6 mm d^{-1}. In 2015, the catchment was dry and due to lack of water. Excessive F_n and F_g strongly affected the plant water stress and microbial inactivity, which was led to decreased ET and R_E affecting NEE. On the other hand, in 2016, there was a more sufficient water reserve. Due to this, F_n controls the photosynthesis and the energy availability controls the rate of photosynthesis affecting the fluxes.

Table 4.4: Wavelet multiple linear regression from February 2016 to December 2016.

	Coefficient	Standard Error	t-Stat	p-Value
fluxes	0.00450	0.001181	3.80716	0.00014
drivers (primary)	0.91981	0.00578	-159.218	≈0
drivers (secondary)	-0.41198	0.00402	-102.475	≈0

From the wavelet analysis (wavelet PCA, coherence, and multiple linear regression) undertaken, the key drivers for the fluxes (NEE, ET, and F_H) were F_n, F_g, θ, T_a, and T_S during the year 2015 (February 9 to November 2) and the year 2016 (February 19 to December 6).

4.3.5 Granger causality test

The Granger causality test was performed to test the causation between the key drivers of fluxes based on the wavelet analysis and the R_E partitioned using both OzFluxQC (ANN) and REddyProc/Reichstein (*Reichstein et al.*, 2005) methods. From equation 2.1, NEE depends on GPP and R_S. Thus, the results of the investigation of key drivers of the fluxes (NEE, ET, and F_H) may also have significant control on GPP and R_E. The causation of the key drivers (F_n, F_g, θ, T_a) of the fluxes to R_E was tested using Granger causality and the results are shown in Table 4.5 for OzFluxQC method and Table 4.5 for REddyProc/Reichstein (*Reichstein et al.*, 2005) method. ET, F_H, and precipitation (*prec.*) were also tested against R_E. However, T_S was neglected to reduce the bias of the analysis since it was used as a variable for the NEE partitioning.

The Granger causality test has a confidence level of 95% with 100 possible lags tested. The F-value is compared to the critical value, if F-value is greater than critical value, the null hypothesis that the variable does not Granger cause R_E was rejected. In 2015, the variables ET, F_n, F_g, T_a, and θ Granger cause R_E. On the other hand, in 2016, the drivers T_a and θ Granger cause R_E.

The partitioned R_E using REddyProc/Reichstein (*Reichstein et al.*, 2005) method for the year 2015 and 2016 was tested using Granger causality with the variables ET, F_H, F_n, F_g, θ, T_a, and *prec.* (Table 4.6). The confidence level and lags were the same with that of the previous Granger

Table 4.5: Granger causality test between R_E partitioned using OzFluxQC (ANN) method and key drivers.

	2015	2015	2016	2016
Variables	F-test	critical value	F-test	critical value
ET	6.27	2.64	2.75	3.87
F_H	0.27	3.88	0.84	3.87
F_n	6.21	2.64	3.00	3.87
T_a	15.94	3.03	5.67	3.03
θ	6.10	3.88	11.13	3.87
F_g	5.51	2.41	1.22	3.87
prec.	0.25	3.88	0.59	3.87

causality analysis. The F-value is compared to the critical value, if F-value is greater than critical value, the null hypothesis that the variable does not Granger cause R_E was rejected. In 2016, the variables F_n, T_a, and θ Granger cause R_E. On the other hand, in 2016, the variables ET, F_n, T_a, θ and F_g Granger cause R_E.

Table 4.6: Granger causality test between R_E partitioned using REddyProc/Reichstein (*Reichstein et al.*, 2005) method and key drivers.

	2015	2015	2016	2016
Variables	F-test	critical value	F-test	critical value
ET	6.27	2.64	2.75	3.87
F_H	0.27	3.88	0.84	3.87
F_n	6.21	2.64	3.00	3.87
T_a	15.94	3.03	5.67	3.03
θ	6.10	3.88	11.13	3.87
F_g	5.51	2.41	1.22	3.87
prec.	0.25	3.88	0.59	3.87

According to the Granger causality test performed for both R_E partitioned using OzfluxQC (ANN) and REddyProc/Reichstein methods, the variables ET, F_n, T_a, θ, and F_g Granger cause R_E. This suggests that these variables would be beneficial to consider to have a more accurate partitioning of NEE into GPP and R_E. Furthermore, among the drivers analyzed, T_a and θ were consistent in Granger causing R_E.

4.3.6 Conclusions

The key drivers of R_E were determined using EC data collection, partitioning, wavelet analysis, and Granger causality test. Partitioning NEE into GPP and R_E using OzFluxQC (ANN) and REddyProc (Reichstein) methods resulted in similar R_E for 2015. However, in 2016, REddyProc estimated higher R_E in mid-September until late-October than the OzFluxQC method. The difference in cumulative R_E for 2016 was around 300 gC m^{-2}.

The wavelet analysis shows that the PCA fluxes were correlated with the drivers from 16 to 64 hours. Furthermore, PCA fluxes (NEE, ET, and F_H) were driven by F_n, F_g, θ, T_S, and T_a. The causation of the variables driving the PCA fluxes were tested with the partitioned R_E using OzFluxQC (ANN) and REddyProc (Reichstein) methods, since R_E is a component of NEE. The result of the Granger causality tests suggested that ET, F_n, T_a, θ, and F_g Granger cause R_E. Moreover, T_a and θ consistently Granger cause R_E for both methods (OzFluxQC and REddyProc) in both years (2015 and 2016).

Due to the difference in partitioning, the Granger causality time series tests obtained different results. For instance, variable ET was a Granger cause for R_E in 2015 but not in 2016 using OzFluxQC method. On the other hand, using REddyProc method, ET Granger caused R_E in 2016 but not in 2015. The same inconsistency of Granger analysis was seen in drivers F_n and F_g due to difference in partitioning methods. Furthermore, precipitation controls carbon assimilation (GPP) and sequestration (NEE) but does not cause R_E. T_a and θ have higher and consistent causation with R_E, according to Granger causality, which may be useful in partitioning NEE more accurately.

In conclusion, adding the drivers T_a and θ in partitioning NEE into GPP and R_E may be more useful than relying on a single parameter, T_S.

Chapter 5

Modelling soil CO_2 efflux

The vertical root distribution and extraction of subsurface water controls the ability of plants to meet their water requirements and thrive. Selecting a root water uptake (RWU) formulation in eco-hydrological models is important since this affects the estimation of actual transpiration as well as soil CO_2 efflux. This study section aims to (i) compare different models, which combine the Richards equation for soil water flow to equations describing heat transfer and air-phase CO_2 production and flow, and to (2) investigate the effect of reduced soil heat flux due to shading and hydraulic redistribution to the daily pattern of soil CO_2 efflux. To compare RWU formulations, a root water uptake model (RWC), accounting only for root water compensation by re-scaling water uptake rates across the vertical profile, was compared to a model (XWP) estimating water uptake as a function of the difference between soil and root xylem water potential; the latter model can account for both compensation (XWP_{RWC}) and hydraulic redistribution (XWP_{HR}). To investigate the daily pattern of soil CO_2 efflux, two cases were simulated to capture the diurnal pattern of the field data given by *Tang et al.* (2005). The first case was a simulation in the open without vegetation, referred as open space, where no hydraulic compensation and redistribution were occurring. The second case was a simulation under the tree, referred as canopy, where hydraulic compensation and redistribution was assumed to take place, simultaneously exposed to shading resulting into reduced soil heat flux.

5.1 Root water uptake influence on soil CO_2 dynamics

The inclusion of root water compensation and hydraulic redistribution in models of soil water dynamics will also affect the modelling of soil CO_2 dynamics. Since different models of root water

uptake are available, the aim of this study is to investigate the effect that different formulations of root water uptake have on the modelling of soil moisture and actual transpiration as well as CO_2 dynamics, focusing on soil CO_2 efflux. In this study, a model for root water uptake (RWC), accounting for root water compensation by re-scaling water uptake rates across the vertical profile, is compared to a model (XWP) estimating water uptake as a function of the difference between soil and root xylem water potential; this second model is used in two modes: one to account for only root water compensation (XWP_{RWC}) and another to account for both root water compensation and hydraulic redistribution (XWP_{HR}).

5.1.1 Methodology

5.1.1.1 Model description

The one-dimensional model of *Simunek and Suarez* (1993) is used to describe the soil water flow, heat transfer, and CO_2 production and transport.

The water flow in variably saturated soil is described using the Richards equation with a sink term for root water uptake (S [s^{-1}]), which reads

$$\frac{\partial \theta}{\partial t} + \frac{\partial}{\partial z} q_w = \frac{\partial \theta}{\partial t} - \frac{\partial}{\partial z}\left[k(h_s)\left(\frac{\partial h_s}{\partial z} + 1\right)\right] = -S, \tag{5.1}$$

where θ [m^3 m^{-3}] is the volumetric water content, q_w [m s^{-1}] is the water flux, h_s [m] is the soil water pressure head, k [m s^{-1}] is the soil hydraulic conductivity, and z [m] is the vertical coordinate (positive upwards). The unsaturated hydraulic properties of the soil are expressed by the soil water retention, $\theta(h_s)$, and hydraulic conductivity, $k(h_s)$, curves.

The water retention curve in equation 5.1 is described by (*Van Genuchten*, 1980)

$$\theta(h_s) = \theta_r + \frac{\theta_s - \theta_r}{(1 + |\alpha h_s|^n)^m}, \tag{5.2}$$

where θ_r [m^3 m^{-3}] is the residual soil water content, θ_s [m^3 m^{-3}] is the soil water content at saturation, α, n ($n > 1$) and m are empirical parameters, with $m = 1 - 1/n$. The hydraulic conductivity is expressed as (*Van Genuchten*, 1980)

$$k(h_s) = k_s S_e^{\frac{1}{2}}[1 - (1 - S_e^{\frac{1}{m}})^m]^2, \tag{5.3}$$

where k_s [m s^{-1}] is the saturated hydraulic conductivity, and S_e is the relative saturation calculated as

$$S_e = \frac{\theta - \theta_r}{\theta_s - \theta_r}. \tag{5.4}$$

Soil temperature is driven by

$$C(\theta)\frac{\partial T_s}{\partial t} = \frac{\partial}{\partial z}\left[\lambda(\theta)\frac{\partial T_s}{\partial z}\right] - C_w\frac{\partial q_w T_s}{\partial z}, \tag{5.5}$$

where T_s [K] is the soil temperature, λ [W m^{-1} K^{-1}] is the apparent thermal conductivity, and C and C_w are the volumetric heat capacities of the soil and the liquid phase, respectively.

The volumetric heat capacity in equation (5.5) is expressed as

$$C(\theta) = C_s(1-\theta_s) + C_w\theta + C_a(\theta_s - \theta), \tag{5.6}$$

where C_s and C_a are the volumetric heat capacity for solid and air, respectively. The apparent thermal conductivity in the heat transfer equation is defined as

$$\lambda(\theta) = b_1 + b_2\theta + b_3\sqrt{\theta}, \tag{5.7}$$

where b_1, b_2 and b_3 [W m^{-1} K^{-1}] are empirical parameters.

The CO_2 production and transport are modeled as

$$\frac{\partial}{\partial t}\left[((\theta_s - \theta) + K_H R T_s \theta)\, c_a\right] = \frac{\partial}{\partial z}\left[D_E(\theta, T_s)\frac{\partial c_a}{\partial z}\right] - \frac{\partial}{\partial z} q_E c_a - S K_H R T_s c_a + \Pi, \tag{5.8}$$

where c_a [m^3 m^{-3}] is the air-phase CO_2 concentration in the soil, θ_s is soil porosity, K_H [mol s^2 kg^{-1} m^2] is the Henry's Law parameter, R [kg m^2 mol^{-1} s^{-2} K^{-1}] is the universal gas constant, D_E [m^2 s^{-1}] is the effective dispersion coefficient, q_E [m s^{-1}] is the effective velocity of CO_2 flux, and Π [m^3 m^{-3} s^{-1}] is the CO_2 production rate. In equation (5.8), the CO_2 dissolved in water, c_w, is assumed to be related to c_a as $c_w = K_H R T_s c_a$ (*Simunek and Suarez*, 1993).

In equation (5.8), the effective dispersion in the soil matrix is given by

$$D_E = (D_{as}\tau_a)[\theta_s - \theta] + \left(D_{ws}\tau_w + \lambda_w\left|\frac{q_w}{\theta}\right|\right) K_H R T_s \theta, \tag{5.9}$$

where D_{as} [m^2 s^{-1}] and D_{ws} [m^2 s^{-1}] are the diffusion coefficients of CO_2 in the gas and dissolved phases, respectively. The parameter λ_w [m] is the dispersivity in the water phase, and τ_a and τ_w are the tortuosity factors in the gas and dissolved phases defined as

$$\tau_a = \frac{(\theta_s - \theta)^{\frac{7}{3}}}{\theta_s^2}, \tag{5.10}$$

and

$$\tau_w = \frac{(\theta)^{\frac{7}{3}}}{\theta_s^2}. \tag{5.11}$$

The term q_E, associated with the water flux, is

$$q_E = K_H R T_s q_w. \tag{5.12}$$

The CO_2 production, Π, is assumed to be the sum of plant root and soil microorganism respiration. Other possible sources and sinks, such as chemical reactions, are neglected. The term Π is thus defined as

$$\Pi = \gamma_s + \gamma_p, \tag{5.13}$$

with the CO_2 production of soil microorganisms, γ_s [m^3 m^{-3} s^{-1}], and plant roots, γ_p [m^3 m^{-3} s^{-1}], calculated as

$$\gamma_s = \gamma_{s_0} f_s(z) f_s(h_s) f(T_s) f_s(c_a), \tag{5.14}$$

and

$$\gamma_p = \gamma_{p_0} r(z) f_p(h_s) f(T_s) f_p(c_a), \tag{5.15}$$

where γ_{s_0} [m^3 m^{-3} s^{-1}] and γ_{p_0} [m^3 m^{-3} s^{-1}] represent the optimal CO_2 production by soil microorganisms and plant roots. The optimal CO_2 production is reduced by functions (f_s and f_p) dependent on depth, soil water pressure head, temperature, and CO_2 concentration; $r(z)$ in equation (5.15) is the root distribution.

Following *Suarez and Simunek* (1993), CO_2 production of soil microorganisms and plant roots is affected by z, h_s, T_s, and c_a. The dependence of Π on these variables is described by a series of functions. The reduction of soil microorganisms respiration with depth is defined as

$$f_s(z) = \frac{a e^{-az}}{\int_{-d}^{0} a e^{-az} dz}, \tag{5.16}$$

where a [m^{-1}] is an empirical constant and d [m] is the root depth.
Root respiration varies in depth according to the root distribution, defined as (*Vrugt et al.*, 2001)

$$r(z) = \frac{\left(1 - \frac{|z|}{d}\right) \exp\left(\frac{-q_z}{d}|z|\right)}{\int_{-d}^{0} \left(1 - \frac{|z|}{d}\right) \exp\left(\frac{-q_z}{d}|z|\right) dz} \qquad -d \leq z \leq 0, \tag{5.17}$$

where q_z is an empirical parameter showing the decrease of root mass with depth.

The reduction coefficient $f_s(h_s)$ reads

$$f_s(h_s) = \begin{cases} 0 & h_1 < h_s \\ \frac{\log h_s - \log h_1}{\log h_2 - \log h_1} & h_2 \leq h_s \leq h_1 \\ \frac{\log h_s - \log h_3}{\log h_2 - \log h_3} & h_3 \leq h_s < h_2 \\ 0 & h_s < h_3, \end{cases} \tag{5.18}$$

where h_1 is the soil water pressure head at the air-entry value of the soil-water retention curve, h_2 is the soil water pressure head where optimal soil respiration occurs, and h_3 is the soil water pressure head where the soil CO_2 production ceases.

The function $f_p(h_s)$ reflects the reduction of the rate of root water uptake affected by the soil moisture condition. The water stress response function of *Feddes et al.* (1978) was used; this is defined as

$$f_p(h_s) = \begin{cases} 0 & h_s \geq h_{s_1} \\ \frac{h_{s_1} - h_s}{h_{s_1} - h_{s_2}} & h_{s_1} > h_s > h_{s_2} \\ 1 & h_{s_2} \geq h_s \geq h_{s_3} \\ \frac{h_s - h_{s_4}}{h_{s_3} - h_{s_4}} & h_{s_3} > h_s > h_{s_4} \\ 0 & h_s \leq h_{s_4}, \end{cases} \tag{5.19}$$

where h_{s_1}, h_{s_2}, h_{s_3} and h_{s_4} are empirical parameters dependent on soil and vegetation type.

The effect of temperature $f(T_s)$ on respiration of both microorganisms and roots is

$$f(T_s) = \exp\left[\frac{E_a(T_s - T_{opt})}{RT_sT_{opt}}\right], \tag{5.20}$$

where E_a [J mol^{-1}] is the activation energy of the reaction and T_{opt} [K] is the optimal temperature for CO_2 production.

The function $f(c_a)$ is based on the simplified Michaelis-Menten equation defined as

$$f(c_a) = \frac{0.21 - c_a}{0.42 - c_a - K_M}, \tag{5.21}$$

where K_M [m^3 m^{-3}] is the Michaelis-Menten constant. The value of K_M can be either for soil microorganisms (K_{M_s}) or plant roots (K_{M_p}).

5.1.1.2 Root water uptake models

Two models for the term S in equation (5.1) will be compared. The first model accounts for root water compensation, and it will be referred to as RWC. The second model includes changes in the xylem water potential (XWP) and describes root water compensation and hydraulic redistribution. This second model will be used with root water compensation only ($\mathrm{XWP_{RWC}}$) and with both root water compensation and hydraulic redistribution ($\mathrm{XWP_{HR}}$).

Root water compensation model

The sink term in equation (5.1) is commonly modelled as

$$S = T_p f_p(h_s) r(z), \tag{5.22}$$

where T_p [m s^{-1}] is the potential transpiration, and $f_p(h_s)$ and $r(z)$ are in equations (5.17) and (5.19). To account for root water compensation, *Jarvis* (1989) modified equation (5.22) as

$$S = \frac{T_p}{\max[\omega(t), \omega_c]} f_p(h_s) r(z), \tag{5.23}$$

where $\omega(t)$ is the water stress index, given by

$$\omega = \int_{-d}^{0} f_p(h_s) r(z) dz, \tag{5.24}$$

and ω_c is the critical value of the water stress index also known as the root adaptability factor. When ω_c is equal to 1, equations (5.22) and (5.23) coincide. On the other hand, a value of ω_c equal to zero triggers a fully-compensated root water uptake. This root water compensation model maintains the total transpiration equal to T_p as long as $\omega \geq \omega_c$. This is achieved by re-scaling the root water uptake using the value of ω; this means that roots experiencing water stress increase their water uptake as well.

Root xylem water potential model

In the XWP models, S is assumed to depend on the water potential difference between soil and roots (*Herkelrath et al.*, 1977; *Molz*, 1981; *Amenu and Kumar*, 2007; *Verma et al.*, 2014) as

$$S = (1 + \beta)[k_{sr}(z) f_p(h_s)(h_s - h_x)], \tag{5.25}$$

where h_x [m] is the water pressure head in the xylem, and β is a factor that regulates hydraulic redistribution; β=1 when $h_s \geq h_x$ and $0 \leq \beta \leq 1$ when $h_s < h_x$. The parameter k_{sr} [m^{-1} s^{-1}] is the soil-root radial conductance expressed as (*Verma et al.*, 2014)

$$k_{sr}(z) = k_{srt} r(z), \tag{5.26}$$

where k_{srt} [s^{-1}] is the total soil-to-root radial conductance. The function $f_p(h_s)$ in equation (5.25) accounts for the reduction of root water uptake due to different soil moisture conditions. This function reads as equation (5.19) but the values of h_{s_3} and h_{s_4} are different from RWC; these will be indicated as h'_{s_3} and h'_{s_4}.

Since S depends on h_x, a model for water flow in the xylem is required. The model defines the xylem as a porous medium and Darcy's law is used to describe the water flow through the xylem as (*Amenu and Kumar*, 2007; *Verma et al.*, 2014)

$$\rho g S_s \frac{\partial h_x}{\partial t} - \frac{\partial}{\partial z}\left[k_p(h_x)\left(\frac{\partial h_x}{\partial z} + 1\right)\right] = S = (1+\beta)[k_{sr}(z) f_p(h_s)(h_s - h_x)], \tag{5.27}$$

where S_s [Pa^{-1}] is the storage within the xylem and k_p [m s^{-1}] is the spatially averaged axial hydraulic conductivity of the xylem.

The parameter k_p is a function of the xylem water potential and is defined as (e.g. *Verma et al.*, 2014)

$$k_p = k_{p_{max}}\left(1 - \frac{1}{1 + \exp(a_p(\rho g h_x - b_p))}\right), \tag{5.28}$$

where a_p [Pa^{-1}] and b_p [Pa] are xylem cavitation parameters.

Due to the water potential gradient in equations (5.25) and (5.27), the roots can both take water from the soil and release water to the soil. XWP thus automatically accounts for both root water compensation and hydraulic redistribution. XWP is used with root water compensation only, XWP_{RWC}, by imposing no flow of water from roots to soil (i.e., $\beta = 0$ when $h_s < h_x$). This allows for a comparison between RWC and XWP_{RWC}. When XWP accounts for both root water compensation and hydraulic redistribution (i.e., XWP_{HR}), the flow of water from roots to the soil is assumed to occur with higher resistance (*Caldwell et al.*, 1998; *Mendel et al.*, 2002; *Neumann and Cardon*, 2012; *Prieto et al.*, 2012); accordingly, $\beta = 0.5$ was assumed when $h_s < h_x$.

The root water uptake in equation (5.27) is driven by T_p by imposing a boundary condition at the surface that defines the actual transpiration as

$$T_{ac} = T_p\left[1 + \left(\frac{h_x}{h_{x_{50}}}\right)^{n_l}\right]^{-1} = T_p f(h_x), \tag{5.29}$$

where $h_{x_{50}}$ [m] represents the pressure head at which the root water extraction is reduced by half; $h_{x_{50}}$ and n_l are both empirical constants. The reduction of T_p is here assumed to depend only on the xylem water potential at the surface. Other sources of stress, such as vapour pressure deficit, solar radiation, and air temperature, could be included; however, since the aim is to compare models, a simplified form is used here for the sake of simplicity.

5.1.1.3 Numerical simulations

The system of equations (5.1), (5.5), (5.8), and (5.27) was solved numerically using COMSOL Multiphysics (Ver. 5.1; http://www.comsol.com/). To compare models, a case similar to the first example of *Simunek and Hopmans* (2009) was selected to define the parameters of the different models. This virtual experiment assumed a loamy soil with a depth of 1.2 m and hydraulic properties as in Table 5.1. The root depth was 0.9 m; differently from *Simunek and Hopmans* (2009), the root distribution here was not linear, but was described by equation (5.17) with the values of the parameters listed in Table 5.1. The geometry, soil type, and root distribution were the same for all simulations.

Selection of parameters

The aim of the first set of simulations was to select the parameters for the $\mathrm{XWP_{RWC}}$ model with that of the RWC model based on *Simunek and Hopmans* (2009). The parameters in the heat transfer and CO_2 equations in the different models were kept the same with the exception of those related to water stress, which are associated with the water flow. The parameters of the water flow equations needed to be selected in order to be able to compare the results from different models.

RWC synthesizes the water stress in one single function (i.e., the Feddes water-stress response function, $f_p(h_s)$) and implements root water compensation through the critical water stress index (ω_c=0.5). Contrarily, XWP has three different forms of water stress (i.e., the Feddes function, $f_p(h_s)$, the vulnerability curve, $k_p(h_x)$, and the stomatal conductance, $f(h_x)$). To compare the different models, the parameters of RWC were selected (Table 5.1) similarly to *Simunek and Hopmans* (2009) and the parameters of $\mathrm{XWP_{RWC}}$ were selected such that T_{ac} of the two models will have a coefficient of determination (R^2) close to unity and a root-mean-square error (RMSE) close to null. The same values of parameters were then used in $\mathrm{XWP_{HR}}$.

The boundary conditions were based on the first example of *Simunek and Hopmans* (2009) that simulated the root water uptake in a one-dimensional soil profile with water table at the bottom. The boundary conditions were adopted to effectively compare the findings of the $\mathrm{XWP_{RWC}}$ with that of the RWC model used in *Simunek and Hopmans* (2009). The boundary conditions were no flux at the ground surface and a pressure head equal to zero at depth of -1.2 m, thereby assuming that the water table was at that depth. The value of T_p in equation (5.23) was assumed to be constant and equal to 0.44 mm h^{-1}; this value, larger than that used by *Simunek and Hopmans* (2009) was selected, to capture large T_p demands in dry areas. $\mathrm{XWP_{RWC}}$ needs conditions for both the soil and the root. The Richards equation (equation (5.1)) of $\mathrm{XWP_{RWC}}$ had the same initial and boundary conditions as RWC. The initial condition of RWC was a hydrostatic pressure head equal to -1.2 m at the soil surface and decreased linearly to zero at

Table 5.1: List of parameters of the Richards equation

Parameter	Units	Value	Description	Reference
Retention curve				
k_s	m s^{-1}	$2.89 \cdot 10^{-6}$	Saturated hydraulic conductivity of the soil	*Simunek and Hopmans* (2009)
θ_s	–	0.43	Saturated volumetric soil moisture content	*Simunek and Hopmans* (2009)
θ_r	–	0.078	Residual volumetric soil moisture content	*Simunek and Hopmans* (2009)
α	m^{-1}	3.6	Soil hydraulic parameter	*Simunek and Hopmans* (2009)
n	–	1.56	Soil hydraulic parameter	*Simunek and Hopmans* (2009)
Xylem flow				
k_{srt}	s^{-1}	$7.2 \cdot 10^{-10}$	Total soil-to-root conductance	*Verma et al.* (2014)
a & q_z	–	10	Root distribution parameter	*Verma et al.* (2014)
S_s	Pa^{-1}	$1 \cdot 10^{-14}$	Xylem storage	Calibrated
$k_{p_{max}}$	m s^{-1}	$1 \cdot 10^{-5}$	Xylem hydraulic conductivity	*Verma et al.* (2014)
a_p	Pa^{-1}	$2 \cdot 10^{-6}$	Xylem cavitation parameter	Calibrated
b_p	Pa	$-3.5 \cdot 10^{6}$	Xylem cavitation parameter	Calibrated
$h_{x_{50}}$	m	-350	Jarvis leaf water potential parameter	Calibrated
n_l	–	8	Jarvis leaf water potential parameter	Calibrated
Water-stress				
ω_c	–	0.5	Critical water index of RWC	*Simunek and Hopmans* (2009)
h_{s_1}	m	-0.1	Feddes parameter	*Simunek and Hopmans* (2009)
h_{s_2}	m	-0.25	Feddes parameter	*Simunek and Hopmans* (2009)
h_{s_3}	m	-5	Feddes parameter	*Simunek and Hopmans* (2009)
h_{s_4}	m	-80	Feddes parameter	*Simunek and Hopmans* (2009)
$h_{s'_3}$	m	-25	adjusted Feddes parameter	Calibrated
$h_{s'_4}$	m	-400	adjusted Feddes parameter	Calibrated

the bottom of the soil profile. The initial condition of the xylem water potential of XWP_{RWC} was as the initial soil water potential, so that no root water uptake occurred at the beginning of the simulation. The boundary conditions at the bottom of the root was no flux and at the top was as in equation (5.29). A shallow water table was used to generate a strong difference in water content between the soil column. The contrast in soil moisture results from the simulations is expected to highlight differences in model structure. Simulations were run for 50 days.

Combinations of parameters of the stress functions in XWP_{RWC} were selected until T_{ac} of XWP_{RWC} almost coincided ($R^2 \approx 1$ and RMSE≈ 0) with that of RWC.

Scenarios

After the parameters were estimated for XWP models, numerical simulations with boundary conditions at the surface changing in time were generated to investigate the effect of changes in these forcing variables and the impact of different formulations of S on T_{ac} and soil CO_2 dynamics. The aim of the second set of simulations was to compare the behaviour of the RWC, XWP_{RWC}, and XWP_{HR} models.

The water flow equation had an initial condition similar to that of the simulations used to estimate water flow parameters for all models. The water flow boundary conditions for the Richards equation of both RWC and XWP models were a pressure head equal to zero at the bottom of the soil column and no flow at the surface, with the exception of a precipitation event of 3.6 mm uniformly distributed on the 25th day of the simulation. Since the focus is on root water compensation, a small rainfall event was selected to generate vertical differences in the water profile, thereby highlighting the different root water uptake mechanisms of the different models. If a large event were used, as, e.g., in *de Willigen et al.* (2012), the whole soil column would be replenished taking the system back to conditions similar to the initial one. Additionally, such small rainfall events are common in semiarid climates and thus this condition is consistent with the conditions associated with the potential transpiration rates and the soil heat flux. The boundary conditions for Darcy's equation (equation (5.27)) of the XWP models (XWP_{RWC} and XWP_{HR}) were no flow at the bottom of the root depth and T_{ac} at the ground surface given by equation (5.29), with T_p changing in time based on values common to semiarid ecosystems in southeastern Australia (Figure 5.1a). Transpiration was assumed to stop during the night and was repeated periodically for the whole simulation of 50 days. The parameters associated with water flow equation are presented in Table 5.1.

For the heat transport calculation, the initial condition of soil temperature profile was based on experimental data shown in Table 5.2. A constant soil temperature (19.85°C) and a periodic soil heat flux (Figure 5.1b) were imposed as boundary conditions at the bottom and at the

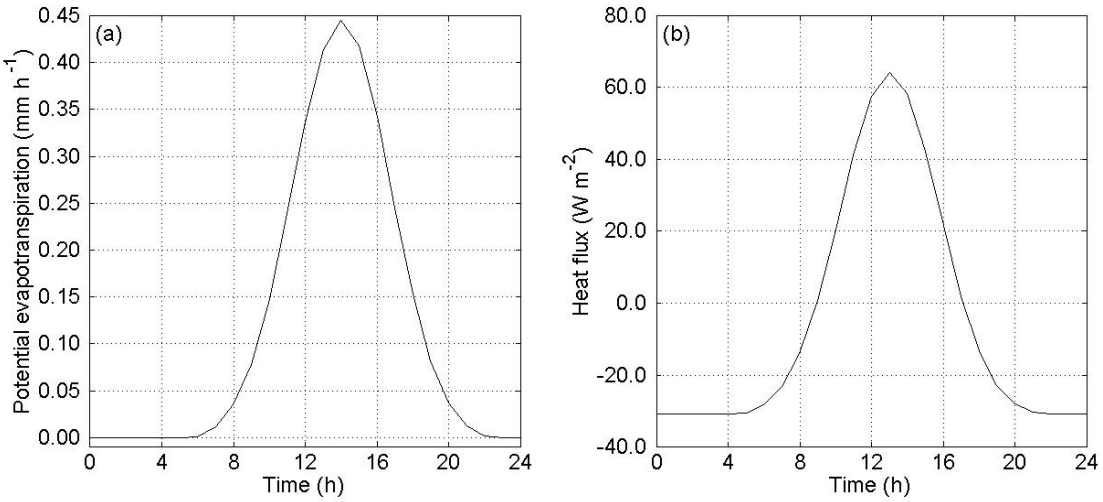

Figure 5.1: (a) Potential transpiration, T_p , used in equations (5.23) and (5.29), and (b) ground heat flux used as boundary condition at the surface in equation (5.5).

top of the soil profile of the heat equation. The soil heat flux input was based on a diurnal soil heat flux pattern common to semiarid ecosystems in southeastern Australia. The parameters associated with the heat equation are in Table 5.3.

Table 5.2: Initial condition of soil temperature

Depth (m)	Soil Temperature (°C)
-0.05	23.85
-0.15	23.70
-0.30	22.82
-0.50	22.24
-0.70	21.69
-1.20	19.85

For the CO_2 production and transport, the initial CO_2 concentration was assumed to decrease linearly from 400 ppm (i.e., atmospheric CO_2 concentration) at the top to $6 \cdot 10^4$ ppm at the bottom of the soil column. These large concentrations are common in soils (e.g., *Daly et al.*, 2009; *Jassal et al.*, 2008). The boundary conditions for top and bottom of the soil were 400 ppm and $6 \cdot 10^4$ ppm, respectively. The parameters associated with CO_2 production and transport are listed in Table 5.4. Fluxes of CO_2 are reported as fluxes of the equivalent carbon (C).

Table 5.3: List of parameters of the heat equation (*Suarez and Simunek*, 1993)

Parameter	Units	Value	Description
C_s	$\mathrm{Jm^{-3}K^{-1}}$	$1.92 \cdot 10^6$	Volumetric heat capacity for solid
C_w	$\mathrm{Jm^{-3}K^{-1}}$	$4.18 \cdot 10^6$	Volumetric heat capacity for water
C_a	$\mathrm{Jm^{-3}K^{-1}}$	$1.20 \cdot 10^3$	Volumetric heat capacity for air
b_1	$\mathrm{Wm^{-1}K^{-1}}$	-0.197	Coefficient of $\lambda(\theta)$
b_2	$\mathrm{Wm^{-1}K^{-1}}$	-0.962	Coefficient of $\lambda(\theta)$
b_3	$\mathrm{Wm^{-1}K^{-1}}$	2.521	Coefficient of $\lambda(\theta)$

5.1.2 Results and discussion

Since soil temperature of all the models had negligible differences, the focus will be on the selection of parameters of XWP models and the role of different formulations of S in determining water fluxes, and CO_2 production and effluxes. The mass balance errors of water in the numerical simulations were deemed reasonable since the discrepancy ranged from 1% (0.04 mm) to 4% (0.14 mm) of the total applied precipitation (i.e., 3.6 mm).

5.1.2.1 Selection of parameters

Parameters of $\mathrm{XWP_{RWC}}$ were selected to match T_{ac} with RWC. The values of T_{ac} of both RWC and XWP were very close in time (Figure 5.2; R^2=0.9975 and RMSE=$2.05 \cdot 10^{-5}$) when the values of XWP water flow parameters were as in Table 5.1.

5.1.2.2 Root water uptake

When different formulations of the sink term were implemented with a periodic T_p and G, the models generated different T_{ac} dynamics. Initially, all the models performed similarly, since the parameters had been calibrated with the same potential transpiration rate and water stress was not yet experienced (Figure 5.3a). RWC and $\mathrm{XWP_{RWC}}$ experienced water stress earlier than $\mathrm{XWP_{HR}}$ and RWC had the largest increase of T_{ac} associated with the rainfall event. As the soil water stress started to play a role, RWC resulted in a slower increase of T_{ac} in the morning and a faster decrease in the evening, even when the peak of T_{ac} was larger than the XWP models (Figure 5.3). The difference in T_{ac} dynamics between RWC and XWP models can also be observed in Figure D.1a, where the diurnal pattern of the average T_{ac} for RWC was narrower than that of XWP models. $\mathrm{XWP_{HR}}$ had the peak of T_{ac} occurring earlier than the other two models (Figure D.1a).

Table 5.4: List of parameters of the CO_2 production and transport equation

Parameter	Units	Value	Description	Reference
K_H	mol s^2 $kg^{-1}m^{-2}$	$5.64 \cdot 10^{-4}$	Henry's Law constant	*Suarez and Simunek* (1993)
R	J $mol^{-1}K^{-1}$	$5.64 \cdot 10^{-4}$	Universal gas constant	*Suarez and Simunek* (1993)
D_{as}	m^2s^{-1}	$1.57 \cdot 10^{-5}$	Molecular gas phase diffusion at 293K	*Yiqi and Zhou* (2010)
D_{ws}	m^2s^{-1}	$2.24 \cdot 10^{-9}$	Molecular liquid phase diffusion at 298K	*Yiqi and Zhou* (2010)
λ_w	m	0.1	Dispersivity of CO_2 in water	*Yiqi and Zhou* (2010)
γ_{s_0}	ms^{-1}	$4.8611 \cdot 10^{-8}$	Optimal CO_2 production for microbes	*Suarez and Simunek* (1993)
γ_{p_0}	ms^{-1}	$3.2407 \cdot 10^{-8}$	Optimal CO_2 production for root	*Suarez and Simunek* (1993)
a	m^{-1}	10	Empirical constant for CO_2 production	*Suarez and Simunek* (1993)
h_1	m	-0.1	Carbon stress parameter for moisture	*Suarez and Simunek* (1993)
h_2	m	-1.0	Carbon stress parameter for moisture	*Suarez and Simunek* (1993)
h_3	m	-1700	Carbon stress parameter for moisture	*Manzoni et al.* (2012)
E_a	J mol^{-1}	55	Activation energy of a reaction	*Suarez and Simunek* (1993)
K_{M_s}	$-$	0.19	Michaelis constant for soil microbes	*Suarez and Simunek* (1993)
K_{M_p}	$-$	0.14	Michaelis constant for plant roots	*Suarez and Simunek* (1993)
T_{opt}	K	317.65	Optimum temperature for C production	*Richardson et al.* (2012)

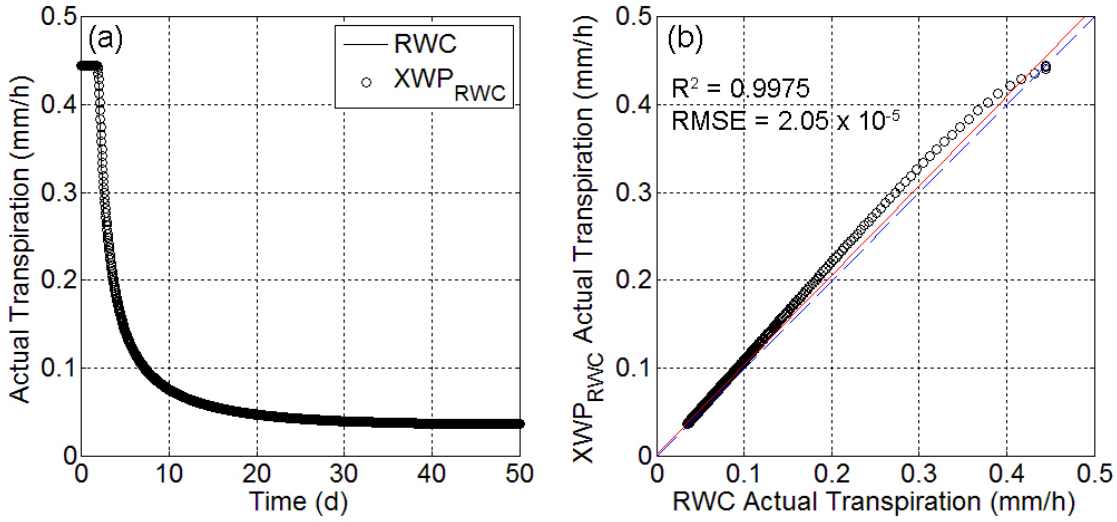

Figure 5.2: (a) Actual transpiration plot of XWP and RWC within the simulation period and (b) comparison of the actual transpiration of XWP and RWC to obtain the parameters in Table 5.1.

Since T_{ac} patterns differed due to the formulations of S, the total amounts of water transpired were also different. The total T_{ac} during the simulation period of the XWP_{RWC} was 13% larger than that of the RWC (Figure D.1b). Even though the XWP_{RWC} and RWC are based on compensation processes, there is a significant difference between the two models due to the way the compensation was applied. In the RWC model, the compensation is adjusted in the whole root leading to a drier soil. The drier soil affects the $f_p(h_s)$ (*Feddes et al.*, 1978) causing the model to experience water stress at an earlier stage. In the XWP_{RWC}, the compensation is adjusted based on the potential head difference based on a more mechanistic approach without overlapping compensation.

XWP_{HR} resulted in higher transpiration, with about 0.10-0.30 mm d^{-1} of water lifted during the nights, which provided an additional water source for the roots near the surface. The magnitude of the lifted soil water was in agreement with the reviewed values by *Neumann and Cardon* (2012). The prolonged transpiration due to soil water lifted increased T_{ac} of XWP_{HR} by an additional 6% within 50 days; this is comparable to the 4% difference over the period of 100 days in the study by *Ryel et al.* (2002).

The soil water extraction profile differed across models. Overall, almost 70% of soil water was taken within 0.40 m below the ground in all models (Figure D.2), reflecting the shape of the root distribution. RWC took soil water near the surface when possible. Applying hydraulic redistribution led to a wetter soil at shallow depths in the morning, such that the root water

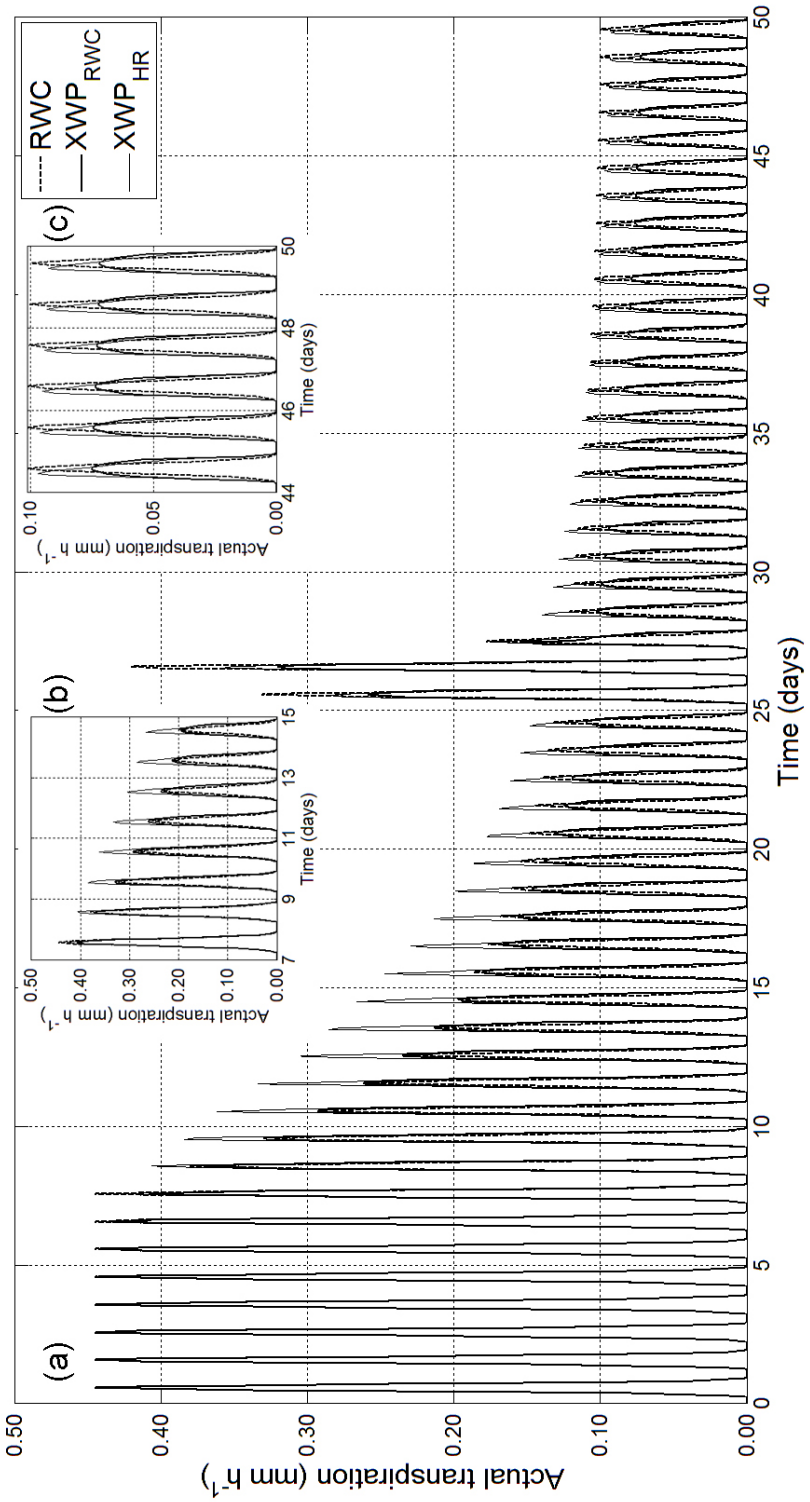

Figure 5.3: Comparison of T_{ac} rates between the 3 models over (a) the length of the simulation period, (b) the period of incipient water stress and (c) the driest part of the simulation period.

uptake of XWP_{HR} was higher at these depths.

The behavior of soil water extraction affected the soil water pressure head and volumetric soil water content. The minimum value of h_s of RWC and XWP was governed by the parameters h_4 and h'_4 equal to -80 m and -400 m, respectively (Figure D.3), which affected the T_{ac} of the models. This explains the reason why the T_{ac} of RWC was higher to that of the XWP models during the latter part of the simulation. Soil moisture in RWC did not reach θ_r due to the root water uptake limitation of h_s at -80 m, which was associated with a value of θ slightly larger than θ_r. The soil of XWP_{RWC} and XWP_{HR} were drier compared to that of RWC, since XWP models generated larger T_{ac}. Hydraulic redistribution thresholds reported in the literature range from -10 to -850 m (*Prieto et al.*, 2010; *Neumann and Cardon*, 2012), which are consistent with the values calculated here.

5.1.2.3 CO_2 production and efflux

The models generated dissimilar CO_2 efflux dynamics due to the different formulations of root water uptake. Although the CO_2 dynamics depend on soil moisture and temperature, the CO_2 production and efflux were mainly driven by soil moisture, since T_s from all models had negligible differences. Initially, all the models resulted in similar CO_2 efflux patterns until the fifth day when the efflux of RWC decreased faster than that of the XWP models (Figure 5.4a). This coincided with incipient water stress, which also led to different transpiration rates as shown in Figure 5.3. After the start of water stress, XWP_{HR} experienced hydraulic redistribution that changed the CO_2 efflux; the efflux calculated with XWP_{HR} experienced lower daily fluctuations than RWC and XWP_{RWC} (Figure 5.4b and 5.4c). In addition, the diurnal average CO_2 efflux of XWP_{HR} had a time lag of almost an hour compared to RWC and XWP_{RWC} (Figure D.4a).

The magnitude of CO_2 production and CO_2 efflux was affected as well due to the different implementations of the S term in RWC and XWP models. XWP_{HR} had the highest diurnal CO_2 efflux from midnight until early afternoon; this was due to the hydraulic redistribution that sustained CO_2 efflux (Figure D.4a). However, RWC had the highest diurnal CO_2 efflux for the rest of the day. The diurnal CO_2 efflux of XWP_{RWC} was consistently lower than those of the two models. Initially, CO_2 efflux of RWC was lower than that of XWP_{RWC}; however, on the 23rd day of the simulation period (Figure D.4b), the cumulative CO_2 efflux of RWC became greater than that of XWP_{RWC} due to the higher soil water reserve for microbial activity. The difference in the implementation of root water compensation between RWC and XWP_{RWC} resulted in a 6% difference of the calculated CO_2 efflux; furthermore, the difference between XWP_{RWC} and XWP_{HR} resulted in an 8% difference within the simulation period.

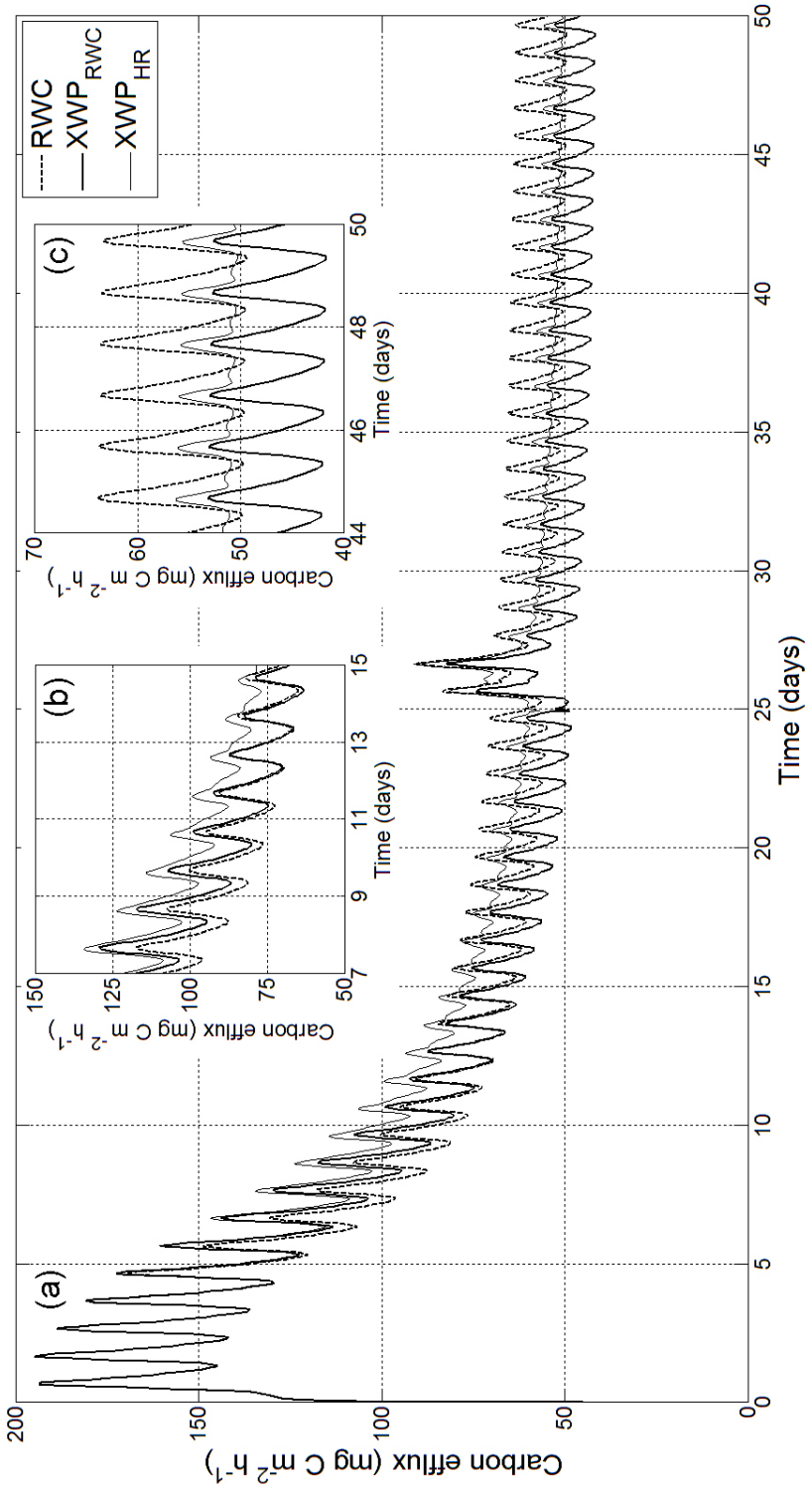

Figure 5.4: Comparison of CO_2 efflux rates between the three models over (a) the length of the simulation period, (b) the period of incipient water stress and (c) the final part of the simulation period.

The CO_2 efflux of RWC was initially lower than that of XWP_{RWC} due to the faster decline of the root C production associated with autotrophic respiration; on the contrary, XWP_{HR} was larger due to the sustained root C production through hydraulic redistribution (Figure D.5a). As the soil water was continuously extracted and reached the maximum possible root water uptake, the shallow layer of RWC produced wetter soil layers than those of XWP models; this resulted in a higher C production of soil microrganisms associated with heterotrophic respiration (Figure D.5b).

The root (Figure D.6a-D.6c) and the microbial (Figure D.6d-D.6f) C production profiles were dependent on the root water uptake (Figure D.2) and the soil water content profiles (Figure D.3), respectively. RWC had relatively higher microbial C production than that of XWP models since T_{ac} was limited to a soil water potential of -80 m. Furthermore, the microbial C production profile of both XWP_{RWC} and XWP_{HR} were almost similar (Figure D.6e-D.6f); thus, hydraulic redistribution has little or insignificant effect on microbial C production.

5.1.3 Conclusions

A one-dimensional model was presented to couple the soil water flow, heat, and CO_2 equations with the aim to compare how different formulations of root water uptake accounting for root water compensation and redistribution affect transpiration rates as well as soil CO_2 production and ground efflux. The cumulative T_{ac} of XWP_{RWC} was 13% higher than that of RWC. RWC model adjusts the whole root leading to a drier soil. The drier soil affects the $f_p(h_s)$ (*Feddes et al.*, 1978) causing the model to experience water stress. A further increased by 6% were experienced when hydraulic redistribution was included in the model.

The CO_2 production and ground efflux were also affected by the different formulations of root water uptake. The cumulative soil CO_2 emissions of RWC were 6% higher than those of XWP_{RWC}. The implementation of hydraulic redistribution resulted into 8% higher CO_2 efflux than that of XWP_{RWC}. In addition, the diurnal average CO_2 efflux of XWP_{HR} had a time lag of almost an hour compared to RWC and XWP_{RWC}.

This study highlight the importance of selecting a root water uptake formulation in eco-hydrological models, since this affects the estimation of magnitudes and patterns of actual transpiration as well as soil CO_2 production and soil CO_2 emissions. Recommendations of what root water uptake formulation are difficult, since, as suggested by *de Willigen et al.* (2012), this depends on the application, computational capability and data availability. However, our study shows that, although it is likely possible to use different models to reproduce the same data through calibration of parameters, the selection of the root water uptake model

may lead to estimates of magnitudes and patterns of important associated variables, such as soil CO_2 emissions, that might be very different from each other. Another important aspect is the selection of root distributions and its potential effects to the water and carbon fluxes due to the varying species and root profile, which can be further studied in future research.

5.2 Daily patterns of soil CO_2 efflux

Soil CO_2 have been observed to have a diurnal cycle, which is often is not in phase with soil temperature (*Tang et al.*, 2005). This lack of direct relationship between CO_2 fluxes and temperature makes it difficult to develop simple models to estimate CO_2 fluxes from variables such as T_S, which are easier to measure. Aditionally, it raises the question on which other variables might drive these daily patterns. Some studies hypothesized that soil CO_2 efflux was driven by photosynthetic activity of the vegetation causing a lag between soil temperature and CO_2 fluxes (*Kuzyakov and Gavrichkova*, 2010).

Empirical approaches have been conducted using CO_2 fluxes time series analysis of soil and photosynthetic parameters to determine the time lag between photosynthesis and soil CO_2 efflux. Among these, field studies were performed by *Tang et al.* (2005) and *Baldocchi et al.* (2006), where R_S was measured continuously and simultaneously with GPP over an oak-grass savanna during summer. There were two cases of measurements: the first case was under a tree and the other was in an open space. The diurnal pattern of R_S in the open space was in phase with T_S. On the other hand, R_S under the tree was decoupled with T_S; it was concluded to be controlled by root respiration strongly correlated with GPP. Some studies employed measurements to investigate if photosynthetic pathway of plants plays an important role in regulating R_S (*Han et al.*, 2014; *Chen et al.*, 2016). A site exposed to N fertilization monitored GPP, leaf area index (LAI), T_S, and θ to determine the seasonal and diurnal responses of R_S (*Zhong et al.*, 2016). Time lags based on experimental studies had a wide range of values from 1 to 20 h for grasses, and from 4 to 5 d for trees depending on height (*Kuzyakov and Gavrichkova*, 2010; *Han et al.*, 2014; *Mencuccini and Hölttä*, 2010).

A limited number of modelling studies investigating the time lag between R_S and GPP were conducted. One of these numerical studies was performed by *Mencuccini and Hölttä* (2010), where a static and dynamic GPP or phloem-transport soil-gas diffusion model were employed. *Goffin et al.* (2015), on the other hand, implemented a mechanism to represent the phloem pressure concentration wave using empirical parameters to capture the diurnal R_S lag. *Scandellari et al.* (2015) assessed the role of GPP, NPP, photosynthetic radiation, T_a using a model to have an improved forecasting of the magnitude and diurnal pattern of R_S. However, the time

lag between R_S and GPP is difficult to implement numerically since it is empirically based on biotic factors (e.g. LAI and GPP). This section aims to offer an alternative approach on the analysis of the diurnal pattern of R_S through numerical simulation with hydraulic compensation and redistribution.

5.2.1 Methodology

5.2.1.1 Model description

The main aim of this section is to compare the diurnal soil respiration under a canopy, where hydraulic redistribution and reduced soil heat flux are experienced, and on an open space, where both are not occuring, in an ideal scenario. The model used was the xylem water potential (XWP) model discussed in 5.1.1.2. Two cases were simulated to capture the diurnal pattern of the experimental data given by *Tang et al.* (2005). The first case was a simulation in the open without trees and grasses, referred herein as open space, where no hydraulic compensation and redistribution were occuring. The second case was a simulation under the tree, referred herein as canopy, where the area was assumed to be subjected to hydraulic compensation and redistribution, and at the same time exposed to shading, leading to reduced soil heat flux and soil temperature. The geometry of both models was changed from 1.2 m to 2.0 m to reduce the hydraulic redistribution, which may be higher compared to field observations.

The CO_2 production of the open space, Π_o, is assumed to be the soil microorganism respiration only. Other possible sources and sinks, such as plant root respiration and chemical reactions, are neglected. Root respiration in the open space is neglected, because in summer, given the high temperature and the low soil moisture, grass is likely to be inactive. The term Π_o is thus defined as

$$\Pi_o = \gamma_{s_0} f_s(z) f_s(h_s) f(T_s) f_s(c_a), \tag{5.30}$$

where γ_{s_0} [m^3 m^{-3} s^{-1}] represent the optimal CO_2 production by soil microorganisms. The optimal CO_2 production is reduced by functions (f_s) dependent on depth, soil water pressure head, temperature, and CO_2 concentration.

On the other hand, the CO_2 production under the canopy (Π), is assumed to be the sum of plant root and soil microorganism respiration shown in equation 5.13. Other possible sources and sinks, such as chemical reactions, were neglected. The reduction factors are described in section 5.1.1.1. The reduction factor for soil temperature $f(T_s)$ is described as (*Bauer et al.*, 2008)

$$f(T_s) = \begin{cases} 2.1^{(T_s - T_{ref})/10} & T_s \leq T_{ref} \\ \\ 1 & T_s > T_{ref} \end{cases} \tag{5.31}$$

where T_{ref} is the reference temperature assumed to be 35°C (Figure 4.5). The evaporation in the open space and the transpiration in the canopy were assumed to be equal, calculated by equation 5.25. Hydraulic redistribution was assumed to occur only in the canopy.

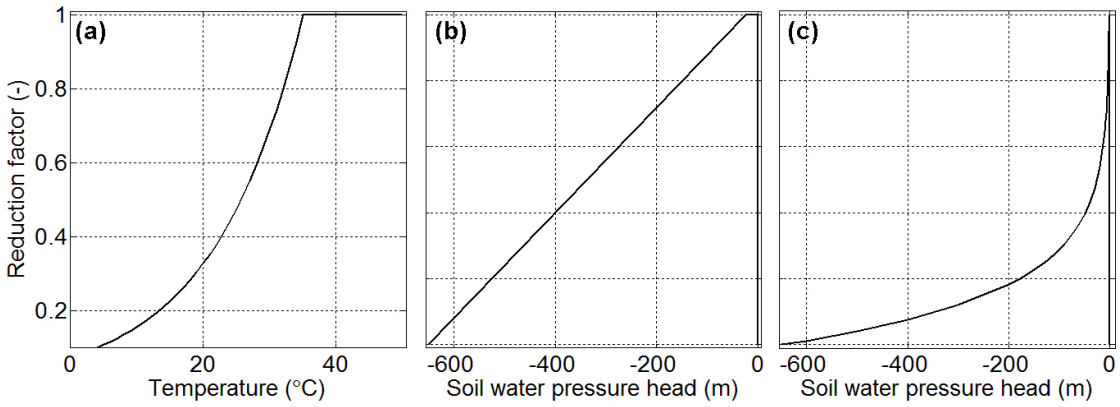

FIGURE 5.5. Reduction factors for (a) soil temperature in both open space and canopy, (b) soil water pressure head for soil microorganisms, and (c) soil water pressure head for plant root C production.

5.2.1.2 Numerical simulations

Equations (5.1), (5.5), (5.8), and (5.27) were solved using COMSOL Multiphysics (Ver. 5.1; http://www.comsol.com/). This numerical analysis assumed a loamy soil with a depth of 2.0 m and hydraulic properties as in Table 5.1. The root depth was 1.2 m with a non-linear root distribution described by equation (5.17) for the canopy case simulation. The parameter a in equation 5.16 was reduced to 5. The values of the other parameters are listed in Table 5.1. The geometry and soil type were the same for both cases (open space and canopy). All the simulations were run for 20 days.

The initial condition for the water flow equation for both open space and canopy cases was a hydrostatic pressure head equal to -2 m at the soil surface and decreased linearly to zero at the bottom of the soil profile. The boundary conditions were no flux at the ground surface, since no rainfall was assumed to occur, and a pressure head equal to zero at depth of -2 m, thereby

assuming that the water table was at that depth.

In the canopy, the boundary conditions for Darcy's equation (equation (5.27)) were no flow at the bottom of the root depth and T_{ac} at the ground surface given by equation (5.29), with T_p changing in time based on values common to semiarid ecosystems in southeastern Australia (Figure 5.1a). Transpiration was assumed to stop during the night and was repeated periodically for the whole simulation of 30 days. The parameters associated with water flow equation are presented in Table 5.1. The hydraulic redistribution factor, β, was assumed to be 1. Also, the parameter h_{s_4} was adjusted to 650 in equation 5.19 to capture the effect of hydraulic redistribution since it limits the CO_2 root production. The h_3 was reduced to -650 m (Equation 5.18).

For the heat transport calculation for both open space and canopy cases, the initial condition of soil temperature profile was based on experimental data shown in Table 5.2. A constant soil temperature (19.85°C) and a periodic soil heat flux (Figure 5.6a for the open space and Figure 5.6b for the canopy) were imposed as boundary conditions at the bottom and at the top of the soil profile of the heat equation. The soil heat flux input was based on the range measured in Tonzi Ranch (*Baldocchi et al.*, 2014) to obtain comparable soil temperature similar to that of *Tang et al.* (2005). The parameters associated with the heat equation are in Table 5.3.

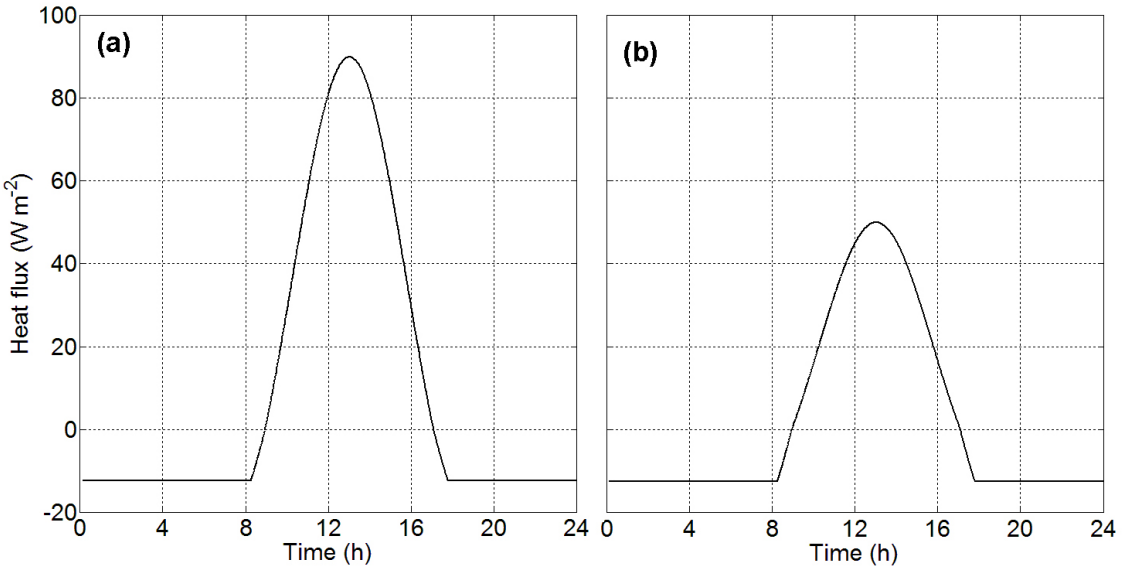

FIGURE 5.6. Soil heat flux boundary input at the surface for (a) the open space and (b) canopy in equation (5.5).

For the CO_2 production and transport for both open space and canopy cases, the initial CO_2 concentration was assumed to have a 2^{nd} degree polynomial distribution given by the function $[CO_2]$=$0.0052z^2 + 0.0144z + 0.0005$ ppm fitted on the data from *Baldocchi et al.* (2006); and

we assumed that the value at the top is 400 ppm (i.e., atmospheric CO_2 concentration) and the value at the bottom of the soil column is $5 \cdot 10^4$ ppm. These large concentrations are common in soils (e.g., *Daly et al.*, 2009; *Jassal et al.*, 2008). The boundary conditions for top and bottom of the soil were 400 ppm and $5 \cdot 10^4$ ppm, respectively. The parameters associated with CO_2 production and transport are listed in Table 5.4.

5.2.2 Results and discussion

The mass balance error of water in the numerical simulations were deemed reasonable since the discrepancies were around 0.9% of the total transpiration.

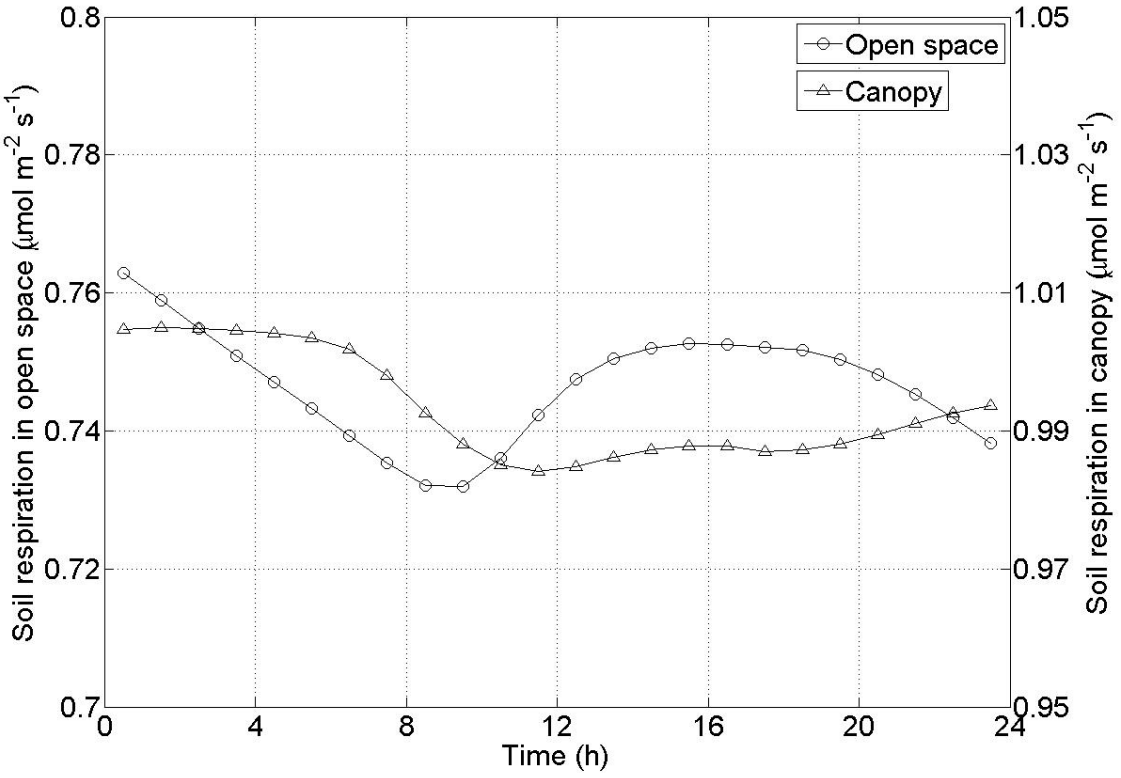

FIGURE 5.7. Simulated daily pattern of R_S, in the open space and canopy.

The daily pattern of CO_2 efflux in the open space and the canopy showed different magnitude and daily patterns (Figure 5.7). The R_S in the canopy was around 50% larger than that of the R_S in the open space. In the field experiment of *Tang et al.* (2005), the R_S under the tree was 5 times greater than that in the open; however, due to different soil type, initial and boundary

conditions, our numerical simulation gave lower R_S. This simulation and the experiment of *Tang et al.* (2005) both indicate a dominant control of autotrophic respiration on R_S. R_S in the open space was 0.73 μmol m^{-2} s^{-1} during the morning and reach its peak at around 16:00 h with an R_S of approximately 0.75 μmol m^{-2} s^{-1} and started to decrease around 20:00 h. On the other hand, R_S in the canopy was around 1.0 μmol m^{-2} s^{-1} during the morning and decreased to 0.98 μmol m^{-2} s^{-1} around 16:00 h; R_S in the canopy increased after 19:00 h. The daily patterns of the R_S simulations in open space and canopy were similar with the field data presented in *Tang et al.* (2005) (Figure E.1).

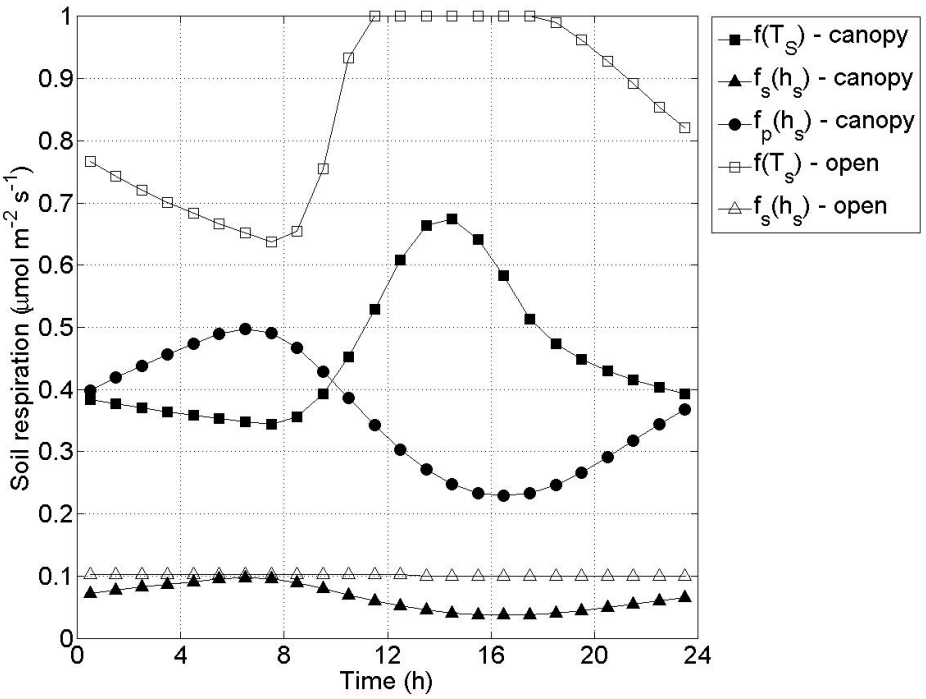

FIGURE 5.8. Simulated daily pattern of the reduction factors in the open space and canopy.

In the canopy, the diurnal change in R_S pattern was due to the reduced soil heat flux and hydraulic redistribution (Figure 5.8). The $f(T_S)$ reduction factor followed the pattern of the R_S on a bare soil. However, due to reduced magnitude of the $f(T_S)$ reduction factor, the phase of the $f_s(h_s)$ and the $f_p(h_s)$ reduction factors governed. The $f_s(h_s)$ and the $f_p(h_s)$ reduction factors captured the daily pattern of R_S in the canopy affected by hydraulic redistribution. In the open space, T_S was almost 30% more than the the magnitude of the T_S in the canopy (Figure 5.9a). The magnitude of T_S was comparable to the T_S presented by *Tang et al.* (2005)

(Figure E.2a). The $f(T_S)$ reduction factor conctrolled the phase of the R_S since the $f_s(h_s)$ in the open space does not have temporal variability. In both canopy and open spaces, the soil moisture content does not have significant variation through time (Figure 5.9b), which is in accordance with *Tang et al.* (2005) (Figure E.3).

A more mechanistic approach to capture the daily pattern of R_S was presented by reducing soil heat flux input and implementing hydraulic redistribution without the necessity of implementing a mechanism to represent the phloem pressure concentration wave using empirical parameters (*Goffin et al.*, 2015) and assessing the role of GPP, NPP, photosynthetic radiation, T_a (*Scandellari et al.*, 2015). The daily pattern of R_S in field studies is achievable when soil heat flux is reduced resulting into reduced T_S. Then, the phase of hydraulic redistribution governs the daily phase of R_S through soil moisture reduction for soil microorganism and plant root carbon production.

5.2.3 Conclusions

At the present time, there are numerous theories about the phase change of soil carbon efflux, whenever proximate to vegetation. The findings of these numerical simulations infer that the daily pattern of R_S, which was commonly explained through a biological time lag between photosynthesis and soil carbon efflux, can be explained through abiotic variables (i.e. reduced soil heat flux and increased soil moisture in shallow layers).

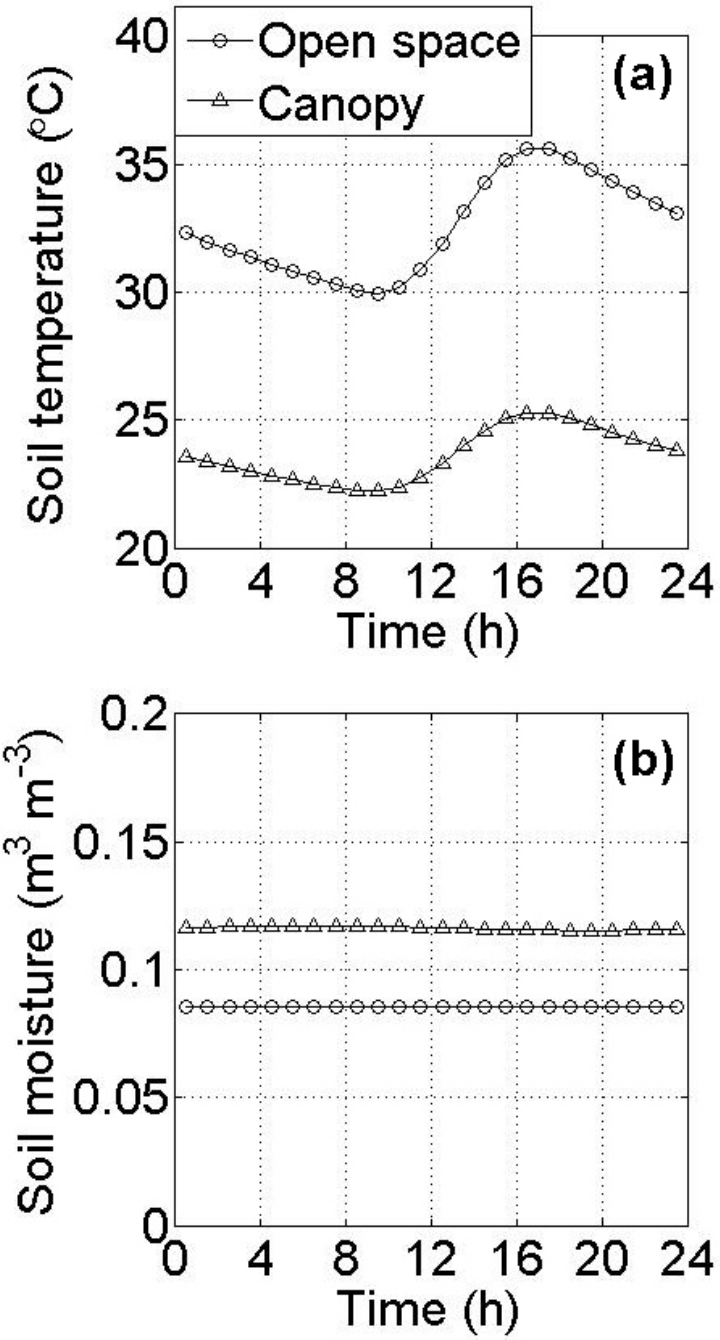

FIGURE 5.9. Simulated daily pattern of (a) T_S and (b) θ in the open space and canopy.

Chapter 6

Conclusions

The CO_2 fluxes in two productive ephemeral catchments (pasture and plantation) were monitored and investigated to supplement the deficiency of studies on CO_2 exchange between land and atmosphere in managed ecosystems.

Plot-scale investigation of the spatial variability of soil CO_2 efflux was conducted in two adjacent study sites to have a deeper understanding on the high uncertainty of soil CO_2 efflux considering land use. The effect of land cover to the variability of soil CO_2 efflux was explored using soil respiration chambers, with simultaneous measurements of soil temperature and soil moisture, taken in four different conditions: pasture, mound near a tree, trail between trees, and open space. The soil CO_2 efflux data suggests that the pasture emits more carbon to the atmosphere particularly during late-autumn, winter, and early-spring when surface soil moisture is greater. The plantation, on the other hand, has relatively higher soil CO_2 efflux during drier periods.

The spatial and temporal variability of soil respiration is mainly driven by soil moisture. Due to the water-limited condition in the study sites, the relationship between soil CO_2 efflux and soil temperature is opposite to the relationship commonly found in temperate areas, where soil respiration tend to increase with soil temperature. This will be helpful in developing more robust soil CO_2 efflux estimation and partitiong models. Furthermore, a regressed model was presented to reflect the influence of soil temperature and soil moisture on soil respiration using a confounding exponential model. The model developed has an acceptable estimating capability with changing coefficients based on the location of soil respiration being considered (i.e. pasture, mound, trail, or open space).

To further investigate the uncertainty of soil CO_2 efflux, possible key drivers were investigated using an eddy-covariance system in the livestock-grazed pasture. The data collected from February 2015 to December 2016 were partitioned using Reichstein (*Reichstein et al.*, 2005) and OzFluxQC (ANN) (*Cleverly and Isaac*, 2015) methods. In 2015, the two partitioning methods resulted into similar soil CO_2 efflux. However, in 2016, the cumulative difference was approximately 300 gC m^{-2} due to different gap-filling methods. Thus, the selection of partitioning technique can affect the accuracy of soil CO_2 efflux estimation from net ecosystem exhange into gross primary productivity and ecosystem respiration.

The eddy-covariance data collected were analyzed using wavelet analysis and Granger causality test. The findings of both analyses suggest that adding the drivers, air temperature, soil moisture, net radiation, and soil heat flux, in estimating soil CO_2 efflux or partitioning net ecosystem exchange into gross primary productivity and ecosystem respiration may be more useful than relying on a single variable, such as soil temperature. It is observable that the sufficiency of water availability changes the influence of the primary drivers on the fluxes. Hence, if water is insufficient, the net radiation and the soil heat flux has a weak and negative effect on soil respiration. On the other hand, if water supply is sufficient, net radiation has a strong and positive effect on soil respiration since energy is the limiting factor that mainly affects the process of photosynthesis that in turn affects the fluxes.

Given the importance of soil moisture in driving soil respiration, this relationship was further investigated using a model. A one-dimensional model was presented to couple the soil water flow with heat and CO_2 equations to compare how different formulations of root water uptake, accounting for root water compensation and hydraulic redistribution, affect transpiration and soil CO_2 efflux. The transpiration and soil CO_2 efflux differed by around 15% to 20%, respectively. Hence, it is important to select an applicable root water uptake formulation based on application, computational capability, and data availability. In addition, the selection of root water uptake model may lead to estimates of magnitude and patterns of important associated variables (i.e. soil CO_2 efflux), that might be dissimilar depending on the formulation used.

The estimation of daily pattern of soil CO_2 efflux has also been a concern in numerous studies. However, there has not been a concrete explanation on the change of soil CO_2 efflux whenever near to a plant. Based on the numerical simulations performed in this study, the daily pattern of soil CO_2 efflux can be explained by reducing soil heat flux due to shading and applying hydraulic redistribution capturing empirical daily pattern from field studies. The findings infer that the daily pattern of soil CO_2 efflux, which was usually explained by a biological time lag between carbon assimilation and soil carbon efflux, can be described by the relationship of soil CO_2 efflux and soil temperature in drier climate and by abiotic variables (i.e. reduction

of soil heat flux due to canopy shading and increase in surface soil moisture due to hydraulic redistribution).

Given time and resources, a better comparison of the fluxes can be performed if an eddy-covariance system was installed in the plantation. Furthermore, a continuous soil respiration data collection using automated chambers would give a more robust time series analysis of soil respiration and its relationship with other meteorological drivers. A Bayesian non-linear regression analysis can also be performed given the availability of time series of soil respiration, net ecosystem exhange, evapotranspiration, heat flux, and other meteorological variables in both the pasture and plantation. Moreover, the monitoring may be extended for a longer period (e.g. 2.5 years), which is not possible for a master's by research student.

Performing sensitivity analysis for the regressed model and a continuous soil respiration data collection to verify the accuracy of the model can be of interest in future research. Furthermore, sensitivity analysis of the XWP models considering soil, boundary conditions, plant species, root distribution and growth can be a viable future research to improve the performance of eco-hydrological models. Lastly, experiments on the diurnal variation of soil respiration considering hydraulic redistribution coupled with more detailed modelling of the soil respiration under the canopy is an interesting topic to delve in.

In summary, the magnitude and pattern of CO_2 fluxes between land and atmosphere are affected by the land cover of catchments. Land cover of catchments has an important role in regulating soil CO_2 efflux since its spatial and architectural features affect the biotic variables (i.e. leaf area index, transpiration, carbon assimilation) and abiotic variables (i.e. soil moisture, soil temperature, soil heat flux, net radiation, and air temperature) driving the soil CO_2 production and transport.

APPENDIX A

Acronyms and Nomenclature

a	Empirical constant for the soil microbes distribution
a_p	Xylem cavitation parameter
AHD	Australian Height Datum
ANN	Artificial Neural Network
b_p	xylem cavitation parameter
b_1	An empirical parameter of the apparent thermal conductivity
b_2	An empirical parameter of the apparent thermal conductivity
b_3	An empirical parameter of the apparent thermal conductivity
C	Volumetric heat capacity of the soil
c_a	Air-phase CO_2 concentration in the soil
c_w	CO_2 dissolved in water
C_a	Volumetric heat capacity of air
C_s	Volumetric heat capacity of the solid
C_w	Volumetric heat capacity of the liquid phase
d	Root depth
D_E	Effective dispersion coefficient
D_{as}	Diffusion coefficients of CO_2 in the gas phase
D_{ws}	Diffusion coefficients of CO_2 in the dissolved phases
E_a	The activation energy of a reaction
EC	Eddy-covariance
ET	Evapotranspiration
f_s	CO_2 reduction factor for soil microorganisms
$f_s(c_a)$	CO_2 reduction factor for soil microorganisms dependent on C concentration

$f_s(h_s)$	CO_2 reduction factor for soil microorganisms dependent on soil water pressure head
$f_s(z)$	CO_2 reduction factor for soil microorganisms dependent on depth
$f_s(T_s)$	CO_2 reduction factor for soil microorganisms dependent on soil temperature
f_p	CO_2 reduction factor for plant roots
$f_p(c_a)$	CO_2 reduction factor for plant roots dependent on C concentration
$f_p(h_s)$	CO_2 reduction factor for plant roots dependent on soil water pressure head
F_H	Sensible heat flux
F_n	Net radiation
F_g	Soil heat flux
GPP	Gross Primary Productivity
h_s	Soil water pressure head
h_{s_1}	Empirical parameters dependent on soil and vegetation type
h_{s_2}	Empirical parameters dependent on soil and vegetation type
h_{s_3}	Empirical parameters dependent on soil and vegetation type
h_{s_4}	Empirical parameters dependent on soil and vegetation type
h_x	Water pressure head in the xylem
$h_{x_{50}}$	Pressure head at which the root water extraction is reduced by half
h_1	Soil water pressure head at the air-entry value of the soil-water retention curve
h_2	Soil water pressure head where optimal soil respiration occurs
h_3	Soil water pressure head where the soil CO_2 production ceases
HDAS	Hydraprobe Data Acquisition System
k	Soil hydraulic conductivity
$k(h_s)$	Hydraulic conductivity curve
k_p	Spatially averaged axial hydraulic conductivity of the xylem
k_s	Saturated hydraulic conductivity
k_{srt}	Total soil-to-root radial conductance
K_H	Henry's Law parameter
K_M	Michaelis-Menten constant
K_{M_s}	Michaelis-Menten constant for soil microorganisms
K_{M_p}	Michaelis-Menten constant for plant roots
LAI	Leaf Area Index
m	Empirical parameter for the soil water retention curve
n	Empirical parameter for the soil water retention curve
n_l	Empirical constant for T_{ac}
NEE	Net Ecosystem Exchange
NPP	Net Primary Productivity
PCA	Principal Component Analysis
q	Specific humidity

q_E	Effective velocity of CO_2 flux
q_w	Water flux
q_z	Empirical parameter showing the decrease of root mass with depth
$r(z)$	Root distribution
R	Universal gas constant
R_a	Authotrophic respiration
R_E	Ecosystem respiration
R_h	Heterotrophic respiration
R_S	Soil respiration
RWC	Root Water Compensation model
RWU	Root Water Uptake
S	Root water uptake/sink term
S_e	Relative saturation
S_s	Storage within the xylem
SOC	Soil Organic Carbon
SRC	Soil Respiration Chamber
T_a	Air temperature
T_{ac}	Actual transpiration
T_{opt}	Optimal temperature for CO_2 production
T_p	Potential transpiration
T_S	Soil temperature
TN	Total Nitrogen
VPD	Vapor Pressure Deficit
XWP	Xylem Water Potential model
XWP_{RWC}	Xylem Water Potential model with root water compensation
XWP_{HR}	Xylem Water Potential model with hydraulic redistribution
z	Vertical coordinate
α	Empirical parameter for the soil water retention curve
β	Factor that regulates hydraulic redistribution
γ_s	CO_2 production of soil microorganisms
γ_{s_0}	Optimal CO_2 production by soil microorganisms
γ_p	CO_2 production of plant roots
γ_{p_0}	Optimal CO_2 production by plant roots
θ	Soil moisture
$\theta(h_s)$	Soil water retention curve
θ_r	Residual water content
θ_s	Saturated water content
$\lambda(\theta)$	Apparent thermal conductivity

λ_w	Dispersivity in the water phase
Π	CO_2 production rate
Π_o	CO_2 production rate in the open space
τ_a	Tortuosity factors in the gas phase
τ_w	Tortuosity factors in dissolved phase
$\omega(t)$	Water stress index
ω_c	Critical value of the water stress index

APPENDIX B

Soil respiration chamber measurement plots

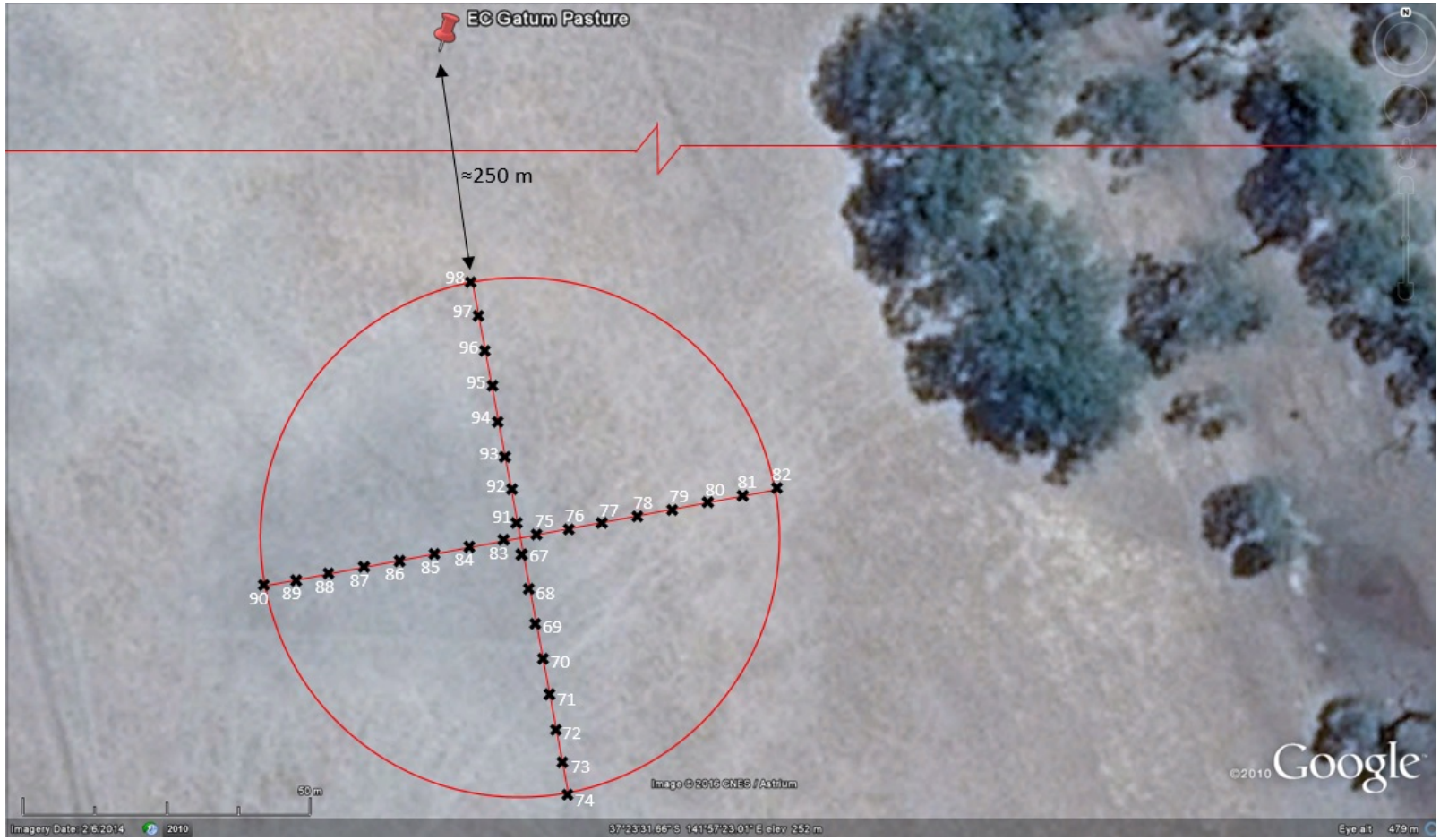

FIGURE B.1. Pasture plot for soil respiration measurements.

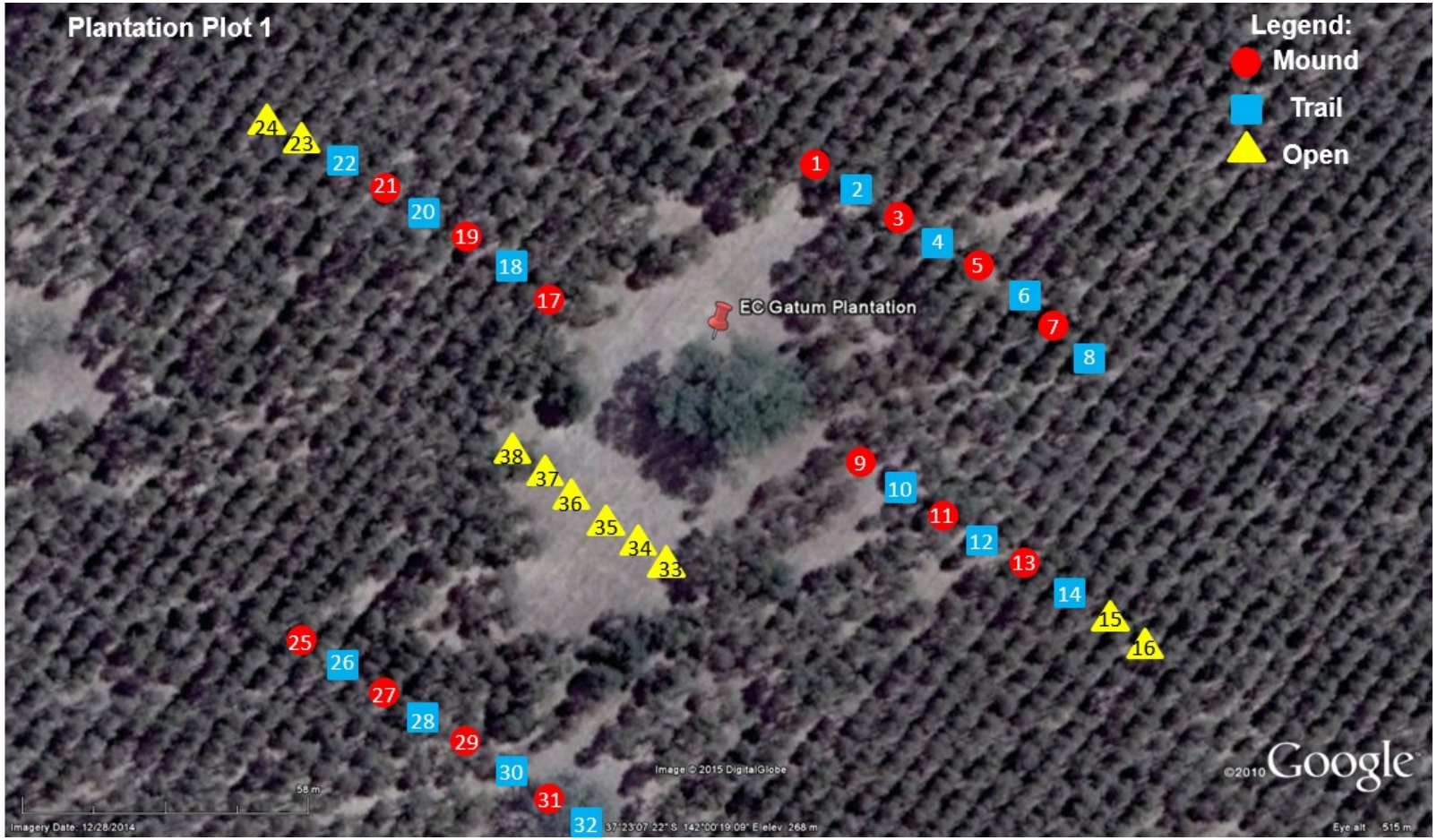

FIGURE B.2. Plot 1 of plantation for soil respiration measurements.

FIGURE B.3. Plot 2 of plantation for soil respiration measurements.

APPENDIX

Eddy-covariance data

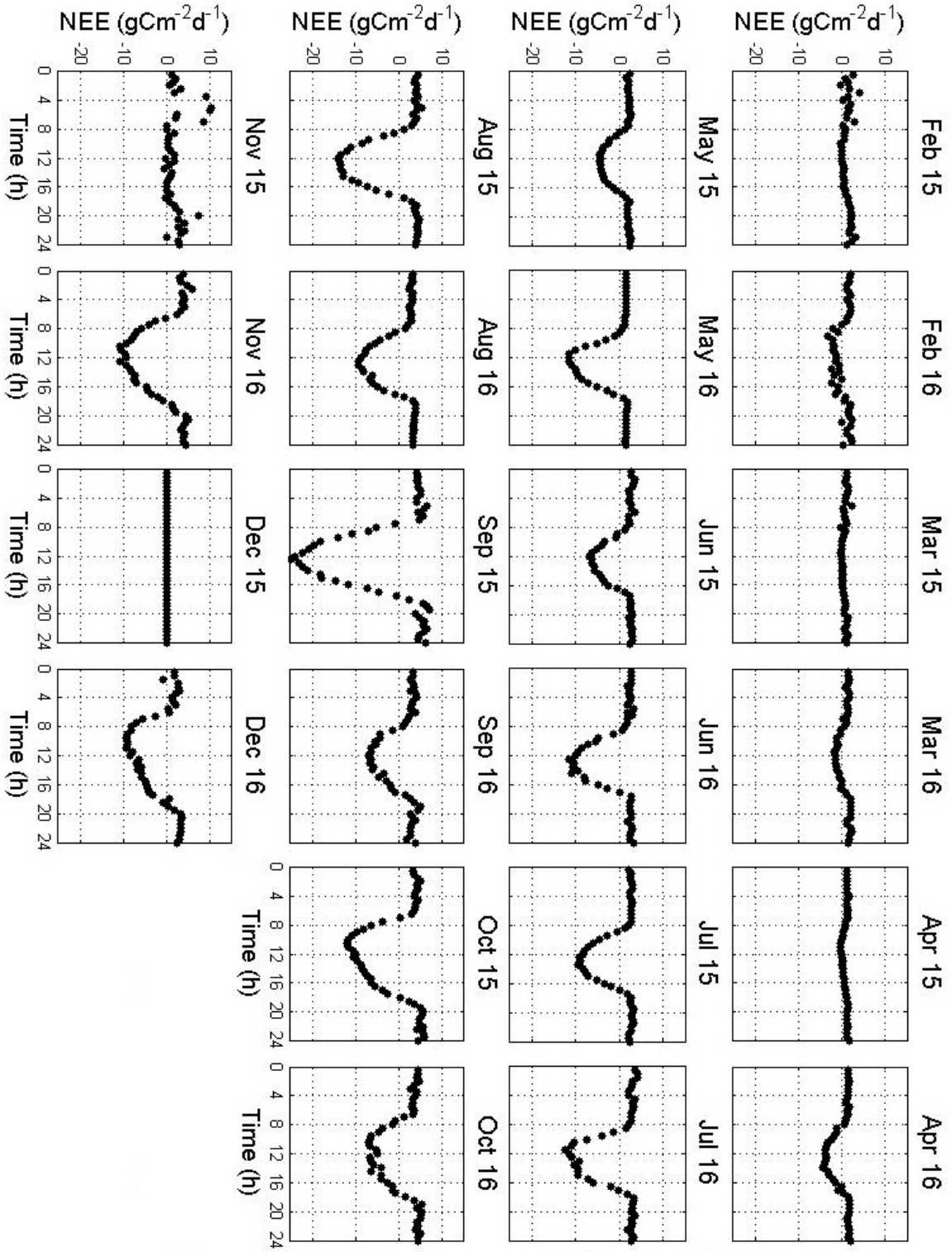

FIGURE C.1. Daily average of Net Ecosystem exchange (NEE)

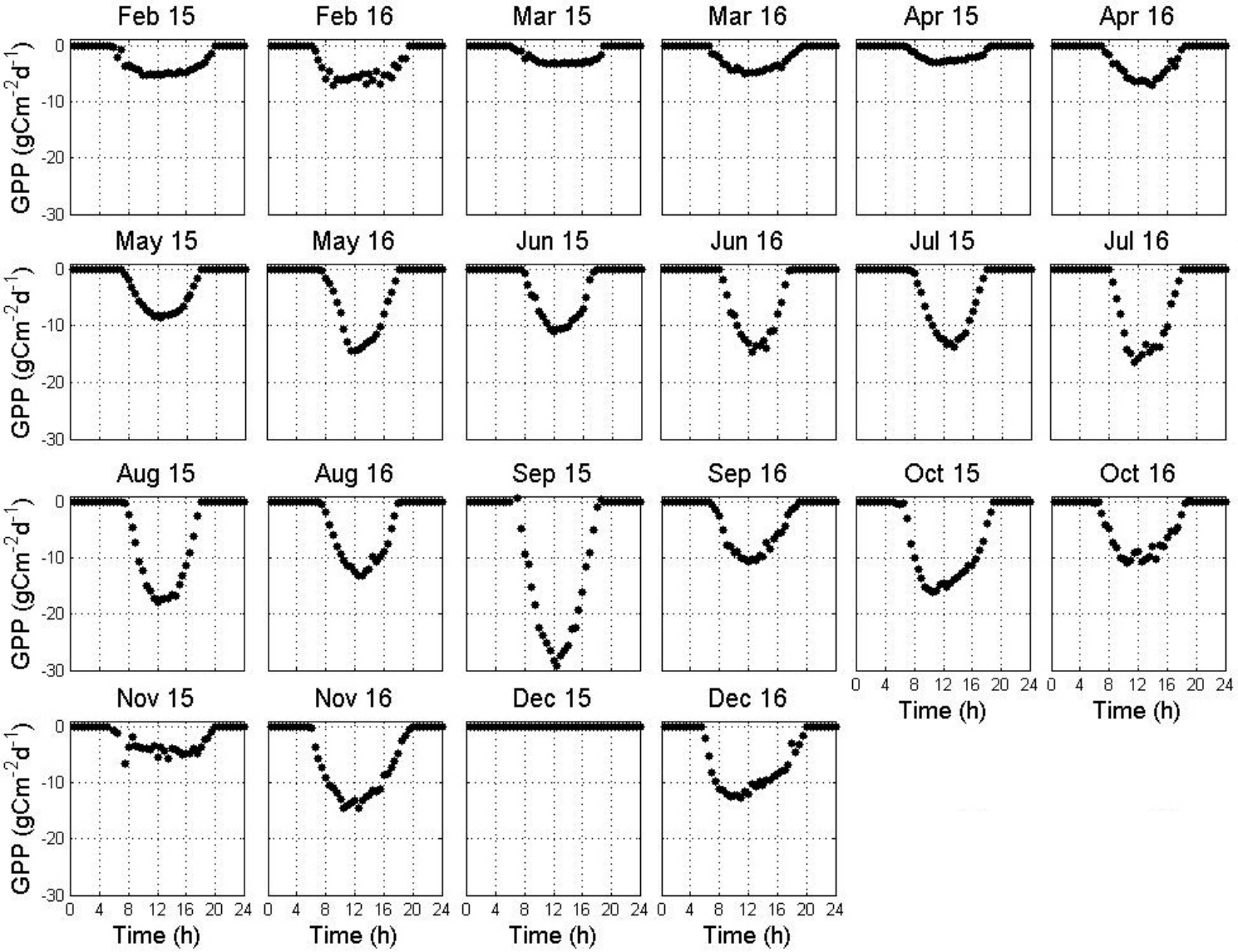

FIGURE C.2. Daily average of Gross Primary Productivity (GPP)

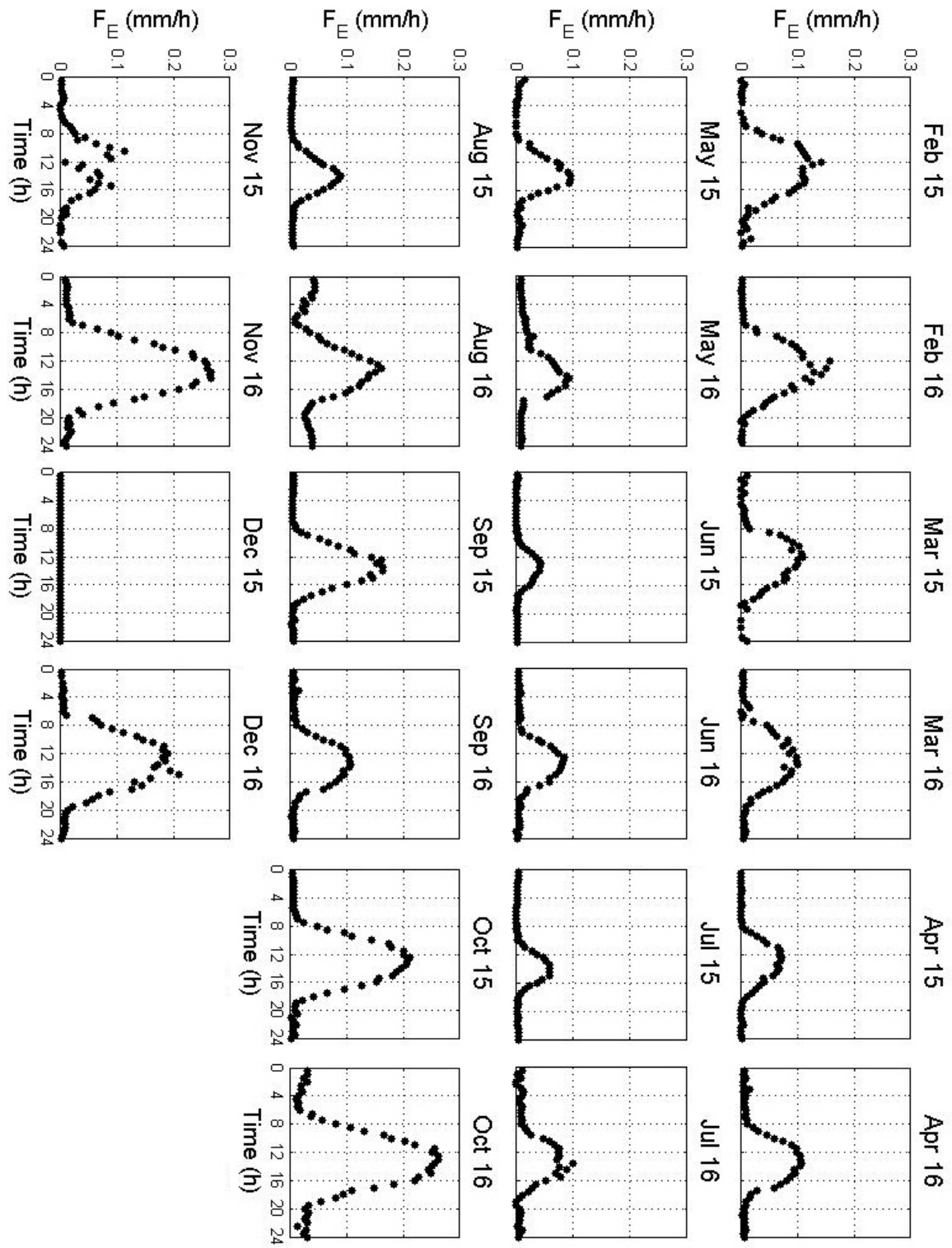

FIGURE C.3. Daily average of evapotranspiration (F_E)

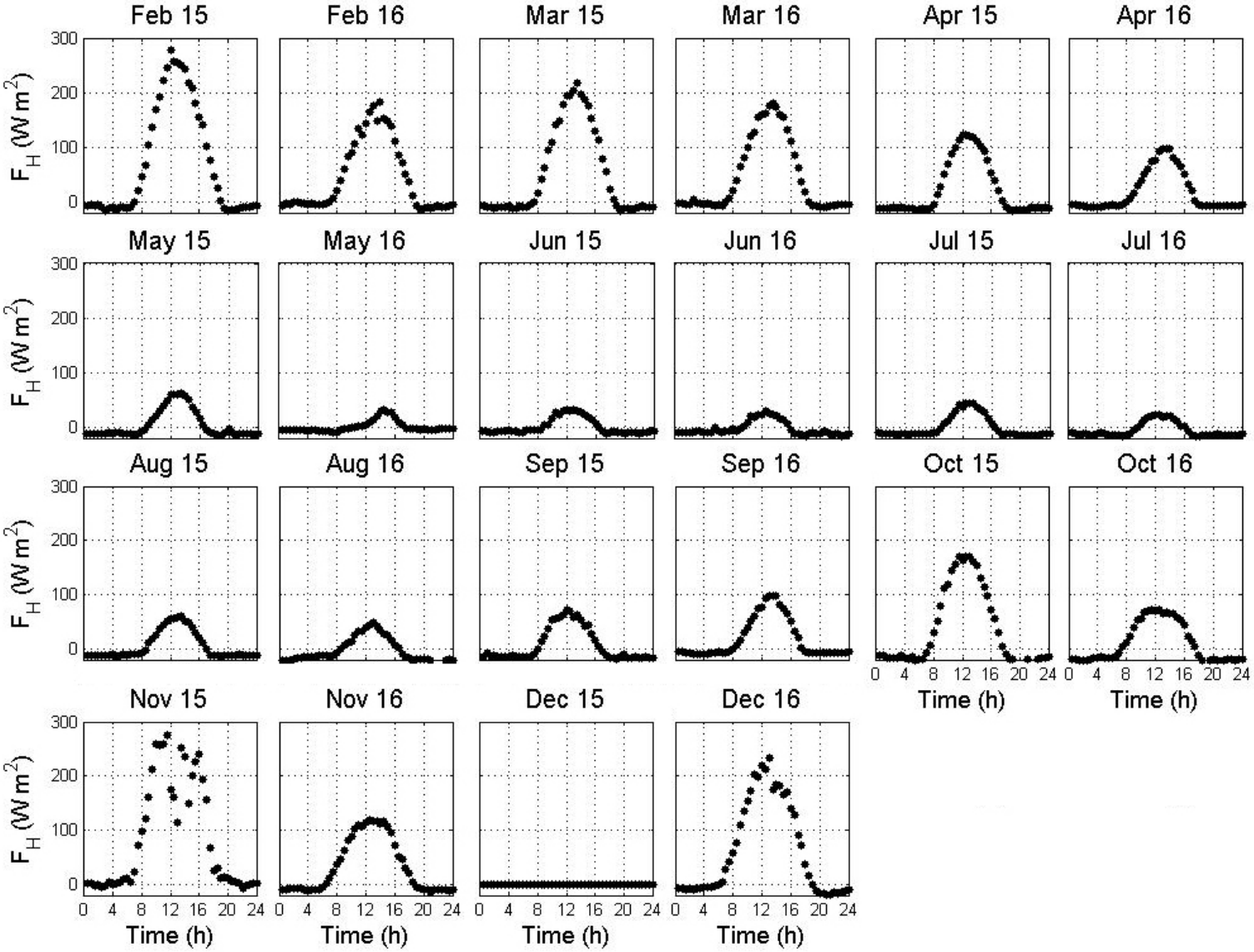

FIGURE C.4. Daily average of sensible heat flux (F_H)

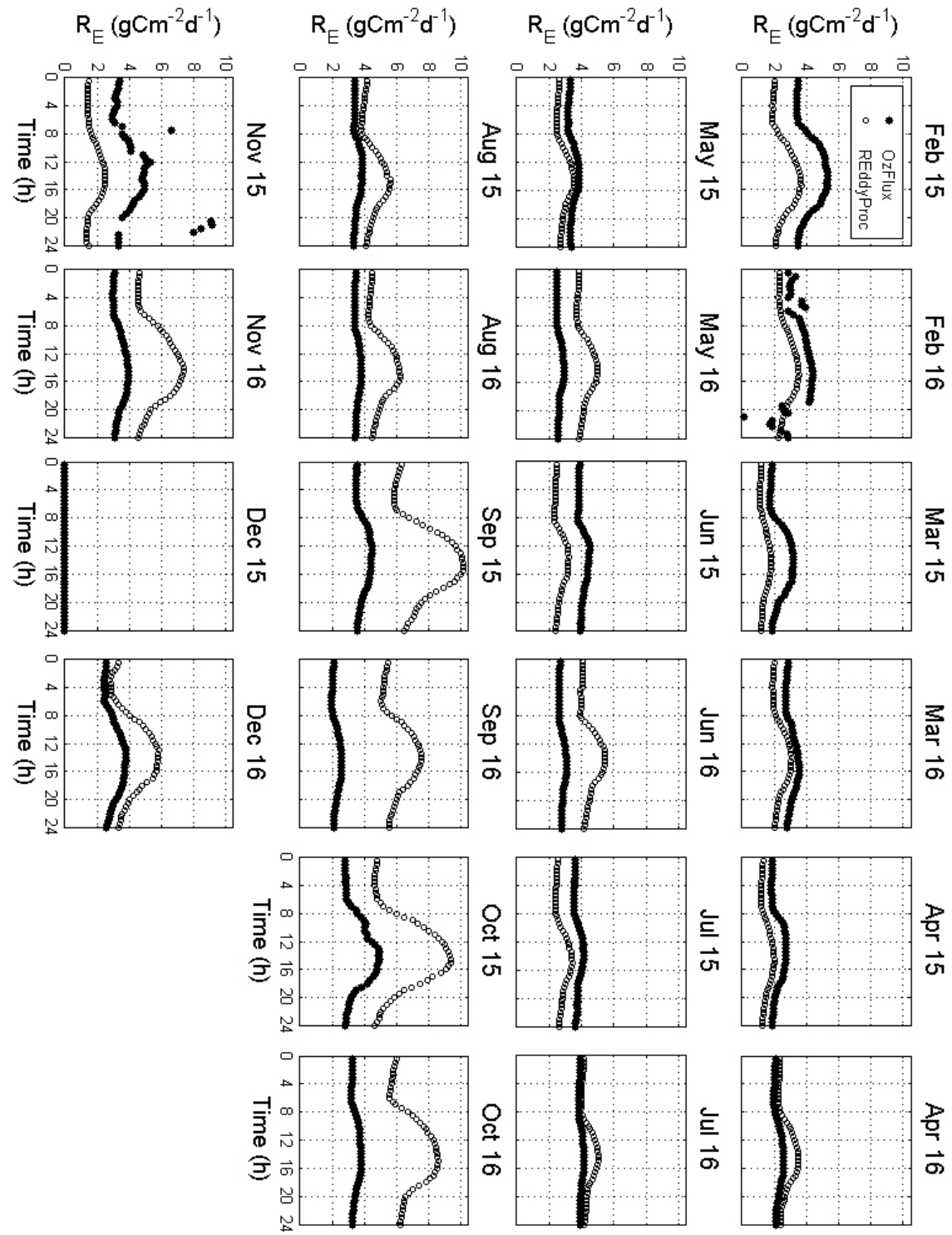

FIGURE C.5. Daily average of ecosystem respiration (R_E)

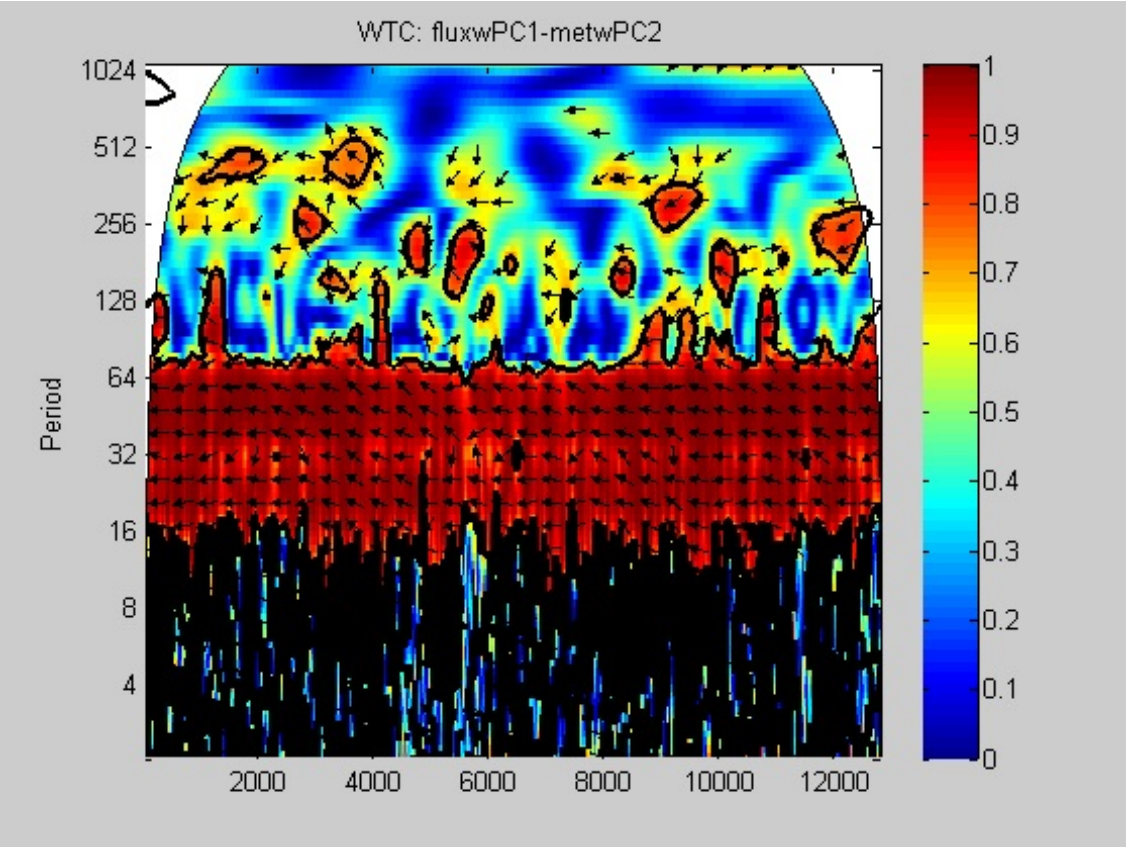

FIGURE C.6. Wavelet coherence between the fluxes and second PCA term of the drivers (2) of the 2015 data.

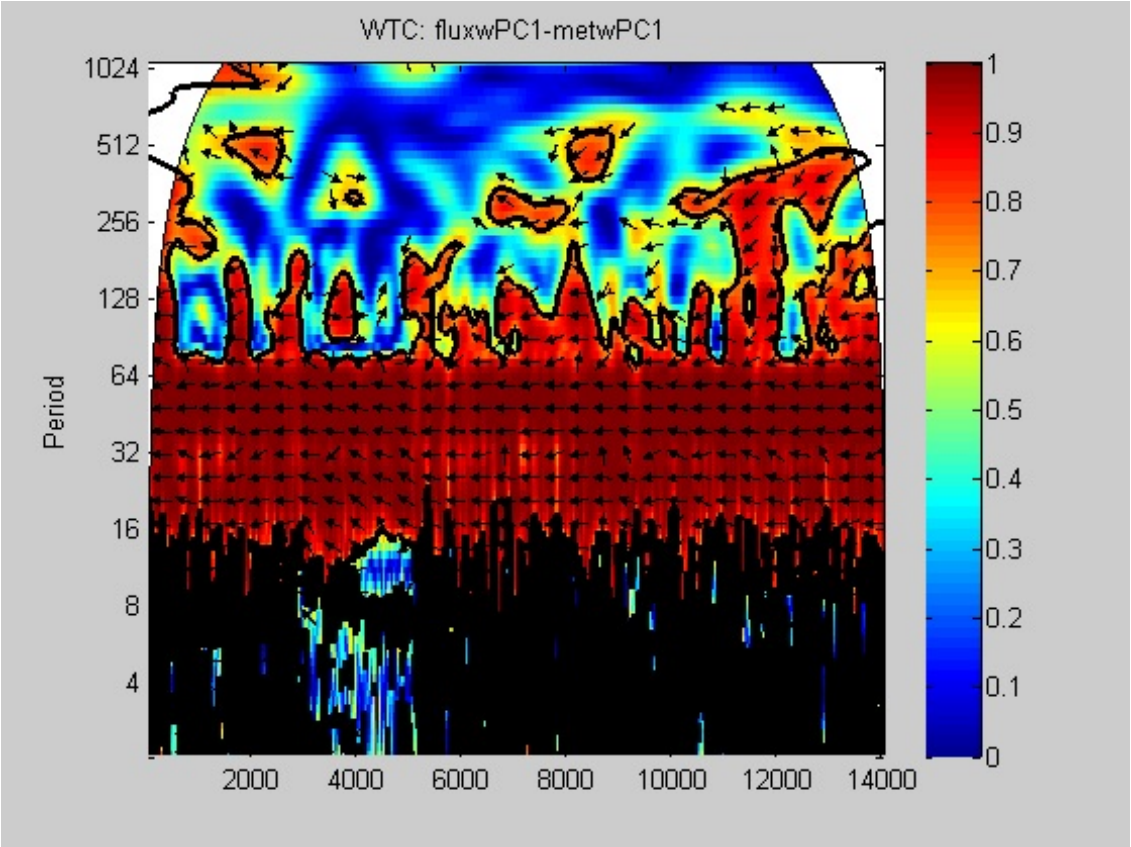

FIGURE C.7. Wavelet coherence between the fluxes and first PCA term of the drivers (1) of the 2016 data.

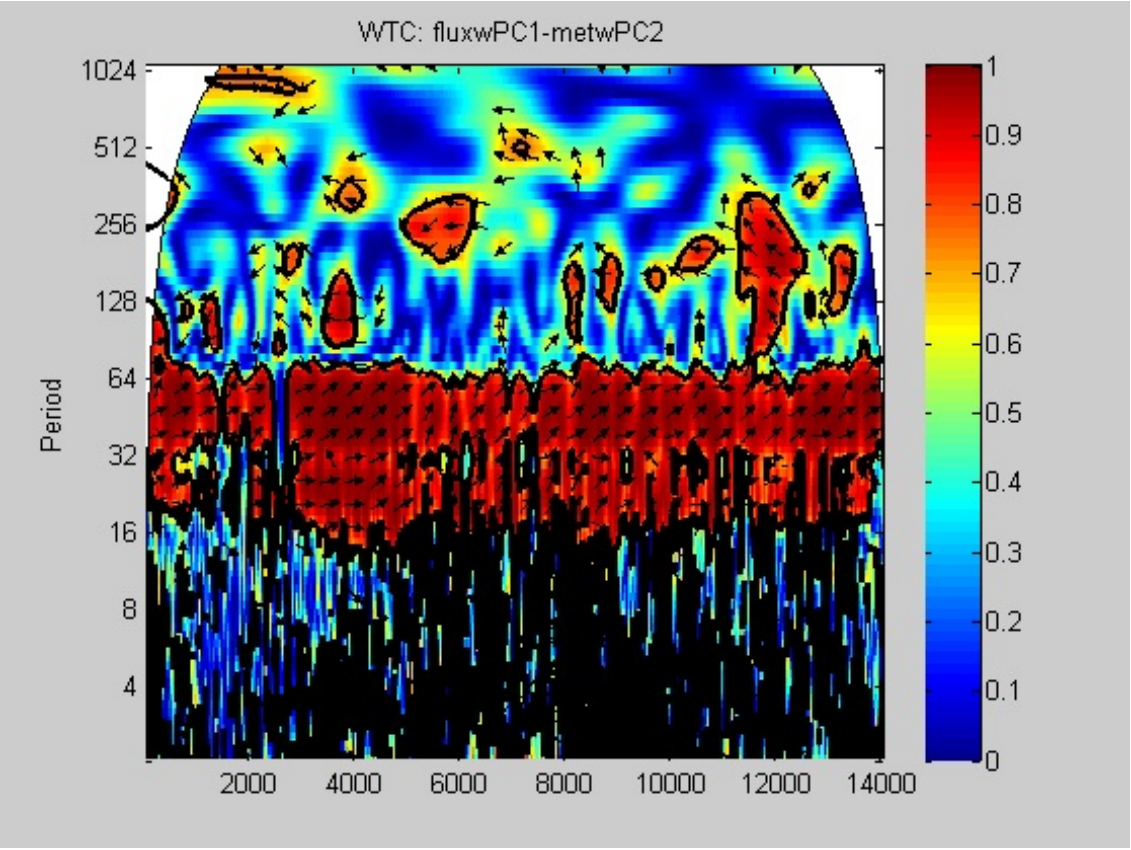

FIGURE C.8. Wavelet coherence between the fluxes and second PCA term of the drivers (2) of the 2016 data.

Appendix D

Comparison of root water uptake models and their influence on modelled soil CO2 dynamics

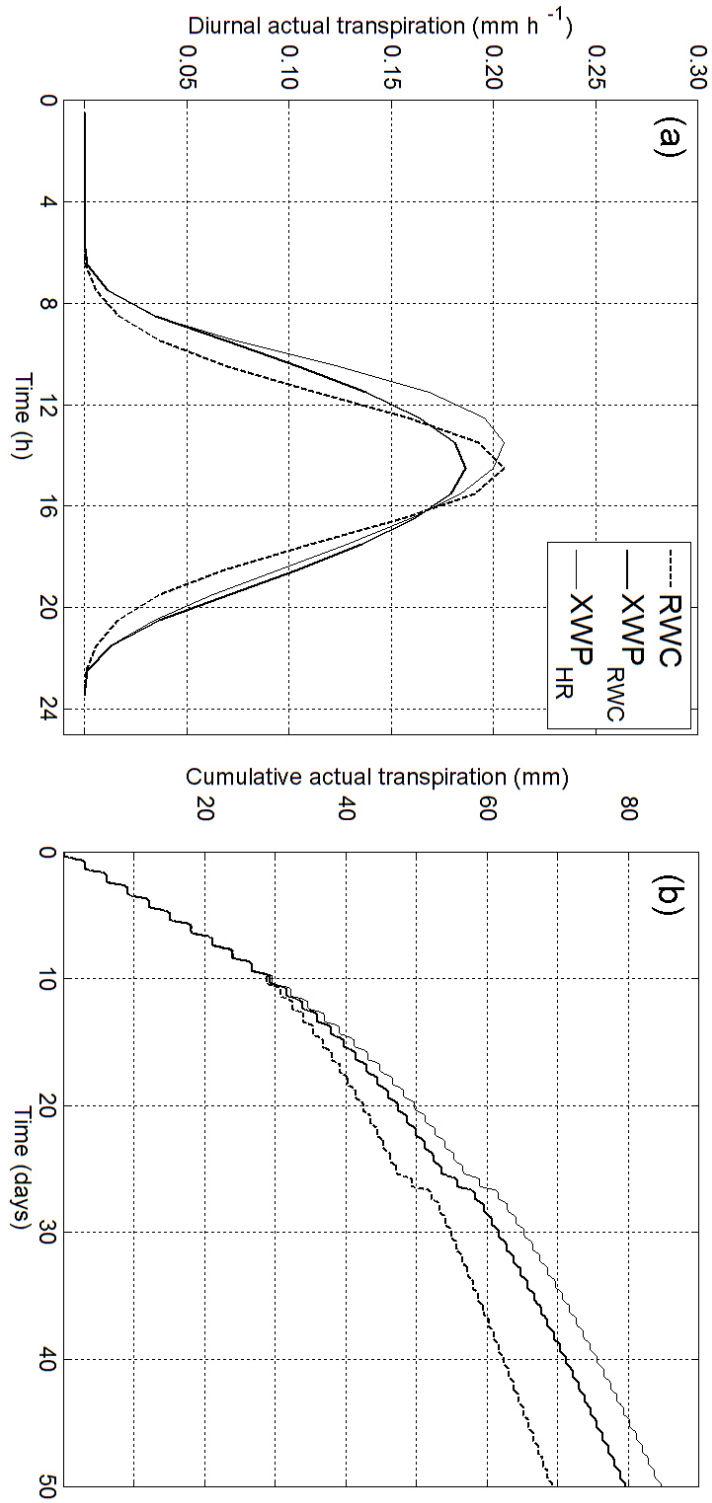

Figure D.1: (a) Average daily pattern of T_{ac} using the three models and (b) cumulative transpiration over the length of the simulation period.

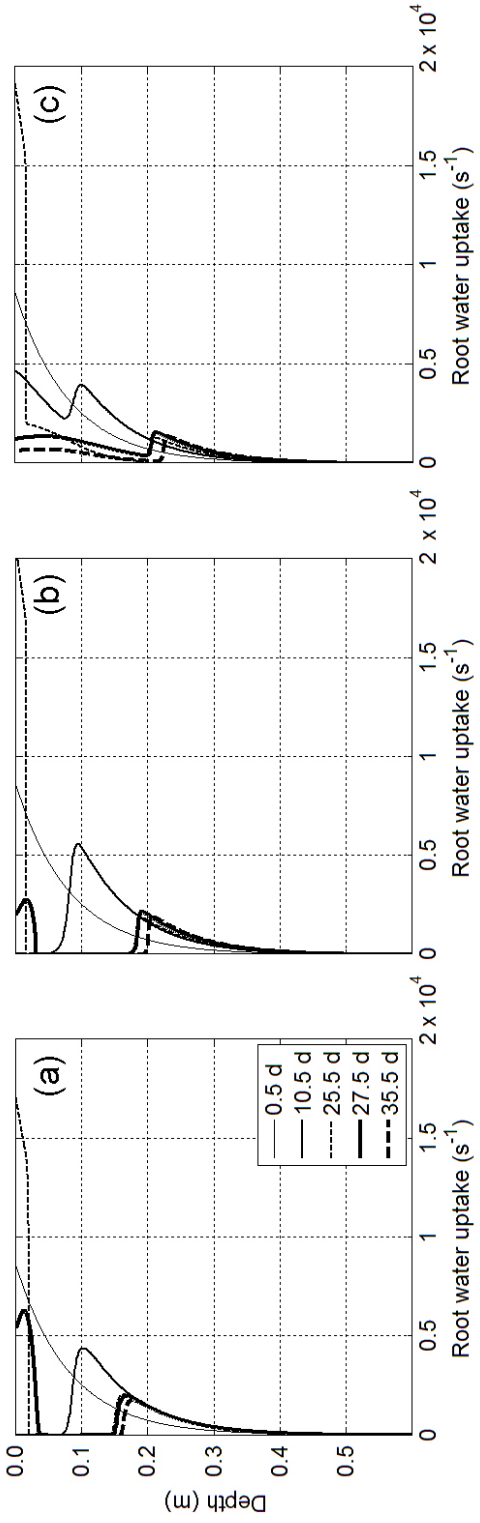

Figure D.2: Root water uptake (S) patterns for (a) RWC, (b) $\mathrm{XWP_{RWC}}$, and (c) $\mathrm{XWP_{HR}}$ in different days.

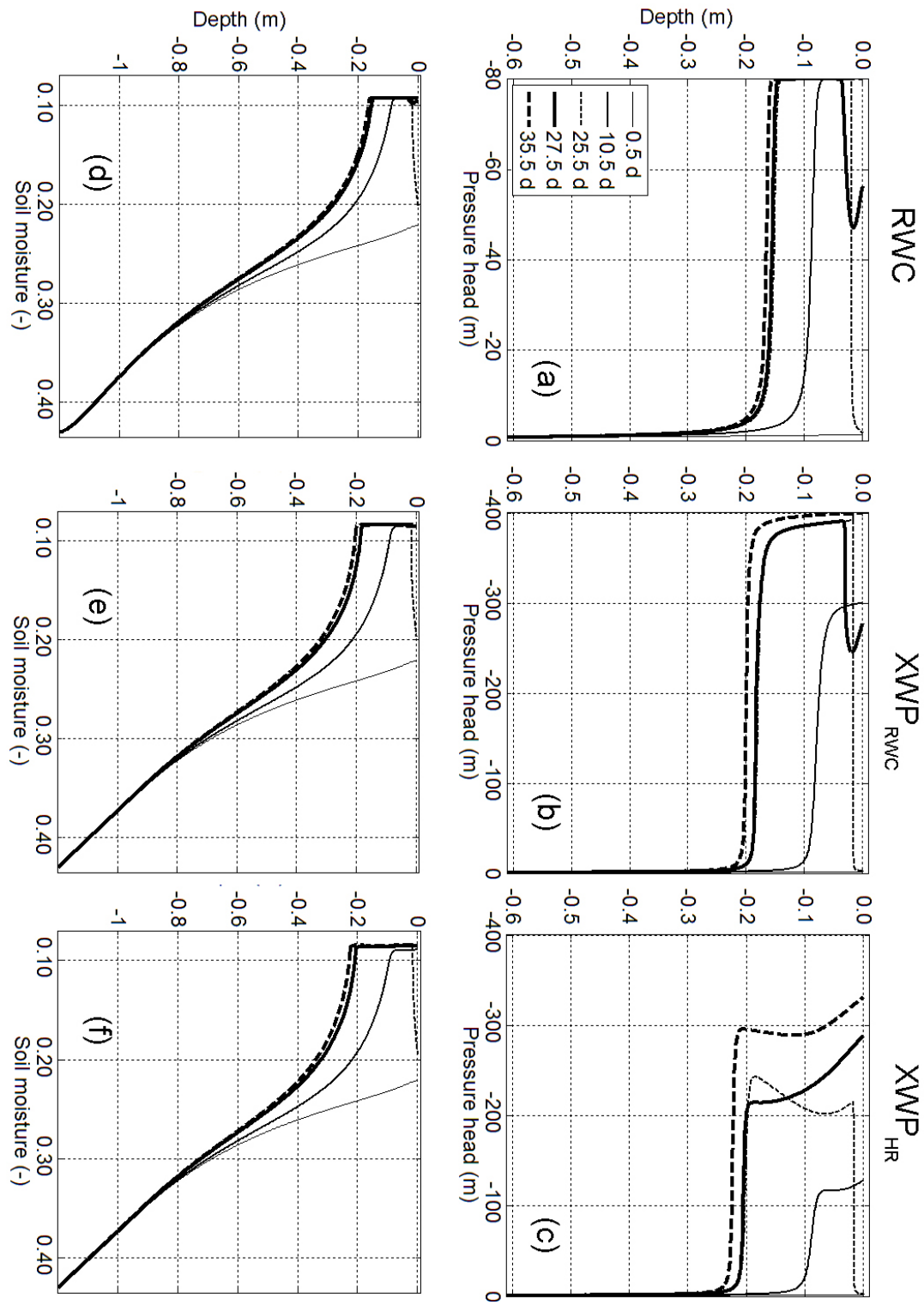

Figure D.3: (a-c) Soil water pressure head and (d-f) volumetric soil moisture (θ) profiles in different days for (a,d) RWC, (b,e) XWP_{RWC}, and (c,f) XWP_{HR}.

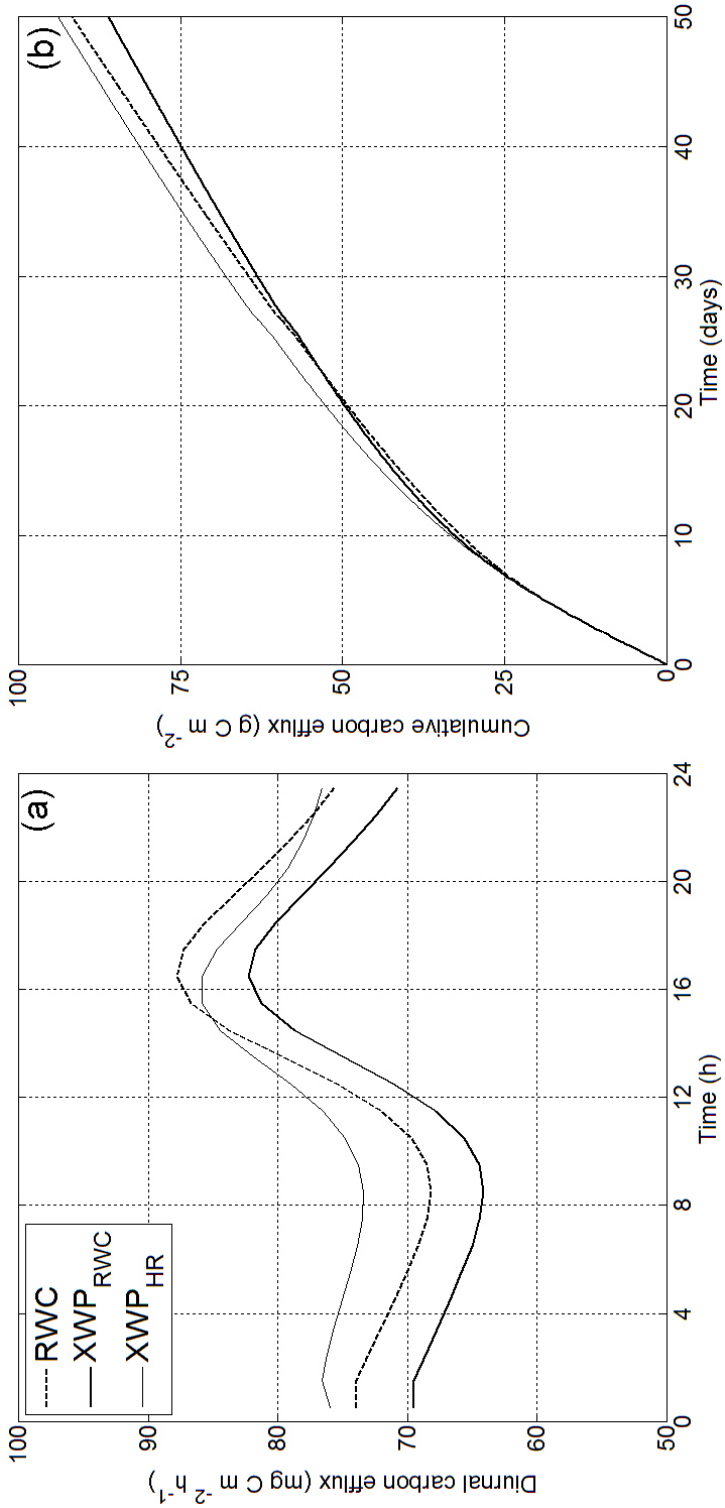

Figure D.4: (a) Average daily pattern of C efflux and (b) cumulative C efflux over the simulation period.

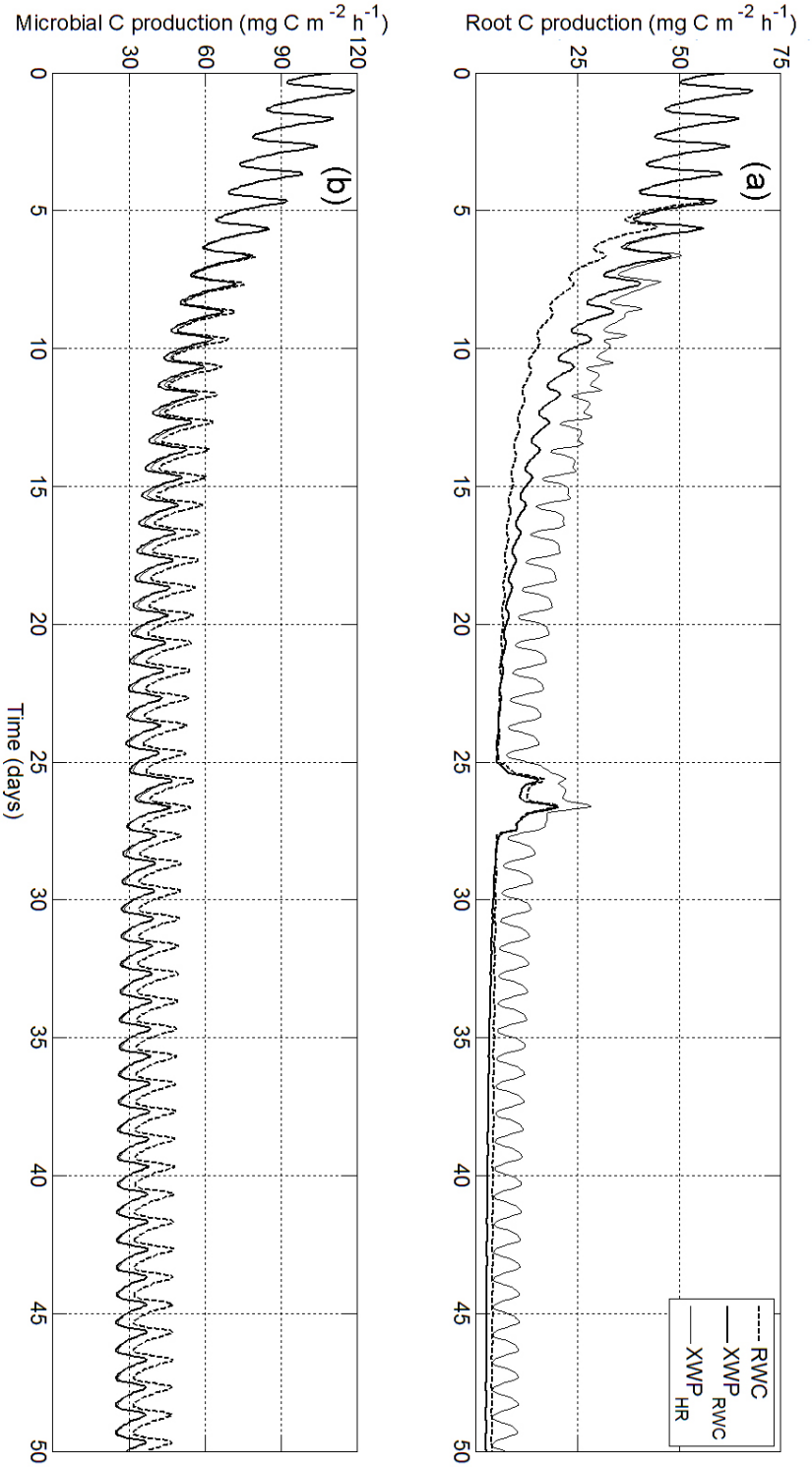

Figure D.5: Comparison between (a) plant root and (b) soil microbial production integrated along the soil profile.

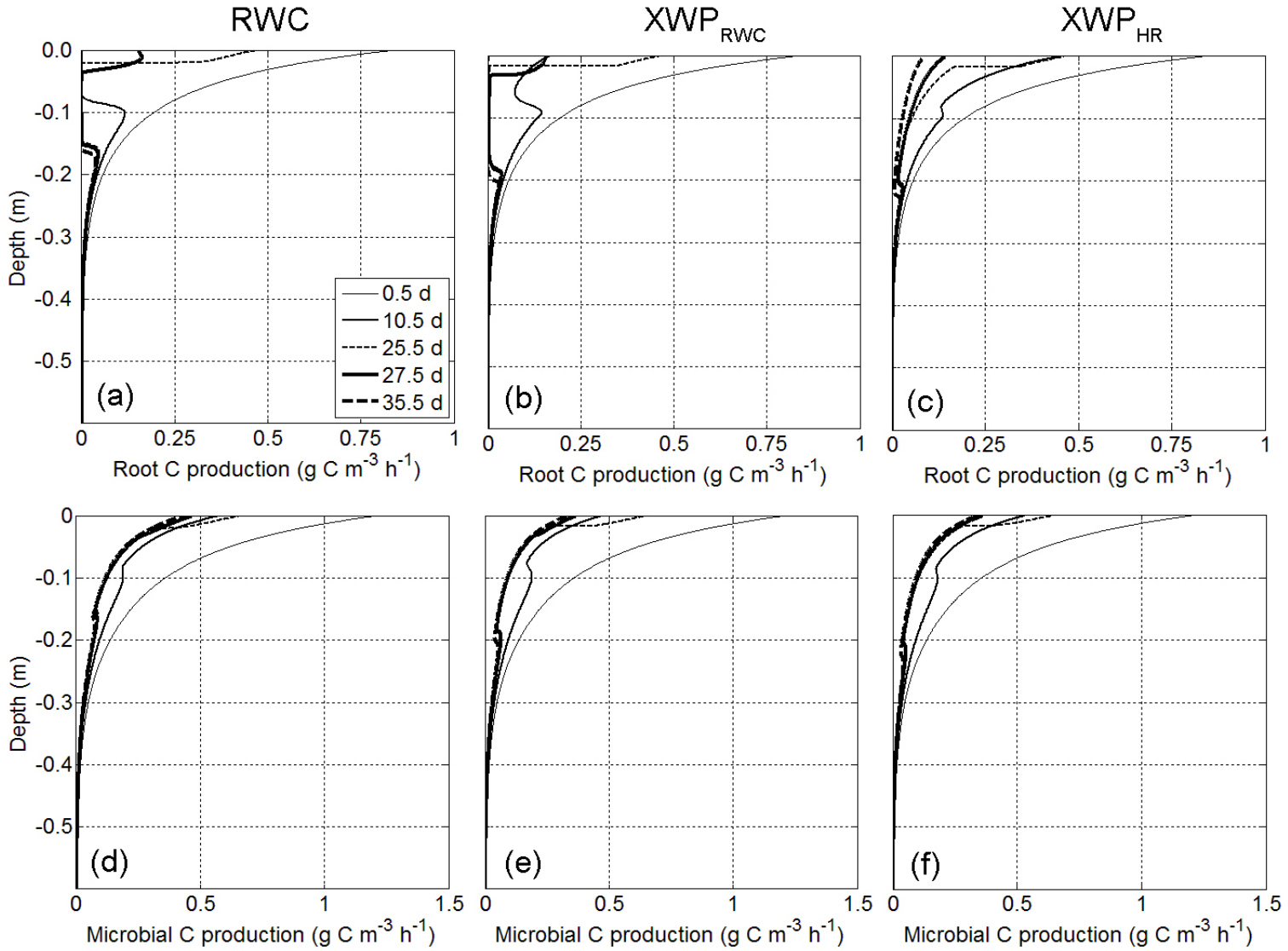

Figure D.6: (a-c) Root C production and (d-f) microbial C production profiles in different days for (a,d) RWC, (b,e) XWP_{RWC}, and (c,f) XWP_{HR}.

Appendix E

Phase change plots

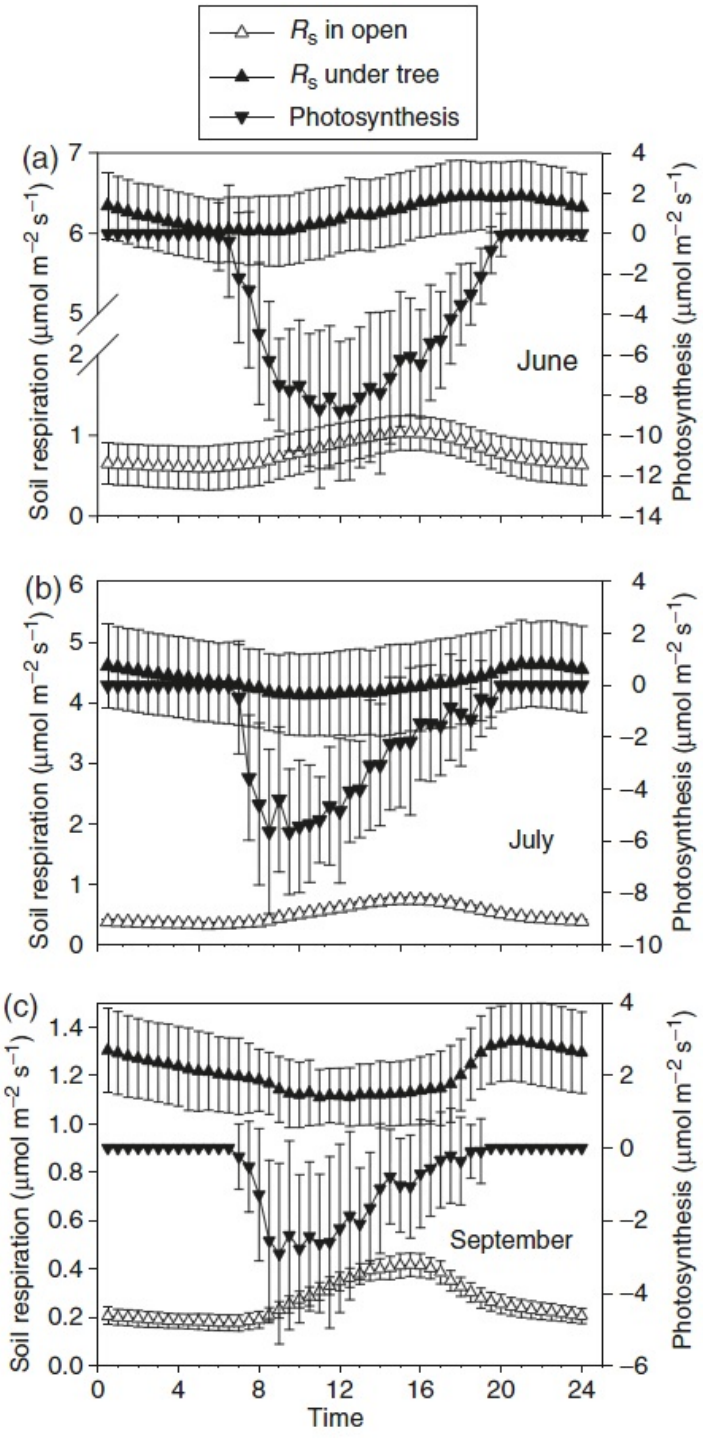

FIGURE E.1. Diurnal patterns of soil respiration (R_S) in the open, under the tree, and photosynthesis in June (a), July (b), and September (c). Values are averages of 30 days of the month (*Tang et al.*, 2005).

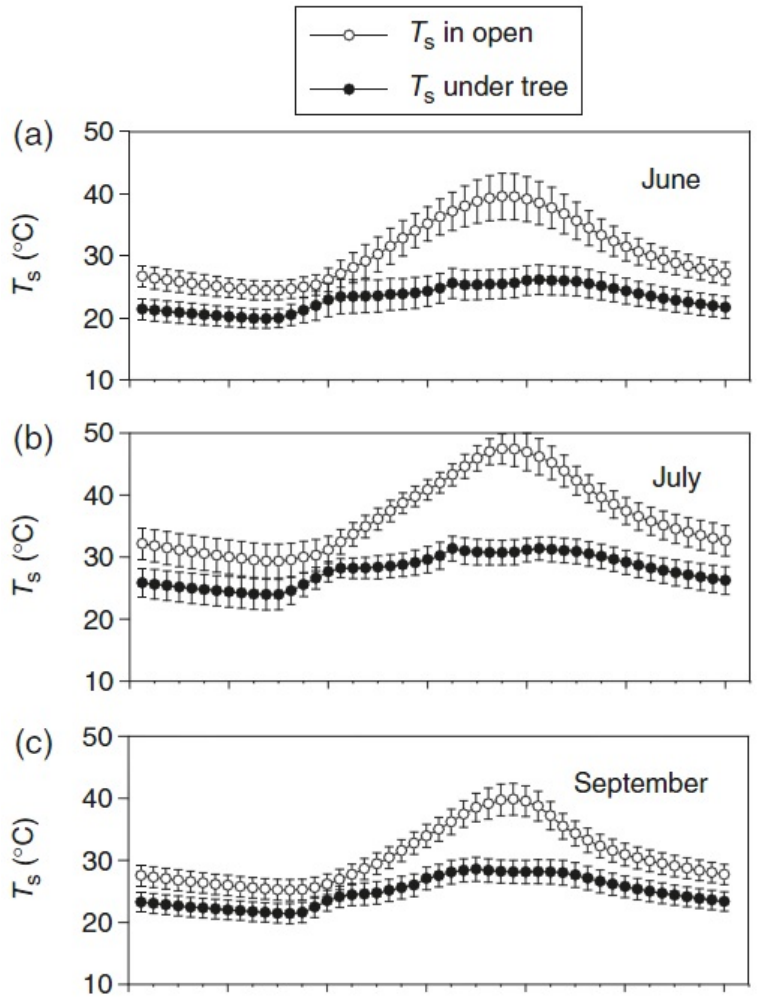

FIGURE E.2. Diurnal patterns of soil temperature (T_S) in the open and under the tree at 0.08m in June (a), July (b), and September (c). Values are averages of 30 days of the month. (*Tang et al.*, 2005).

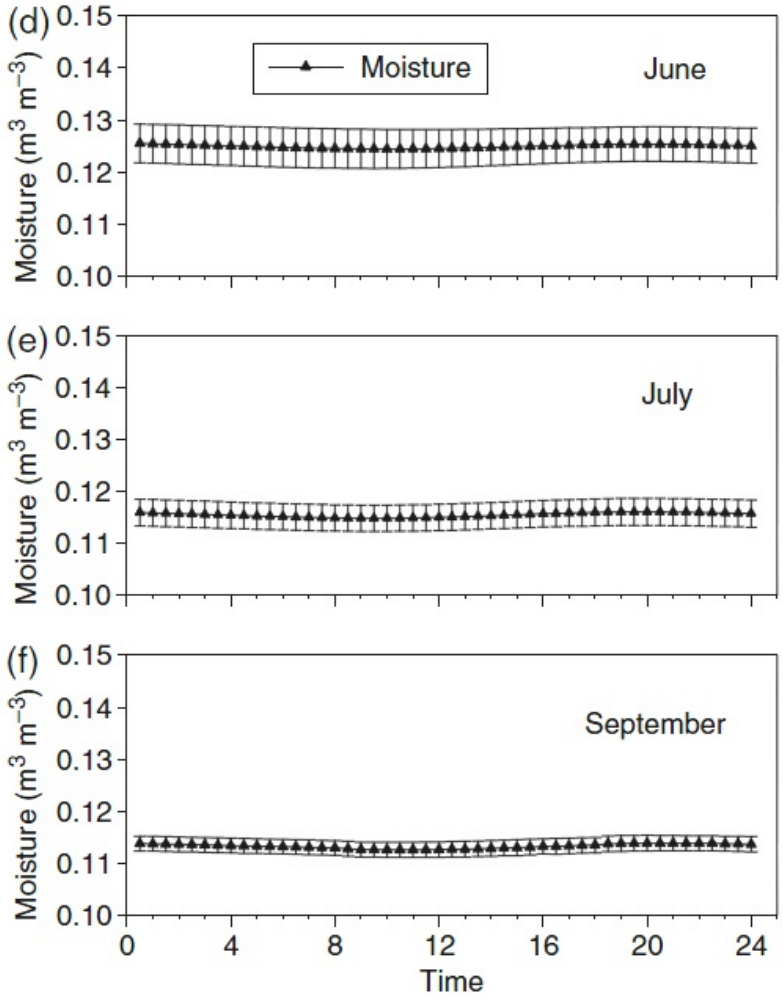

FIGURE E.3. Diurnal patterns of soil volumetric moisture under the tree at 0.1m in June (d), July (e), and September (f). Values are averages of 30 days of the month (*Tang et al.*, 2005).

References

Abdalla, M., M. Saunders, A. Hastings, M. Williams, P. Smith, B. Osborne, G. Lanigan, and M. B. Jones (2013), Simulating the impacts of land use in Northwest Europe on Net Ecosystem Exchange (NEE): The role of arable ecosystems, grasslands and forest plantations in climate change mitigation, *Science of the Total Environment*, *465*, 325–336.

Adelana, S. M., P. E. Dresel, P. Hekmeijer, H. Zydor, J. A. Webb, M. Reynolds, and M. Ryan (2015), A comparison of streamflow, salt and water balances in adjacent farmland and forest catchments in south-western victoria, australia, *Hydrological Processes*, *29*(6), 1630–1643.

Almagro, M., J. López, J. Querejeta, and M. Martínez-Mena (2009), Temperature dependence of soil co 2 efflux is strongly modulated by seasonal patterns of moisture availability in a mediterranean ecosystem, *Soil Biology and Biochemistry*, *41*(3), 594–605.

Almagro, M., J. I. Querejeta, C. Boix-Fayos, and M. Martínez-Mena (2013), Links between vegetation patterns, soil c and n pools and respiration rate under three different land uses in a dry mediterranean ecosystem, *Journal of Soils and Sediments*, *13*(4), 641–653.

Amenu, G., and P. Kumar (2007), A model for hydraulic redistribution incorporating coupled soil-root moisture transport, *Hydrology and Earth System Sciences Discussions*, *4*(5), 3719–3769.

Archibald, S., A. Kirton, M. Van der Merwe, R. Scholes, C. Williams, and N. Hanan (2009), Drivers of inter-annual variability in net ecosystem exchange in a semi-arid savanna ecosystem, south africa, *Biogeosciences*, *6*(2), 251–266.

Arneth, A., F. Kelliher, T. McSeveny, and J. Byers (1998), Net ecosystem productivity, net primary productivity and ecosystem carbon sequestration in a pinus radiata plantation subject to soil water deficit, *Tree Physiology*, *18*(12), 785–793.

Aroca, R., R. Porcel, and J. M. Ruiz-Lozano (2012), Regulation of root water uptake under abiotic stress conditions, *Journal of experimental botany*, *63*(1), 43–57.

Baldocchi, D. (2014), Measuring fluxes of trace gases and energy between ecosystems and the atmosphere–the state and future of the eddy covariance method, *Global change biology*, *20*(12), 3600–3609.

Baldocchi, D., J. Tang, and L. Xu (2006), How switches and lags in biophysical regulators affect spatial-temporal variation of soil respiration in an oak-grass savanna, *Journal of Geophysical Research: Biogeosciences*, *111*(G2).

Baldocchi, D., J. Verfaillie, and S. Ma (2014), *Thirteen years flux observations at Tonzi (US-Ton) and Vaira (US-Var).*

Balogh, J., S. Fóti, K. Pintér, S. Burri, W. Eugster, M. Papp, and Z. Nagy (2015), Soil co2 efflux and production rates as influenced by evapotranspiration in a dry grassland, *Plant and Soil*, *388*(1-2), 157–173.

Barba, J., J. C. Yuste, J. Martínez-Vilalta, and F. Lloret (2013), Drought-induced tree species replacement is reflected in the spatial variability of soil respiration in a mixed mediterranean forest, *Forest Ecology and Management*, *306*, 79–87.

Bauer, J., M. Herbst, J. Huisman, L. Weihermueller, and H. Vereecken (2008), Sensitivity of simulated soil heterotrophic respiration to temperature and moisture reduction functions, *Geoderma*, *145*(1), 17–27.

Benyon, R., T. Doody, S. Theiveyanathan, and V. Koul (2009), Plantation forest water use in southwest victoria: report prepared for the forest and wood products australia, *Project No: PNC064-0607, 103p.*

Benyon, R. G., S. Theiveyanathan, and T. M. Doody (2006), Impacts of tree plantations on groundwater in south-eastern australia, *Australian Journal of Botany*, *54*(2), 181–192.

Biosciences, L. (2012), Eddypro eddy covariance software version 4.0 userâĂŹs guide & reference, *LI-COR Inc., Lincoln.*

Bonan, G. (2015), *Ecological climatology: concepts and applications*, Cambridge University Press.

Bond-Lamberty, B., and A. Thomson (2010), Temperature-associated increases in the global soil respiration record, *Nature*, *464*(7288), 579–582.

Buysse, P., C. R. Flechard, Y. Hamon, and V. Viaud (2016), Impacts of water regime and land-use on soil co2 efflux in a small temperate agricultural catchment, *Biogeochemistry*, *130*(3), 267–288.

Caldwell, M. M., T. E. Dawson, and J. H. Richards (1998), Hydraulic lift: consequences of water efflux from the roots of plants, *Oecologia*, *113*(2), 151–161.

Camargo, G., and A. Kemanian (2016), Six crop models differ in their simulation of water uptake, *Agricultural and Forest Meteorology*, *220*, 116–129.

Campioli, M., S. Vicca, S. Luyssaert, J. Bilcke, E. Ceschia, F. Chapin III, P. Ciais, M. Fernández-Martínez, Y. Malhi, M. Obersteiner, et al. (2015), Biomass production efficiency controlled by management in temperate and boreal ecosystems, *Nature Geoscience*, *8*(11), 843–846.

Carbone, M. S., C. J. Still, A. R. Ambrose, T. E. Dawson, A. P. Williams, C. M. Boot, S. M. Schaeffer, and J. P. Schimel (2011), Seasonal and episodic moisture controls on plant and microbial contributions to soil respiration, *Oecologia*, *167*(1), 265–278.

Chen, D., J. Molina, C. Clapp, R. Venterea, and A. Palazzo (2005), Corn root influence on automated measurement of soil carbon dioxide concentrations, *Soil science*, *170*(10), 779–787.

Chen, J., Q. Wang, M. Li, F. Liu, and W. Li (2016), Does the different photosynthetic pathway of plants affect soil respiration in a subtropical wetland?, *Ecology and Evolution*, *6*(22), 8010–8017.

Cleverly, J., and P. Isaac (2015), Ozfluxqc simulator version 2.8. 6, *GitHub repository*.

Correia, A., F. Minunno, M. Caldeira, J. Banza, J. Mateus, M. Carneiro, L. Wingate, A. Shvaleva, A. Ramos, M. Jongen, et al. (2012), Soil water availability strongly modulates soil co 2 efflux in different mediterranean ecosystems: Model calibration using the bayesian approach, *Agriculture, ecosystems & environment*, *161*, 88–100.

Couvreur, V., J. Vanderborght, and M. Javaux (2012), A simple three-dimensional macroscopic root water uptake model based on the hydraulic architecture approach, *Hydrology and earth system sciences*, *16*(8), 2957–2971.

Da Rocha, H. R., M. L. Goulden, S. D. Miller, M. C. Menton, L. D. Pinto, H. C. de Freitas, et al. (2004), Seasonality of water and heat fluxes over a tropical forest in eastern amazonia, *Ecological applications*, *14*(sp4), 22–32.

Daly, E., S. Palmroth, P. Stoy, M. Siqueira, A. C. Oishi, J.-Y. Juang, R. Oren, A. Porporato, and G. G. Katul (2009), The effects of elevated atmospheric co2 and nitrogen amendments on subsurface co2 production and concentration dynamics in a maturing pine forest, *Biogeochemistry*, *94*(3), 271–287.

Davidson, E., E. Belk, R. D. Boone, et al. (1998), Soil water content and temperature as independent or confounded factors controlling soil respiration in a temperate mixed hardwood forest, *Global change biology*, *4*(2), 217–227.

de Jong van Lier, Q., J. C. van Dam, A. Durigon, M. A. Dos Santos, and K. Metselaar (2013), Modeling water potentials and flows in the soil–plant system comparing hydraulic resistances and transpiration reduction functions, *Vadose Zone Journal*, *12*(3).

de Willigen, P., J. C. van Dam, M. Javaux, and M. Heinen (2012), Root water uptake as simulated by three soil water flow models, *Vadose Zone Journal*, *11*(3).

Dean, J., M. Camporese, J. Webb, S. Grover, P. Dresel, and E. Daly (2016), Water balance complexities in ephemeral catchments with different land uses: Insights from monitoring and distributed hydrologic modeling, *Water Resources Research*.

Domec, J. C., F. Scholz, S. Bucci, F. Meinzer, G. Goldstein, and R. Villalobos-Vega (2006), Diurnal and seasonal variation in root xylem embolism in neotropical savanna woody species: impact on stomatal control of plant water status, *Plant, Cell & Environment*, *29*(1), 26–35.

Domec, J.-C., J. S. King, A. Noormets, E. Treasure, M. J. Gavazzi, G. Sun, and S. G. McNulty (2010), Hydraulic redistribution of soil water by roots affects whole-stand evapotranspiration and net ecosystem carbon exchange, *New Phytologist*, *187*(1), 171–183.

Etzold, S., N. K. Ruehr, R. Zweifel, M. Dobbertin, A. Zingg, P. Pluess, R. Häsler, W. Eugster, and N. Buchmann (2011), The carbon balance of two contrasting mountain forest ecosystems in switzerland: similar annual trends, but seasonal differences, *Ecosystems*, *14*(8), 1289–1309.

Fang, C., and J. B. Moncrieff (1999), A model for soil co 2 production and transport 1:: Model development, *Agricultural and Forest Meteorology*, *95*(4), 225–236.

Feddes, R. A., P. J. Kowalik, H. Zaradny, et al. (1978), *Simulation of field water use and crop yield.*, Centre for Agricultural Publishing and Documentation.

Gilmanov, T. G., S. B. Verma, P. L. Sims, T. P. Meyers, J. A. Bradford, G. G. Burba, and A. E. Suyker (2003), Gross primary production and light response parameters of four southern plains ecosystems estimated using long-term co2-flux tower measurements, *Global Biogeochemical Cycles*, *17*(2).

Goffin, S., C. Wylock, B. Haut, M. Maier, B. Longdoz, and M. Aubinet (2015), Modeling soil co2 production and transport to investigate the intra-day variability of surface efflux and soil co2 concentration measurements in a scots pine forest (pinus sylvestris, l.), *Plant and soil*, *390*(1-2), 195–211.

Granier, A., E. Ceschia, C. Damesin, E. Dufrêne, D. Epron, P. Gross, S. Lebaube, V. Le Dantec, N. Le Goff, D. Lemoine, et al. (2000), The carbon balance of a young beech forest, *Functional ecology*, *14*(3), 312–325.

Grindlay, D. (Updated: August 2015), *Port of Portland now biggest exporter of blue gum hardwood chips in the world*, ABC News. http://www.abc.net.au/news/2015-08-18/blue-gum-portland-woodchips-exports-china-japan-forestry/6704158. Accessed: January 2016.

Han, G., Y. Luo, D. Li, J. Xia, Q. Xing, and J. Yu (2014), Ecosystem photosynthesis regulates soil respiration on a diurnal scale with a short-term time lag in a coastal wetland, *Soil Biology and Biochemistry*, *68*, 85–94.

Hanson, P., S. Wullschleger, S. Bohlman, and D. Todd (1993), Seasonal and topographic patterns of forest floor co2 efflux from an upland oak forest, *Tree physiology*, *13*(1), 1–15.

Heinemeyer, A., M. Wilkinson, R. Vargas, J.-A. Subke, E. Casella, J. I. Morison, and P. Ineson (2012), Exploring the" overflow tap" theory: linking forest soil co2 fluxes and individual mycorrhizosphere components to photosynthesis, *Biogeosciences*, *9*(1), 79.

Henzell, T. (2007), *Australian agriculture: its history and challenges*, CSIRO publishing.

Herbst, M., N. Prolingheuer, A. Graf, J. Huisman, L. Weihermüller, and J. Vanderborght (2009), Characterization and understanding of bare soil respiration spatial variability at plot scale, *Vadose Zone Journal*, *8*(3), 762–771.

Herkelrath, W., E. Miller, and W. Gardner (1977), Water uptake by plants: Ii. the root contact model, *Soil Science Society of America Journal*, *41*(6), 1039–1043.

Hirano, T., H. Kim, and Y. Tanaka (2003), Long-term half-hourly measurement of soil co2 concentration and soil respiration in a temperate deciduous forest, *Journal of Geophysical Research: Atmospheres*, *108*(D20).

Howard, A. R., M. W. Van Iersel, J. H. Richards, and L. A. Donovan (2009), Night-time transpiration can decrease hydraulic redistribution, *Plant, Cell & Environment*, *32*(8), 1060–1070.

Jackson, R. B., E. G. Jobbágy, R. Avissar, S. B. Roy, D. J. Barrett, C. W. Cook, K. A. Farley, D. C. Le Maitre, B. A. McCarl, and B. C. Murray (2005), Trading water for carbon with biological carbon sequestration, *science*, *310*(5756), 1944–1947.

Jarvis, N. (1989), A simple empirical model of root water uptake, *Journal of Hydrology*, *107*(1-4), 57–72.

Jarvis, N. (2010), Comment on macroscopic root water uptake distribution using a matric flux potential approach, *Vadose Zone Journal*, *9*(2), 499–502.

Jarvis, N. (2011), Simple physics-based models of compensatory plant water uptake: Concepts and eco-hydrological consequences, *Hydrology and Earth System Sciences*, *15*(11), 3431–3446.

Jassal, R. S., T. A. Black, M. D. Novak, D. Gaumont-Guay, and Z. Nesic (2008), Effect of soil water stress on soil respiration and its temperature sensitivity in an 18-year-old temperate douglas-fir stand, *Global Change Biology*, *14*(6), 1305–1318.

Javaux, M., V. Couvreur, J. Vanderborght, and H. Vereecken (2013), Root water uptake: from three-dimensional biophysical processes to macroscopic modeling approaches, *Vadose Zone Journal*, *12*(4).

Kilinc, M., J. Beringer, L. B. Hutley, N. J. Tapper, and D. A. McGuire (2013), Carbon and water exchange of the world's tallest angiosperm forest, *Agricultural and forest meteorology*, *182*, 215–224.

Kuzyakov, Y., and O. Gavrichkova (2010), Review: Time lag between photosynthesis and carbon dioxide efflux from soil: a review of mechanisms and controls, *Global Change Biology*, *16*(12), 3386–3406.

Lasslop, G., M. Reichstein, D. Papale, A. D. Richardson, A. Arneth, A. Barr, P. Stoy, and G. Wohlfahrt (2010), Separation of net ecosystem exchange into assimilation and respiration using a light response curve approach: critical issues and global evaluation, *Global Change Biology*, *16*(1), 187–208.

Latimer, R. N., and D. A. Risk (2016), An inversion approach for determining distribution of production and temperature sensitivity of soil respiration, *Biogeosciences*, *13*(7), 2111.

Lee, J.-E., R. S. Oliveira, T. E. Dawson, and I. Fung (2005), Root functioning modifies seasonal climate, *Proceedings of the National Academy of Sciences of the United States of America*, *102*(49), 17,576–17,581.

Lellei-Kovács, E., Z. Botta-Dukát, G. de Dato, M. Estiarte, G. Guidolotti, G. R. Kopittke, E. Kovács-Láng, G. Kröel-Dulay, K. S. Larsen, J. Peñuelas, et al. (2016), Temperature dependence of soil respiration modulated by thresholds in soil water availability across european shrubland ecosystems, *Ecosystems*, pp. 1–18.

Liang, N., T. Hirano, Z.-M. Zheng, J. Tang, and Y. Fujinuma (2010), Soil co2 efflux of a larch forest in northern japan, *Biogeosciences*, *7*(11), 3447–3457.

Liu, W., Z. Zhang, and S. Wan (2009), Predominant role of water in regulating soil and microbial respiration and their responses to climate change in a semiarid grassland, *Global Change Biology*, *15*(1), 184–195.

Livesley, S., R. Kiese, P. Miehle, C. Weston, K. Butterbach-Bahl, and S. Arndt (2009), Soil–atmosphere exchange of greenhouse gases in a eucalyptus marginata woodland, a clover-grass pasture, and pinus radiata and eucalyptus globulus plantations, *Global Change Biology*, *15*(2), 425–440.

Lloyd, J. and Taylor, J.A. (1994), On the temperature dependence of soil respiration, *Functional Ecology*, 315–323.

Luyssaert, S., M. Jammet, P. C. Stoy, S. Estel, J. Pongratz, E. Ceschia, G. Churkina, A. Don, K. Erb, M. Ferlicoq, et al. (2014), Land management and land-cover change have impacts of similar magnitude on surface temperature, *Nature Climate Change*, *4*(5), 389–393.

Malhi, Y., D. Baldocchi, and P. Jarvis (1999), The carbon balance of tropical, temperate and boreal forests, *Plant, Cell & Environment*, *22*(6), 715–740.

Manzoni, S., J. Schimel, and A. Porporato (2012), Responses of soil microbial communities to water stress: results from a meta-analysis, *Ecology*, *93*(4), 930–938.

Mencuccini, M., and T. Hölttä (2010), The significance of phloem transport for the speed with which canopy photosynthesis and belowground respiration are linked, *New Phytologist*, *185*(1), 189–203.

Mendel, M., S. Hergarten, and H. Neugebauer (2002), On a better understanding of hydraulic lift: a numerical study, *Water Resources Research*, *38*(10).

Molz, F. J. (1981), Models of water transport in the soil-plant system: A review, *Water Resources Research*, *17*(5), 1245–1260.

Moncrieff, J. B., and C. Fang (1999), A model for soil co 2 production and transport 2: application to a florida pinus elliotte plantation, *Agricultural and Forest Meteorology*, *95*(4), 237–256.

Moyes, A. B., and D. R. Bowling (2013), Interannual variation in seasonal drivers of soil respiration in a semi-arid rocky mountain meadow, *Biogeochemistry*, *113*(1-3), 683–697.

Neumann, R. B., and Z. G. Cardon (2012), The magnitude of hydraulic redistribution by plant roots: a review and synthesis of empirical and modeling studies, *New Phytologist*, *194*(2), 337–352.

Novick, K., P. Stoy, G. Katul, D. Ellsworth, M. Siqueira, J. Juang, and R. Oren (2004), Carbon dioxide and water vapor exchange in a warm temperate grassland, *Oecologia*, *138*(2), 259–274.

Panciera, M. O. Y. R., R., and J. Walker (2006), *The Hydraprobe Data Acquisition System (HDAS): User guide.*, University of Melbourne.

Patwardhan, A., J. Nieber, and I. Moore (1988), Oxygen, carbon dioxide, and water transfer in soils: mechanism and crop response, *Transaction of ASEA*, *31*(5), 1383–1395.

Prieto, I., and R. J. Ryel (2014), Internal hydraulic redistribution prevents the loss of root conductivity during drought, *Tree physiology*, p. tpt115.

Prieto, I., Z. Kikvidze, and F. I. Pugnaire (2010), Hydraulic lift: soil processes and transpiration in the mediterranean leguminous shrub *Retama sphaerocarpa (L.) Boiss*, *Plant and Soil*, *329*(1-2), 447–456.

Prieto, I., F. M. Padilla, C. Armas, and F. I. Pugnaire (2011), The role of hydraulic lift on seedling establishment under a nurse plant species in a semi-arid environment, *Perspectives in Plant Ecology, Evolution and Systematics*, *13*(3), 181–187.

Prieto, I., C. Armas, and F. I. Pugnaire (2012), Water release through plant roots: new insights into its consequences at the plant and ecosystem level, *New Phytologist*, *193*(4), 830–841.

Reichstein, M., E. Falge, D. Baldocchi, D. Papale, M. Aubinet, P. Berbigier, C. Bernhofer, N. Buchmann, T. Gilmanov, A. Granier, et al. (2005), On the separation of net ecosystem exchange into assimilation and ecosystem respiration: review and improved algorithm, *Global Change Biology*, *11*(9), 1424–1439.

Reichstein, M., M. Bahn, P. Ciais, D. Frank, M. D. Mahecha, S. I. Seneviratne, J. Zscheischler, C. Beer, N. Buchmann, D. C. Frank, et al. (2013), Climate extremes and the carbon cycle, *Nature*, *500*(7462), 287–295.

Reynolds, L. L., B. R. Johnson, L. Pfeifer-Meister, and S. D. Bridgham (2015), Soil respiration response to climate change in pacific northwest prairies is mediated by a regional mediterranean climate gradient, *Global change biology*, *21*(1), 487–500.

Richardson, J., A. Chatterjee, and G. D. Jenerette (2012), Optimum temperatures for soil respiration along a semi-arid elevation gradient in southern california, *Soil Biology and Biochemistry*, *46*, 89–95.

Riveros-Iregui, D. A., B. L. McGlynn, L. A. Marshall, D. L. Welsch, R. E. Emanuel, and H. E. Epstein (2011), A watershed-scale assessment of a process soil co2 production and efflux model, *Water Resources Research*, *47*(10).

Robson, B. (2008), Managing flows for ephemeral streams, *Land and Water Australia: Fact sheet*, *2*.

Robson, B. J., E. T. Chester, B. D. Mitchell, and T. G. Matthews (2013), Disturbance and the role of refuges in mediterranean climate streams, *Hydrobiologia*, *719*(1), 77–91.

Rochette, P., R. Desjardins, and E. Pattey (1991), Spatial and temporal variability of soil respiration in agricultural fields, *Canadian Journal of Soil Science*, *71*(2), 189–196.

Ryel, R., M. Caldwell, C. Yoder, D. Or, and A. Leffler (2002), Hydraulic redistribution in a stand of artemisia tridentata: evaluation of benefits to transpiration assessed with a simulation model, *Oecologia*, *130*(2), 173–184.

Santos, M. A. d., J. van Lier, J. C. v. Dam, A. H. Freire Bezerra, et al. (2017), Benchmarking test of empirical root water uptake models, *Hydrology and Earth System Sciences*, *21*(1), 473–493.

Scandellari, F., D. Zanotelli, C. Ceccon, M. Bolognesi, L. Montagnani, P. Cassol, G. Melo, and M. Tagliavini (2015), Enhancing prediction accuracy of soil respiration in an apple orchard by integrating photosynthetic activity into a temperature-related model, *European Journal of Soil Biology*, *70*, 77–87.

Schulze, E.-D. (2006), Biological control of the terrestrial carbon sink, *Biogeosciences*, *3*(2), 147–166.

Serrano-Ortiz, P., C. Oyonarte, O. Pérez-Priego, B. R. Reverter, E. P. Sánchez-Cañete, A. Were, O. Uclés, L. Morillas, and F. Domingo (2014), Ecological functioning in grass–shrub mediterranean ecosystems measured by eddy covariance, *Oecologia*, *175*(3), 1005–1017.

Simunek, J., and J. W. Hopmans (2009), Modeling compensated root water and nutrient uptake, *Ecological modelling*, *220*(4), 505–521.

Simunek, J., and D. L. Suarez (1993), Modeling of carbon dioxide transport and production in soil: 1. model development, *Water Resources Research*, *29*(2), 487–497.

Siqueira, M., G. Katul, D. Sampson, P. Stoy, J.-Y. Juang, H. McCarthy, and R. Oren (2006), Multiscale model intercomparisons of co2 and h2o exchange rates in a maturing southeastern us pine forest, *Global Change Biology*, *12*(7), 1189–1207.

Skaggs, T. H., M. T. van Genuchten, P. J. Shouse, and J. A. Poss (2006), Macroscopic approaches to root water uptake as a function of water and salinity stress, *agricultural water management*, *86*(1), 140–149.

Stoy, P. C., G. G. Katul, M. B. Siqueira, J.-Y. Juang, K. A. Novick, J. M. Uebelherr, and R. Oren (2006), An evaluation of models for partitioning eddy covariance-measured net ecosystem exchange into photosynthesis and respiration, *Agricultural and Forest Meteorology*, *141*(1), 2–18.

Suarez, D. L., and J. Simunek (1993), Modeling of carbon dioxide transport and production in soil: 2. parameter selection, sensitivity analysis, and comparison of model predictions to field data, *Water Resources Research*, *29*(2), 499–513.

Subke, J.-A., and M. Bahn (2010), On the âĂŸtemperature sensitivityâĂŹof soil respiration: Can we use the immeasurable to predict the unknown?, *Soil Biology and Biochemistry*, *42*(9), 1653–1656.

Suseela, V., R. T. Conant, M. D. Wallenstein, and J. S. Dukes (2012), Effects of soil moisture on the temperature sensitivity of heterotrophic respiration vary seasonally in an old-field climate change experiment, *Global Change Biology*, *18*(1), 336–348.

Tang, J., D. D. Baldocchi, and L. Xu (2005), Tree photosynthesis modulates soil respiration on a diurnal time scale, *Global Change Biology*, *11*(8), 1298–1304.

Valentini, R., G. Matteucci, A. Dolman, E.-D. Schulze, C. Rebmann, E. Moors, A. Granier, P. Gross, N. Jensen, K. Pilegaard, et al. (2000), Respiration as the main determinant of carbon balance in european forests, *Nature*, *404*(6780), 861–865.

Van Genuchten, M. T. (1980), A closed-form equation for predicting the hydraulic conductivity of unsaturated soils, *Soil science society of America journal*, *44*(5), 892–898.

Verma, P., S. P. Loheide, D. Eamus, and E. Daly (2014), Root water compensation sustains transpiration rates in an australian woodland, *Advances in Water Resources*, *74*, 91–101.

Vrugt, J., M. v. Wijk, J. W. Hopmans, and J. Šimunek (2001), One-, two-, and three-dimensional root water uptake functions for transient modeling, *Water Resources Research*, *37*(10), 2457–2470.

Wang, B., T. Zha, X. Jia, J. Gong, B. Wu, C. Bourque, Y. Zhang, S. Qin, G. Chen, and H. Peltola (2015), Microtopographic variation in soil respiration and its controlling factors vary with plant phenophases in a desert-shrub ecosystem, *Biogeosciences*, *12*(19), 5705.

Welsch, D. L., and G. M. Hornberger (2004), Spatial and temporal simulation of soil co 2 concentrations in a small forested catchment in virginia, *Biogeochemistry*, *71*(3), 413–434.

Wiaux, F., M. Vanclooster, and K. Van Oost (2015), Vertical partitioning and controlling factors of gradient-based soil carbon dioxide fluxes in two contrasted soil profiles along a loamy hillslope, *Biogeosciences*, *12*(15), 4637–4649.

Wolfe, E. (2009), Country pasture/forage resource profiles: Australia, *Available at: w ww. fao. org/ag/AGP/AGPC/doc/Counprof/Australia/australia. htm.*

Wu, J., K. S. Larsen, L. van der Linden, C. Beier, K. Pilegaard, and A. Ibrom (2013), Synthesis on the carbon budget and cycling in a danish, temperate deciduous forest, *Agricultural and forest meteorology*, *181*, 94–107.

Yiqi, L., and X. Zhou (2010), *Soil respiration and the environment*, Academic press.

Zanotelli, D., L. Montagnani, G. Manca, and M. Tagliavini (2013), Net primary productivity, allocation pattern and carbon use efficiency in an apple orchard assessed by integrating eddy covariance, biometric and continuous soil chamber measurements, *Biogeosciences*, *10*(5), 3089–3108.

Zhong, Y., W. Yan, Y. Zong, and Z. Shangguan (2016), Biotic and abiotic controls on the diel and seasonal variation in soil respiration and its components in a wheat field under long-term nitrogen fertilization, *Field Crops Research*, *199*, 1–9.